
THE UNIVERSITY
*of* EDINBURGH

This thesis has been submitted in fulfilment of the requirements for a postgraduate degree (e.g. PhD, MPhil, DClinPsychol) at the University of Edinburgh. Please note the following terms and conditions of use:

This work is protected by copyright and other intellectual property rights, which are retained by the thesis author, unless otherwise stated.
A copy can be downloaded for personal non-commercial research or study, without prior permission or charge.
This thesis cannot be reproduced or quoted extensively from without first obtaining permission in writing from the author.
The content must not be changed in any way or sold commercially in any format or medium without the formal permission of the author.
When referring to this work, full bibliographic details including the author, title, awarding institution and date of the thesis must be given.

# Role of $^{18}$F FDG PET/CT as a novel non-invasive biomarker of inflammation in Chronic Obstructive Pulmonary Disease

Gourab Choudhury
MBBS, MRCP


Doctor of Medicine

University of Edinburgh

2018

# Declaration

This study represents original work carried out at the Wellcome Trust Clinical Research Facility, Royal Infirmary of Edinburgh, in the Clinical Research Imaging Centre (CRIC), and ELEGI Laboratories in the Queens Medical Research Institute, University of Edinburgh.

This research was funded by a Pfizer Inc Academic Grant. I solely conducted the study, with assistance in performing the FDG PET physics analyses from the experienced staff of the CRIC physics and radiology team, and my research nurses as acknowledged below. I had sole responsibility for obtaining the blood samples for measurement of FDG activity in the study subjects. In addition, I undertook the laboratory measures myself with assistance from colleagues in the Centre for Inflammation Research, as also acknowledged below.

None of this work has been previously submitted for any other degree. The study was performed, following ethical approval by Lothian Regional Ethics Committee, and written informed consent was obtained from each subject prior to entry into the studies.

Gourab Choudhury

# Acknowledgements

There are a very large number of people I need to thank; both for making this work possible and for helping me persevere to the end. This research was undertaken under the supervision of Professor William MacNee (Professor of Respiratory Medicine) and Professor Edwin Van Beek (Professor of Radiology). I am grateful for their support and guidance over the past few years. They have allowed my good ideas to prosper while quickly and politely glossing over those with less potential. I am also thankful for the many opportunities they have given to me; especially to Bill during my early days as a consultant, enabling me to further myself and my career.

I would like to thank my research nurses, Susie Ferguson and Andrew Deans, who helped me all through the study with recruitment, initial screening and on the scan days. Their professionalism made every patient visit run smoothly and they were always available for help and advice. I would also like to thank the nurses in the clinical research facility for their help on the screening days. A big thanks to all the staff in CRIC for their help during this period. It really helped to keep me right on the PET scan days, making these challenging days enjoyable.

As a clinician entering a research laboratory, one relies on experienced scientists to lend a guiding hand. I am grateful to Dr Ellen Drost, Dr Jennifer Raftis, Dr Len Li and Dr Roberto Rabinovich for their general help within the ELEGI labs; Ellen particularly for her supervision in performing the sputum analyses, Jen for her input with the ELISA experiments, and Roberto who guided me with the statistical analyses.

It is important to acknowledge Dr Alison Fletcher and Dr Tim Clarke, from CRIC, as it was their drive and zeal that initially helped me set up the PET imaging in CRIC including advice with radiation dose and imaging protocol. Also, a huge thanks to Mrs Sheila Marshall from CIR, whose astounding organizational skills are inspirational; many thanks to Sheila also for helping me with proof reading my thesis. I would also like to extend a huge thanks to Dr William Vennart from Pfizer,

for his constant enthusiasm, advice and help during the study. I also acknowledge the funding support from Pfizer Inc, which enabled me to perform this study.

Also, a huge thanks to Dr Susan Fernandez who helped me with the analyses of the vascular sub-study.

This acknowledgment section would be incomplete without mentioning the Late Martin Connell, principal physicist of NHS Lothian and CRIC. This study would have been impossible without your input with all the physics analyses. Your constant involvement and suggestions to make this study more robust will always be remembered. Thank you for your ceaseless help during my thesis writing phase too; you will always be reminisced as an exceptionally gifted physicist.

Finally, I would like to thank my friends and my family, especially my parents who have always been a pillar of support in my life.

Gourab Choudhury, February 2018

# Abstract

A characteristic feature of Chronic Obstructive Pulmonary Disease (COPD) is an abnormal inflammatory response in the lungs to inhaled particles or gases. The ability to assess and monitor this response in the lungs of COPD patients is important for understanding the pathogenic mechanisms, but also provides a measure of the activity of the disease. Disease activity is more likely to relate to lung inflammation rather than the degree of airflow limitation as measured by the $FEV_1$. Preliminary studies have shown the $^{18}F$ fluorodeoxyglucose positron emission tomography ($^{18}F$ FDG-PET) signal, as a measure of lung inflammation, is quantifiable in the lungs and is increased in COPD patients compared to controls. However, the methodology requires standardisation and any further enhancement of the methodology would improve its application to assess inflammation in the lungs.

I investigated various methods of assessing FDG uptake in the lungs and assessed the reproducibility of these methods, and particularly evaluated whether the data was reproducible or not in the COPD patients (smokers and ex-smokers). This data was then compared with a group of healthy controls to assess the role of dynamic $^{18}F$ FDG-PET scanning as a surrogate marker of lung inflammation.

My data showed a good reproducibility of all methods of assessing FDG lung uptake. However, using conventional Patlak analysis, the uptake was not statistically different between COPD and the control group. Encouraging results in favour of COPD patients were nonetheless shown using compartmental methods of assessing the FDG lung uptake, suggesting the need to correct for the effect of air and blood (tissue fraction effect) when assessing this in a highly vascular organ like the lungs.

A prospective study analysis involving a bigger cohort of COPD patients would be desirable to investigate this further.

# Lay Summary

Chronic Obstructive Pulmonary Disease (COPD) is a debilitating chronic lung disease condition. It is associated with inflammation in the lungs. The ability to measure this inflammation in the lung would be helpful in testing novel anti-inflammatory drugs in the future. In this study I used imaging techniques which combined positron emission tomography (PET) with radioactive tracer and computerized tomography (CT) scans to assess lung inflammation in a group of COPD patients (smokers and ex-smokers), and compared this to a group of healthy volunteers. The study developed a reproducible method to assess lung inflammation in the lungs of COPD patients.

# Thesis Overview

The first chapter deals with overview of COPD, including causes, comorbidities and pathogenic mechanisms; highlighting the importance of inflammation and the need for inflammatory biomarkers. It also gives a synopsis of the current evidence based on pre-existing work in the literature, supporting the use of dynamic PET scans using radioactive tracers to measure lung inflammation.

Chapter 2 deals with detailed methodology, including details of the study set-up, patient characterisation and principles of various methodologies applied to assess lung inflammation in my study cohort using FDG labelled PET scans.

Chapter 3 highlights all the findings from my study including demographics of the study subjects and results from the feasibility, reproducibility and the comparative phases of this study. This has been subdivided into smaller sections highlighting the various ways of assessing lung inflammation including Patlak analyses, compartmental modelling and static PET analyses using SUV measurement. A section has also been added reporting results to look at the vascular inflammation in this cohort, which was performed as a sub-study in this research project.

Finally, Chapter 4 deals with a detailed discussion of all these methodologies, including the highlights and the shortcomings of this study and ways to potentially improve these methodological challenges in the future.

# Contents

**Page No**

**Page No**

# Chapter 1. Introduction

## 1.1 COPD and its clinical significance

Chronic Obstructive Pulmonary Disease (COPD) is a major cause of morbidity and mortality worldwide. It has been projected to move from the sixth to the third most common cause of death worldwide by 2020, whilst rising from fourth to third in terms of morbidity within the same timeframe [1].

The prevalence of COPD in the general population is estimated to be around 1% of the adult population, but rises sharply amongst those aged ≥40 years. The prevalence continues to increase with age [2]. COPD is known to primarily affect the lung structure and function, resulting in emphysematous lung tissue destruction and large and small airway disease that occur in varying proportions and severity in different individuals [3].

### 1.1.1 Definitions of chronic obstructive pulmonary disease

***American Thoracic Society/European Respiratory Society consensus definition:*** Having previously developed definitions for COPD separately, the ATS and ERS derived a global definition of COPD in their consensus statement in 2004 [3]. This highlighted the importance of obstructive spirometry for a diagnosis of COPD and stated the criteria for chronic airflow limitation as – "not fully reversible". It acknowledges the most common aetiology and local pulmonary pathological changes as an "abnormal inflammatory response of the lungs to noxious particles or gases". Finally, reflecting current thinking, there is reference to the association with "systemic consequences".

The complete definition is as follows:

***"Chronic obstructive pulmonary disease (COPD) is a preventable and treatable disease state characterised by airflow limitation that is not fully reversible. The airflow limitation is usually progressive and is associated with an abnormal***

***inflammatory response of the lungs to noxious particles or gases, primarily caused by cigarette smoking. Although COPD affects the lungs, it also produces significant systemic consequences."***

***Global Initiative for Chronic obstructive lung disease (GOLD) definition:***

The Global Initiative for Chronic Obstructive Lung Disease (GOLD) is a collaborative project of the US National Heart, Lung, and Blood Institute (NHLBI) and the World Health Organization (WHO) [4]. Its goals have been to increase awareness of COPD and decrease morbidity and mortality from this disease. GOLD aims to improve prevention and management of COPD through a concerted worldwide effort of people involved in all facets of healthcare and healthcare policy, and to encourage a renewed research interest in this extremely prevalent disease.

This project provides an updated definition of COPD with references to risk stratification (exacerbation history and hospital admissions; high risk: two or more exacerbations in the preceding 12 months or one or more hospital admissions; low risk: one or no exacerbation not leading to a hospital admission and symptom load (modified MRC dyspnoea score, [**see appendix for table**]) [4]. It also focuses on the pathological response of the lungs to the injury and the systemic effects and associated comorbidities of the condition [4].

The 2017 GOLD complete definition of COPD is as follows:

***"Chronic Obstructive Pulmonary Disease (COPD) is a common, preventable and treatable disease that is characterized by persistent respiratory symptoms and airflow limitation that is due to airway and/or alveolar abnormalities usually caused by significant exposure to noxious particles or gases. The chronic airflow limitation that is characteristic of COPD is caused by a mixture of small airways disease (e.g. obstructive bronchiolitis) and parenchymal destruction (emphysema), the relative contributions of which vary from person to person."***

The terms 'pink puffer' and 'blue bloater' are now historical, however they were an early attempt at describing phenotypes of COPD. Recent studies have begun to describe and validate subgroups or phenotypes of this heterogeneous disease that have unique prognostic or therapeutic characteristics [5].

### 1.1.2 Burden of the disease

Data on mortality from COPD published by the National Records of Scotland shows that between 1996 and 2013 the annual number (per 100,000 population) of deaths among males where COPD was the underlying cause of death fell, while during the same period the rate for females increased. The data also shows that the standardised mortality rate (using the 2013 European Standard Population) in the male population fell by 32% from 97.6 deaths per 100,000 per year in 1996 to 66.31 in 2013, and in females increased by 4% from 48.6 per 100,000 in 1996 to 50.4 in 2013 (Figure 1.1) [6]. This is most likely related to improved smoking cessation and better management of COPD and increased self-awareness amongst the patients.

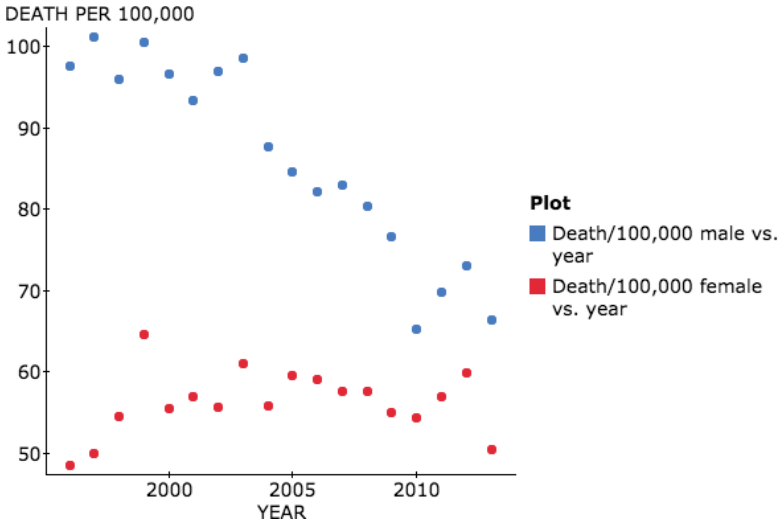


**Figure 1.1: Mortality rate for COPD as primary underlying cause of death, by gender, Scotland 1996-2013 (Data adapted from Scottish Public Health Observatory [6]).**

Despite this, COPD continues to be a major burden on healthcare services and is a major cause of mortality both in the UK and worldwide. [1,7]. The National Institute for Clinical Excellence (NICE) estimates that COPD accounts for £800 million in healthcare costs and is the cause of 90,000 admissions per year, with an average length of stay of 11 days [8]. Furthermore, 31% of patients will be readmitted within 90 days of their discharge. The 2012-2013 data also shows that approximately about 150,000 COPD patients reside across Scotland (3.8% of the adult pollution).

The trend for admissions due to COPD is to rise as well, with emergency admissions due to COPD increasing in Scotland by 2.5-fold in 2006 compared to 1981 (Figure 1.2) [9]. This change is particularly marked in females most likely because of the changes in incidence of smoking, which, whilst going down in males, shows an upward trend amongst females.

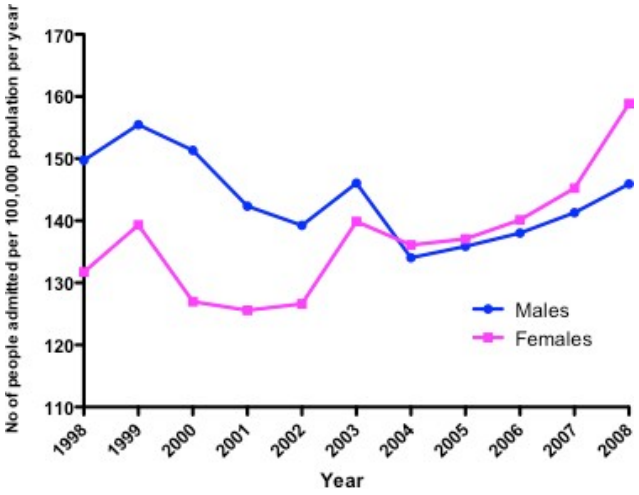


**Figure 1.2: Number of people with at least one emergency admission with a principal diagnosis of COPD per 100,000 populations in Scotland, 1998-2008 ((adapted from Scottish Public Health Observatory, 2010).**

## 1.2 Causes of COPD

### 1.2.1 Cigarette smoking

Cigarette smoking is responsible for at least 90% of all cases of COPD. Fifteen to twenty per cent of cigarette smokers could develop clinically significant COPD [10]. Abstaining from this is clearly related to lower prevalence of tobacco related diseases such as COPD [11]. Despite health promotion campaigns worldwide, the prevalence of cigarette smoking globally continues to increase.

Fletcher and colleagues described the effect of smoking on lung function in the 1960s [12]. They described an increase in the decline in the forced expiratory volume in the first second ($FEV_1$) in working men of 18mls/year in smokers in comparison with non-smokers.

Kohansal *et al* also described lung function changes in healthy never-smoking males and females, from adolescence to old age, and in smokers also to determine the effects of this and quitting [13]. This was a prospective cohort study in all participants of the Framingham Offspring cohort who had two or more valid spirometry measurements during follow-up (n = 4391; age range at baseline 13 to 71 years), with a median follow-up time of 23 years. The study showed that: (i) healthy never-smoker females achieved full lung growth earlier than males, and their rate of decline with age was slightly, but not significantly, lower; (ii) smoking increases the rate of lung function decline, both in males and in females: rate of decline of $FEV_1$ of 38ml per year in male and 23ml per year in female smokers, compared with 20ml and 18ml in non-smoking males and females respectively, and (iii) quitting smoking has a beneficial effect on the rate of lung function decline at any age, but it is more pronounced in earlier quitters.

Compared to *active smoking*, very little data is available on the role of *passive smoking* in causing COPD. Data from three cross-sectional studies within the Obstructive Lung Disease in Northern Sweden (OLIN) database showed that COPD prevalence was independently associated with increased environmental tobacco smoke (ETS) exposure, related to work and home circumstances [14]. The prevalence was associated with increased ETS exposure: 4.2% (no ETS), 8.0% (ETS ever at home), 8.3% (ETS at previous work), and 14.7% (ETS ever at home and at both previous and current work), and therefore showed that ETS in multiple settings was, after age, the strongest risk factor for COPD and comparable to personal smoking of up to 14 cigarettes/day. People aged greater than 65 years were excluded from this study and ageing therefore could not have contributed to these findings.

With the introduction of indoor smoking bans across Europe and the concurrent improvement of respiratory ailments in workers previously exposed to a smoky environment, it is anticipated that there will be a reduction in COPD in individuals previously exposed passively to cigarette smoke.

### 1.2.2 Inhalation of other noxious substances

Cannabis is the most commonly used illicit recreational substance across the globe. The drug is most commonly smoked in a hand-rolled cigarette or in a designed water pipe; it may also be added to food and eaten. It contains many chemicals unique to the plant (referred to as cannabinoids), including the desired psychoactive component - delta-9-tetrahydrocannabinol (THC) [15]. Concerns regarding the respiratory effects of inhaling cannabis smoke are heightened by the knowledge regarding the harm caused by tobacco smoke and the different way in which cannabis is smoked. That is, when smoking cannabis compared with tobacco, there is a prolonged and deeper inhalation and this inhalation technique results in an approximately fivefold increase in carboxyhaemoglobin concentration, fourfold greater amount of tar inhaled, and the retention of one third more tar in the lower

airways [16]. The presence of bullous lung disease or emphysema therefore has been reported among chronic cannabis smokers, although whether the association should be considered causal or causative is in contention. An Australian group has also described early bullous disease in cannabis smokers that occurs much earlier than in cigarette smokers [17] although this has not been confirmed in another study [18]. A growing body of literature also supports the impact on lung function of cannabis use in terms of developing COPD, most commonly by measuring $FEV_1$ and the forced vital capacity (FVC). Using these measures, a few studies have found a relationship between regular cannabis use and increased airway obstruction compared with those who do not use the product [16, 19].

While smoking is thus the major cause of COPD, occupational exposures to vapours, gases, dusts, and fumes (VGDF) can also increase the risk [20]. There is now an abundant support in the literature linking COPD to exposure to dusts in the workplace. Groups at particular risk are coal miners and hard rock miners, as well as workers exposed to mineral dusts and fine metal articulate such as cadmium and vanadium. Dement *et al* showed an 18% increased risk attributed to construction-related exposures, which are additive to the risk contributed by smoking [21].

In the developing world, indoor wood and other biomass fuel burning stoves have also been implicated as a causal factor in the development of COPD, particularly in women engaged in household work [22].

### 1.2.3 Genetic implications

***Alpha-1-antitrypsin deficiency:*** This is a well-known causative factor for COPD. Alpha-1 antitrypsin (A1AT) is produced in the liver, and one of its functions is to protect the lungs from neutrophil elastase, an enzyme that can disrupt connective tissue. A1AT deficiency therefore can, in younger people, lead to development of emphysematous lung disease [23]. In a minority of cases of COPD, deficiency of the antiprotease α-1-antitrypsin (AAT), which is an autosomal recessive disease, could

be the causative factor [24]. The primary function of the anti-protease AAT is to inhibit neutrophil elastase. In severe deficiency, anti-elastase protection in the lung interstitium and alveolar space is markedly decreased to about 15-20% of normal levels, similar to the decrease in plasma levels. An imbalance of elastase and anti-elastase, along with increased innate inflammation in the lung that increases the elastase burden, is believed to cause lung destruction resulting in emphysema in this disease. It is now apparent that AAT has important immune-regulatory roles that would be lost in AATD [25]. Beraldo *et al* [26] showed that the adaptive immune inflammation, comprising B, CD4 (+), and CD8 (+) lymphocytes, and lymphoid follicles, is a prominent feature in AATD. These results change the paradigm of the mechanism of AATD-induced emphysema from a pure elastase/anti-elastase imbalance to a much more complex one involving the adaptive immune system, similar to that which occurs in usual COPD.

Genetic influences on lung function as measured by $FEV_1$ and consequent increased risk of developing COPD have been reported from twin and family studies [23]. In one such study, Zhai and colleagues [23] studied unselected monozygotic (MZ) and dizygotic (DZ) twin pairs from the Twins UK registry to estimate the heritability of the ratio of measured $FEV_1$ ($mFEV_1$) to expected $FEV_1$ ($eFEV_1$) in a white population, and to examine the interaction between genetic factors and smoking on this ratio. The heritability estimate for $mFEV_1/eFEV_1$ ratio was 66% in non-smokers but was significantly reduced to 32% in current smokers. No clear difference was found in the heritability of this ratio between non-smokers and ex-smokers, suggesting that genetics could be a major influence in non-smokers. However, this genetic influence indeed could be further amplified in a major way by interaction with external factors such as cigarette smoking.

***Other genetic influences:*** Silverman *et al* studied a cohort of 44 probands with severe, early-onset COPD, who did not have severe alpha-1-antitrypsin deficiency in a population [25]. This cohort had a high prevalence of females (79.6%) and the study found that the first-degree relatives of early-onset COPD probands had

significantly lower $FEV_1$ and $FEV_1/FVC$ values than control subjects ($p<0.01$), despite similar pack-years of smoking. Reduced spirometric values in these relatives of early-onset COPD probands were seen only in current or ex-cigarette smokers, indicating that the incidence of the disease is possibly higher in the first- degree relatives of the COPD patients, and also reinforces the detrimental additive effect of cigarette smoking in this group.

Data from the COPDGene and ECLIPSE studies also show that there could be genetic differences between subjects with various phenotypes of COPD (eg, the chronic bronchitis [CB] phenotype) [27]. One such study showed that the CB phenotype of COPD relative to smoking controls is more common in a new genome-wide significant locus on chromosome 11p15.5, as well as with significant associations of known COPD single-nucleotide polymorphisms within the FAM13A gene. This provides further evidence that genetic variants may also contribute to phenotypic heterogeneity of COPD.

### 1.2.4 Childhood risk factors

There are several well-known associations with risk factors in childhood and development of COPD in later life.

***Poor socioeconomic status*** along with adverse childhood experiences (ACEs) before age 18 has been associated with several chronic diseases in adulthood, including COPD [28]. Cunningham *et al* [28] studied data from a large cohort of adults and used a regression analysis model to estimate prevalence ratios and their corresponding 95% confidence intervals (CIs) for the relationship of eight ACEs with COPD after adjustment for age group, race/ethnicity, marital status, educational attainment, employment, asthma history, health insurance coverage, and smoking status. The data showed that 63.8% of women and 62.2% of men reported ≥1 ACE. 4.9% of women and 4.0% of men reported COPD. In women, but not in

men, there was a higher likelihood of COPD-associated variety of childhood adverse experiences. There was a higher likelihood of COPD associated with verbal abuse (PR =1.30, 95% CI: 1.05, 1.61), sexual abuse (PR =1.69, 95% CI: 1.36, 2.10), living with a substance abusing household member (PR =1.49, 95% CI: 1.23, 1.81), witnessing domestic violence (PR =1.40, 95% CI: 1.14, 1.72), and parental separation/divorce (PR =1.47, 95% CI: 1.21, 1.80) during childhood compared to those with no individual ACEs. Reporting ≥5 ACEs (prevalence ratio =2.08, 95% CI: 1.55, 2.80) compared to none was associated with a higher likelihood of COPD amongst women, reinforcing the need for the need for further research that examines sex-specific differences and the possible mechanisms that links ACEs and COPD.

***Childhood respiratory infections:*** both viral and bacterial infections are important risk factors for the pathogenesis of COPD. Several recent cohort studies suggest that lung growth is impaired by childhood lower respiratory tract infection, making these individuals more vulnerable to developing COPD on exposure to additional risk factors [29]. The majority of these childhood infections are viral in origin, such as adenovirus, that appear to persist as latent infections in the airways of patients with COPD, and adenoviral E1A protein is capable of amplifying host genes, possibly including those involved in cigarette smoke-induced lung inflammation at a later stage in life [30]. In this context a DNA virus, adenovirus (Ad), early gene 1A (ElA gene) has been identified in lung tissue of COPD. The E1A gene expression can augment the soluble intercellular adhesion molecule (ICAM) 1 expression and the recruitment of inflammatory cells into airways of COPD lungs [30].

Similarly, ***low birth weight*** has been reported as a poor prognostic marker for development of adult respiratory diseases including COPD. Barker and colleagues reported an association between low birth weight and adult respiratory function, and this relationship appeared to be present in all socioeconomic classes [31] and was

also associated with death from COPD. Stern *et al* also investigated whether lung function in early adulthood is affected by airway function measured shortly after birth [32]. This study showed that the participants who had infant Vmax (maximal flow at functional residual capacity) in the lowest quartile also had lower values for the FEV1/FVC ratio (-5.2%, $p<0.0001$), FEF25-75 (-663 mL/s, $p<0.0001$), and FEV1 (-233 mL, $p=0.001$) up to age 22, after adjustment for height, weight, age, and sex, than those in the upper three quartiles combined. This suggests that very early life factors can have a big impact on the development of airways disease in the future. Similarly the Danish Inter99 study looked at adults aged 30-60 years, providing information on birth weight and lung function on 4428 participants [33]. The study showed that birth weight was positively associated with spirometric variables: for a 1 kg increase in birth weight, $FEV_1$ increased by 86 ml (95% CI: 34-139) and FVC by 88 ml (95% CI 27-148); again showing the negative implication of low birth weight in the potential development of COPD at a later life.

## 1.3 Pathogenesis of COPD

The pathogenesis of COPD is thought to be multifactorial [34] and inflammation plays a major role.

Table 1.1 summarises the important factors causative in the pathogenesis of COPD and gives insight into the role of the inflammatory cascade in development of the disease.

**Table 1.1 summarises all the pathogenic mechanisms in causing COPD**

| Mechanism | Pathogenic contribution in COPD |
|---|---|
| **Oxidative stress** | Circulating inflammatory cells produce reactive oxygen species (ROS) promoting inflammation [35] |
| **Role of premature ageing (senescence)** | • Shortened telomere length is associated with reduced lung function emphysema and increased risk of COPD [36]<br>• Senescence markers P16/p21/s-β gal are increased in COPD lungs [37]<br>• Reduced level of anti-ageing molecules SIRT1 and Klotho in lungs of COPD patients [38-39] |
| **Inflammation** | In COPD patients -<br>**Neutrophils:** show enhanced ROS production [18]<br>**Monocytes**: have defective phagocytosis, increase matrix metalloproteinase (MMP)-9 release [40]<br>**Lymphocytes**: peripheral blood T cells show increased apoptosis and Senescent T-cell phenotype [40]<br>**NK cells**: Reduction of cytotoxic and phagocytic function [40-42].<br>Persistent high levels of systemic and pulmonary IL6, TNFα and acute phase reactants such as CRP, Fibrinogen and surfactant protein D seen in COPD [40] |
| **Advanced glycation end-product (AGE)** | COPD patients have lower levels of circulating AGEs<br>correlating with the presence of emphysema [43] |
| **Protease–antiprotease imbalance** | Leads to lung parenchymal destruction [44] |
| **Autoimmune Hypothesis** | The hypothesis is that COPD has an autoimmune component that may account for the persistent enhanced airway inflammation that develops with exposure to cigarette smoke [45] |

The following section will discuss some of these aspects in greater detail.

### 1.3.1 Pulmonary inflammation

Chronic lung inflammation is a characteristic feature of COPD and plays a key role in the pathogenesis of the disease. This involves a number of cells including neutrophils, macrophages, T lymphocytes and augmented concentrations of proinflammatory mediators such as leukotriene B4, Interleukin (IL)-1, IL-6 and IL-8b and TNF-α [32]. Bronchoalveolar lavage fluid and sputum have also been shown to demonstrate increased levels of inflammatory biomarkers such as cytokines, soluble cytokine receptors and proteases in COPD patients [46].

An exaggerated inflammatory response of the airways to chronic irritants, primarily cigarette smoke, is thus an important feature of COPD. After smoking cessation, this inflammation can persist and the levels of pro-inflammatory cytokines in the lungs and bloodstream remain high in many patients with COPD, even those with mild and stable forms of the disease [47].

Pulmonary emphysema has also been shown to be associated with increased activity of proteolytic enzymes, which are activated due to inflammation and oxidative stress occurring in COPD [48]. Mucus hyper secretion, a feature predominantly of the chronic bronchitic phenotype of COPD has been associated with an increased number of exacerbations, and is associated with increased inflammation around the submucosal glands as well as enhanced severity of inflammation in peripheral airways [49]. Chronic lung inflammation in COPD can thus result in remodelling of the airways (small airways disease) and destruction of the lung parenchyma (emphysema). This persistent lung inflammation is therefore considered a major driver of COPD progression.

In addition, systemic inflammation, present in a proportion of COPD patients, may also contribute to the development of systemic complications of COPD [50] that adversely affect clinical outcomes. Agusti *et al* showed that persistent systemic inflammation, defined as having two or more elevated blood inflammatory biomarkers (high sensitivity CRP, IL-6, white blood cell count, fibrinogen) on two occasions one year apart, occurred in a proportion of COPD patients (16%) and was associated with worse clinical outcomes, including increased mortality [51]. Lung and systemic inflammation are further amplified during exacerbations of COPD and hence are of great importance in risk stratification [52].

There is much debate around whether the systemic inflammation in COPD arises from a "spill-over" of inflammatory mediators from lung inflammation [40, 51-53], or whether the systemic inflammation in COPD represents a systemic component of the disease that develops in parallel with, or prior to, pulmonary inflammation [50]. The absence of a relationship between inflammatory biomarkers in the sputum and blood of COPD patients has provided some evidence against the "spill-over theory" [54, 55]. Smoking, lung hyperinflation, tissue hypoxia, skeletal muscle, bone marrow stimulation, immunological disorders, and infections are all cited as possible sources of systemic inflammation in COPD [56]. Thus, this is now considered a systemic effect of COPD as well and will be explained in more detail in section 1.4.

### 1.3.2 Oxidative stress

Oxidative stress reflects an imbalance between the manifestation of oxidants and the ability of a biological system to detoxify these reactive oxidants or to repair the resulting damage. There is good evidence that such an imbalance between oxidants and antioxidants occurs in patients with COPD and is another major driver force in the pathogenesis of the disease in conjunction with inflammation [57]. Increased levels of biomarkers of oxidative stress have been shown to be present in COPD

patients in many studies [58]. An increased level of 8-hydroxy-deoxyguansoine, a marker of oxidative DNA damage, is present in peripheral lung tissue of smokers (with and without COPD) compared with non-smokers [59]. Increased expression of 8-hydroxydeoxyguanosine (8-OHdG), an oxidized nucleoside of DNA, leads to further generation of ROS, diminished DNA auto-repair ability and ultimately somatic mutations even after smoking cessation, thus promulgating further inflammation. Raised levels of 3-nitrotyrosine a marker of nitrosive stress and the lipid peroxidation product F2α isoprostanes have also been detected in the lungs of COPD patients, and these showed a strong correlation with the severity of airflow limitation as measured by $FEV_1$ in COPD patients [60]. Other studies have shown increased levels of the lipid peroxidation product 4-hydroxynonenol in the lungs of COPD patients compared with smokers who have not developed COPD [61]. Increased markers of oxidative stress are also found systemically in COPD patients [62]. Thus, increased oxidative stress is a feature in COPD lungs and systemically in COPD patients and is a major driver of the pathogenesis of the disease in conjunction with inflammatory processes.

### 1.3.3 Protease-antiprotease imbalance in COPD

The interactions between Reactive Oxygen Species (ROS), proteases and antiproteases can trigger a protease/antiprotease imbalance leading to lung parenchymal destruction and emphysema [44, 63]. This protease/ antiprotease imbalance is thought to result from an increased release of proteases by inflammatory cells and from oxidative inactivation of protease inhibitors [64, 65]. Smoke exposure from cigarettes or other biomass smoke can inactivate endogenous antiproteases, activate resident alveolar macrophages and promote neutrophil influx into lungs [63, 66]. This is therefore an important adjunct mechanism to the inflammation and oxidative stress observed in COPD. These activated leukocytes release proteases, such as neutrophil elastase, proteinase 3, matrix metalloproteinases (MMPs), and cathepsins [63]. These proteinases act as

potentiators of each other and also impede the action of their endogenous inhibitors [63, 67]. These proteinases act on components of the extracellular matrix, elastin fibres and collagen and produce chemotactic peptide fragments that attract the further macrophage and neutrophil influx and lung damage.

This imbalance could further be triggered by infection and bacterial colonization. Sethi and colleagues studied 39 consecutive COPD patients in a prospective observational study and identified 76 acquisitions of a new strain of M. catarrhalis in sputum over a 6-year period [68]. Pre-acquisition sputum supernatant samples, obtained just before acquisition of M. catarrhalis, and post-acquisition samples (associated with exacerbation and some with colonization) were analyzed for IL-8, TNF-α, Neutrophil Elastase (NE) and Secretory leukocyte protease inhibitor (SLPI). IL-8, TNF-α and NE were significantly elevated after acquisition of M. catarrhalis, compared to pre-acquisition samples ($p=<0.001$ for all three). These inflammatory biomarkers were also present in colonization ($p=0.015$ for IL-8; $p=<0.001$ for TNF-α and NE) as well as in exacerbation ($p=<0.001$ for all three), compared to pre-acquisition levels. SLPI was significantly lower after acquisition ($p=<0.001$), in colonization ($p=<0.001$) as well as in exacerbation ($p=0.004$), compared to pre-acquisition levels. This is an important study as this further confirms that there is increased airway inflammation and worsening protease-antiprotease imbalance can happen during exacerbations and also in sputum colonization, adding to the inflammatory cascade of the disease pathogenesis and progression.

### 1.3.4 Accelerated ageing

***Telomere length shortening in COPD:*** Evidence suggests that there is occurrence of premature senescence in COPD patients [36].

In many human somatic tissues and cells including lung fibroblasts, there is a progressive waning in cellular division capacity with age or a restricted division

potential before undergoing so-called "replicative senescence". This process is linked to the fact that the telomeres, which protect the ends of chromosomes, get progressively shorter as cells divide.

Telomeres are repetitive DNA sequences (TTAGGG/CCCTAA) located at the end of chromosomes, protecting chromosomes against degradation and remodelling [69]. Due to the end-replication problem in mature somatic cells, telomere repeats are lost with each replicative cycle, until a critical length is attained when the cells undergo senescence. Inflammation or oxidative stress can amplify this process significantly leading to shortened telomere length [70]. Assessing telomere length is therefore considered to be a marker of biological age.

As a part of the Lung Health Study, 5887 smokers, aged 35-60 years with mild to moderate airflow limitation were recruited across North America [71]. In this cohort telomere length of peripheral blood leukocytes of patients with COPD was significantly related to the risk of all-cause (Hazard Ratio, HR, 1.29; p=0.0425) and cancer mortality (HR, 1.48; p=0.0324) over a median follow-up of 7.5 years, irrespective of potential confounders such as chronological age, smoking status and lung function [72].

In another observational study, Rode *et al* studied almost 10,000 patients with COPD and performed telomere length analysis on peripheral blood leukocytes and showed that telomere length decreased significantly with increasing age and with decreased FEV1/FVC ratio, indicating a relationship between telomere length and the degree of airflow limitation [36]. Sin and colleagues had also shown similar results in another cohort of patients [73]. Interestingly, Debigaire *et al* has also recently shown shortened telomere length from the quadriceps muscle biopsy of COPD patients compared to healthy subjects, suggesting a role of premature ageing in the observed muscle dysfunction in COPD [74]. This study reinforces that in COPD patients accelerated ageing plays an important role in pathogenesis of the disease as well as disease progression.

Cigarette smoking may play an important role in this accelerated aging process. Animal studies have shown that animals with shorter telomeres in their lung cells have increased susceptibility to cigarette smoke-induced emphysema [75]. Studies also have shown that in circulating leukocytes, both current and ex-smokers had shorter telomeres than their age-matched non-smokers with a dose-dependent relationship between the telomere length and the years smoked, and that telomere length in COPD patients were shorter than that of control subjects in any age range [76].

In this context of accelerated aging in COPD, *sirtuins* deserve a special mention.

Sirtuins are Type III histone deacetylases (HDAC) that act on histone residues in DNA that regulate various cellular processes, such as cell cycle differentiation, apoptosis, autophagy and senescence [77, 78]. Within the histone deacetylases (HDACs), sirtuins maintain a special position since they are structurally different from other HDACs and are inhibited by different compounds as they have the unique characteristic of being NAD+-dependent [79]. Amongst the sirtuins, sirtuin1 (SIRT1) is important in the context of COPD and is thought to be involved in the clearance of old and damaged mitochondria by prompting autophagy. It also aids in the activation peroxisome proliferator-activated receptor γ coactivator-1α (PGC- α), the mitochondrial biogenesis regulator, and thereby facilitates the recruitment of new mitochondria [80]. Given the central role of mitochondria in the ageing process [81, 82], activation of Sirt1 by maintaining and potentially rejuvenating the pool of mitochondria is a potential therapeutic option. In this respect, resveratrol (3, 4′, 5-trihydroxystilbene), a plant polyphenol, deserves mention [83]. Resveratrol appears to facilitate its anti-ageing effects partly by stimulating SIRT1 and is also reported to be a powerful antioxidant as well as with anti-inflammatory properties (PI3K inhibitor). This is of clinical significance in COPD as a potential anti-inflammatory and an anti-ageing agent given the observed levels of reduced SIRT1 in the COPD

lungs and the associated premature ageing and inflammatory burden as observed in this cohort [83].

***Advanced glycation end products (AGEs)***: Though not directly implicated in the pathogenesis of COPD, advanced glycation end products (AGEs) also deserve a mention as a potential contributor to the inflammatory disease load.

Advanced glycosylation end products of proteins (AGEs) are non-enzymatically glycosylated proteins, which accumulate in vascular tissue with age [84]. AGEs have a broad range of cellular functions, especially in endothelial cells and macrophage expression of procoagulant activity, inducing migration of mononuclear phagocytes, as well as production of platelet derived growth factor and cytokines [84, 85] adding to the inflammatory cascade.

The receptor for advanced glycation end products (RAGE) is a multi-ligand signal transduction receptor that can initiate and propagate inflammation induced by a variety of stimuli including hyperglycaemia, oxidative stress, ageing and hypoxia [86]. RAGE has several isoforms including a soluble form known as sRAGE that appears to act as a decoy receptor, binding RAGE ligands in the extracellular fluid and thus providing protection against inflammation and oxidative stress [84] and so is a potential therapeutic target.

A recent study showed that membrane RAGE is overexpressed in the airway smooth muscles and epithelium of COPD patients [87]. Acute exacerbations of COPD were associated with further reductions in plasma sRAGE and high serum CRP concentrations. Miniati and co-workers in another study involving a large group of COPD patients and age- and sex-matched controls showed that a decrease in sRAGE in COPD was strongly associated with the impairment of lung diffusing capacity, and the severity of emphysema measured by CT scanning [43].

In this context, high mobility group protein B1 (HMGB1) an abundant chromatin protein that acts as a cytokine when released into the extracellular milieu by necrotic and inflammatory cells deserves a mention. It is considered a marker of tissue injury and a mediator of inflammation. Recent studies also report an enhanced level of HMGB1 in BAL fluid, sputum and in blood in patients with COPD [87]. sRAGE presumably inhibits the activity of HMGB1, and therefore might be of potential therapeutic importance in breaking the inflammatory cascade that contributes to accelerated ageing in COPD.

### 1.3.5 Autoimmune hypothesis

Autoimmune conditions are characterised by B- and T-cell responses to self-epitopes and thus the demonstration of B-cell immunoglobulin production and/or T-cell reactivity against autologous antigens is a defining feature of autoimmunity. An autoimmune hypothesis has also been suggested in the pathogenesis of COPD. Lee and colleagues described anti-elastin antibodies in a cohort of emphysematous patients in comparison with a non-emphysematous control group [88]. In addition, they also reported enhanced T-helper cell responses in the emphysema cohort to elastin peptides in comparison with healthy controls and an asthmatic control population, with the production of both interferon-gamma and IL-10. Both cytokines were closely associated with CT-quantified emphysema severity. The authors suggested that exposure to cigarette smoke leads to proliferation and activity of B- and T-cells against elastin that propagates inflammation after withdrawal of the cigarette smoke stimulus.

This is an interesting theory as it could provide an explanation as to why airway inflammation that develops with exposure to cigarette smoke persists following the cessation of smoking [89]. Furthermore, it may explain why some smokers are more susceptible to lung damage on exposure to cigarette smoking. Finally, the autoimmune theory might help us understand the development of COPD as a

condition with extra-pulmonary effects as is observed in this cohort, in a similar way to connective tissue disorders such as rheumatoid arthritis.

## 1.4 Manifestations

### 1.4.1 Systemic effects of COPD and co-morbidities

Besides the lung abnormalities, COPD is now recognised as a condition that has an impact on other organs, the so-called "systemic effects" and comorbidities of COPD [32, 39, 44]. Conventionally, comorbidity has been defined as a disease coexisting with the primary disease of interest. In COPD, however, the definition becomes even more challenging, as certain coexisting illnesses may be a consequence of the patients' underlying COPD [90].

It is as yet unclear whether these associations are a consequence of shared risk factors such as cigarette smoking and poor physical activity, or whether COPD is a true causal factor. Nevertheless, these extra-pulmonary features of COPD add to the challenge of assessing and managing the disease and to the added burden of inflammation.

Table 1.2 lists the various described systemic effects and comorbidities associated with COPD.

**Table 1.2**

| Systemic effects of COPD [32, 39, 44] | Comorbidities in COPD [32, 39, 44] |
|---|---|
| • Muscle dysfunction<br>• Cachexia<br>• Autonomic dysfunction<br>• Systemic inflammation | • Cardiovascular co- morbidities<br>• Lung cancer<br>• Osteoporosis<br>• Nutritional abnormalities<br>• Anaemia<br>• Diabetes<br>• Psychological issues<br>• Obstructive sleep apnoea |

### 1.4.2 Systemic inflammation

Although more an association interlinked with pulmonary inflammation than a causative effect in the pathogenesis of the disease and its extra pulmonary effects, it is nonetheless important to understand the effects of systemic inflammation in COPD [45].

Several recent studies have clearly shown that COPD is associated not only with an abnormal inflammatory response of the lung parenchyma, but also with evidence of systemic inflammation, including systemic oxidative stress, activation of circulating inflammatory cells and increased levels of pro-inflammatory cytokines [33, 34].

This inflammatory response is thus similar to that observed in the lung, and this concept is key to understanding the development of the various systemic effects as seen in this disease.

Systemic inflammation has been implicated as a causative factor for many of the systemic manifestations and the comorbidities of the disease [32]. In a systematic review of 14 original studies, Gan and co-workers demonstrated that peripheral blood leukocyte count and C-reactive protein (CRP) levels were raised in COPD patients, compared to smokers without COPD [91]. Systemic inflammation may thus also contribute to the extra-pulmonary features associated with COPD, such as skeletal muscle dysfunction, osteoporosis and an increased risk of cardiovascular disease, and these in turn can add to the inflammatory burden of COPD.

Figure 1.3 summarises these interrelations between inflammation and the co-morbidities and systemic effects in COPD.

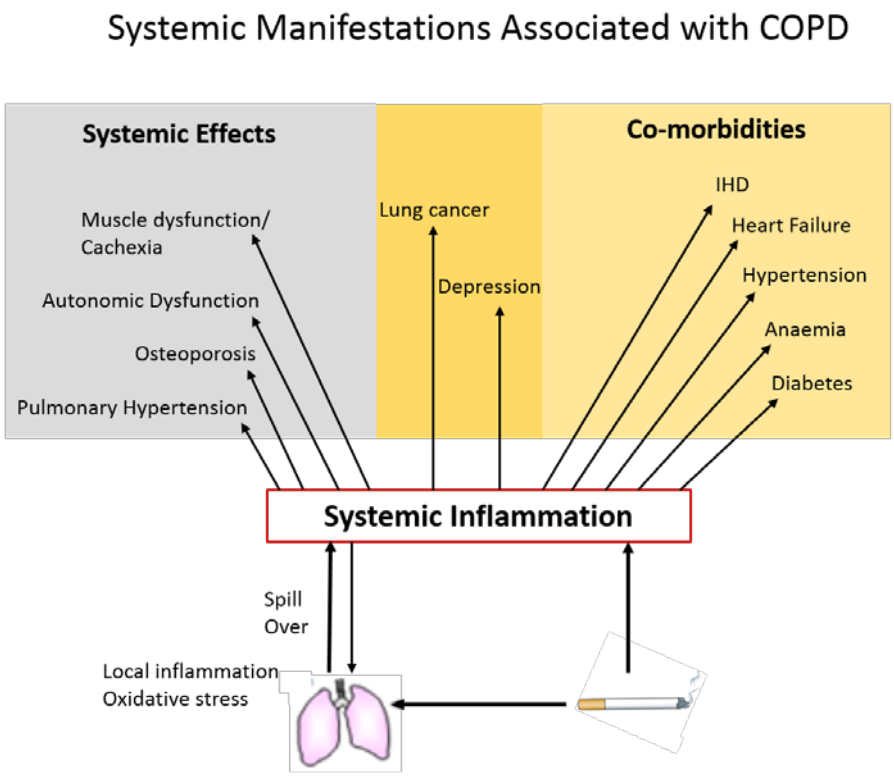


**Figure 1.3: shows interchanging role of systemic inflammation in COPD as a cause and an effect of disease pathogenesis.**

Table 1.3 summarises the predominant mediators that have been implicated in causing the systemic inflammation in COPD and also responsible for the pathogenesis of the other systemic effects and comorbidities as observed in this cohort.

| Mediators | | Actions |
|---|---|---|
| ***Cytokines*** | **IL6 (↑)** | Cardiovascular and skeletal muscle dysfunction [92] |
| | **TNF-α (↑)** | Metabolic and skeletal muscle dysfunction [93, 94] |
| | **IL-1β (↑)** | Cachexia in COPD [44] |
| | **CXCL8 (IL-8) and other CXC chemokines (↑)** | Neutrophil and monocyte recruitment and also contributes to SMD [44] |
| | **Adipokines such as leptins (↑)** | Possible role in cachexia in COPD [44] |
| ***Acute phase proteins*** | **CRP (↑)** | Raised in infective exacerbations potentiates cardiovascular effects and SMD [32, 95] |
| | **Fibrinogen (↑)** | Raised in COPD associated with cardiovascular complications [96, 97] |
| | **Surfactant protein D (↓)** | Derived from lung tissue, circulating levels of this is inversely associated with lung function and health status of patients with advanced COPD [98] |
| | **Serum amyloid A (SA-A) (↑)** | Released by circulating pro-inflammatory cytokines, SA-A levels are raised during acute exacerbations of COPD and its concentrations are correlated with the severity of exacerbation [99] |
| ***Circulating cells*** | **Neutrophils (↑)** | Inverse correlation between neutrophil numbers in the circulation and $FEV_1$ [100], increased turnover in smokers [44], enhanced production of reactive oxygen species [101] |
| | **Monocytes (↑)** | Increase macrophage accumulation in the lungs with defective phagocytosis [44], increase matrix metalloproteinase (MMP)-9 levels in the lungs in COPD compared to non-smokers [102] |
| | **Lymphocytes (↑)** | Increased apoptosis of peripheral T lymphocytes from COPD patients, with increased expression of Fas. TNF- α and transforming growth factor (TGF)- β [44,103], increase in apoptosis of CD8+ T- cells in COPD [104] |
| | **Natural killer cells (NK) cells (↓)** | Reduction of cytotoxic and phagocytic function of circulating NK cells has been reported in COPD [42, 44] |

**Table 1.3: Inflammatory mediators as observed in COPD**

Undeniably, inflammation (both local and systemic) plays a major role in the pathogenesis of COPD, and makes it all the more pertinent to develop novel biomarkers that will help us to quantify the disease burden better and also aid to assess the efficacy of newer anti-inflammatory treatments in the future.

### 1.4.3 Comorbidities in COPD

Although not directly relevant to this study, a brief understanding of some of the comorbidities of COPD may also help us to understand the underlying inflammatory cascade that has an implication in the pathogenesis and progression of the disease.

***Cardiovascular complication***: Cardiovascular disease is the most significant non-respiratory contributor to both morbidity and mortality in COPD and has been reinforced in many research studies. In one such large cohort of COPD patients admitted to a Veterans Administration Hospital or clinic, the prevalence of coronary artery disease was 33.6%, appreciably higher than the 27.1% prevalence seen in a matched cohort without COPD [105]. In the lung health study that assessed deaths and hospitalizations over a 5-year period in a cohort of COPD patients, mortality in 5,887 patients aged 35 to 46 years with COPD and mild to moderate airways obstruction was 2.5%, of which 25% died of cardiovascular complications [106], and cardiovascular disease accounted for 42% of the first hospitalisation and 44% of the second hospitalisation over a follow up period of 5 years in patients with relatively mild COPD. Compared to this, only 14% of the hospitalisations in this cohort were from respiratory causes.

Divo and co-workers also studied 1,664 patients with COPD for over 4 years to assess COPD comorbidities and mortality risk [107]. They generated a COPD comorbidity index based on the comorbidities that increase mortality risk using a multivariate analysis. The prevalence of coronary artery disease in this study was unsurprisingly high at 30.2%, with congestive heart failure and dysrhythmias making up another 15.7% and 13% of the cases respectively, and was strongly

associated with an increased risk of death (p value <0.05).

Mannino and co-workers also assessed the prevalence of COPD deaths in the US between 1979 and 2001 [108]. They found there were about 47 million hospital discharges (8.5% of all hospitalizations in adults) with a primary or secondary diagnosis of COPD (21% and 79%, respectively). Hospital mortality was 43% related to heart disease, compared to 37% related to respiratory failure and another 25% related to pneumonia in this combined cohort (primary or secondary diagnosis of COPD).

$FEV_1$ is also known to be an independent predictor of cardiovascular complications in COPD patients. In the Lung Health Study for every 10% decrease in $FEV_1$, cardiovascular mortality increased by approximately 28% and non-fatal coronary events increased by approximately 20% in mild to moderate COPD [106]. Even a moderate reduction of expiratory flow volumes manifolds the risk of cardiovascular morbidity and sudden cardiac deaths by 2-3 times, independent of other risk factors [109-112]. COPD patients also have shown evidence of increased atherosclerotic plaque burden as assessed by increased carotid intimal medial thickening (CIMT) which is associated with increased cardiovascular and all-cause mortality [113].

Studies have also shown that patients with COPD can have significantly increased coronary artery calcification as observed on CT than controls, and this is associated with increased dyspnoea, reduced exercise capacity and increased mortality in the cohort [114]. In another study, circulating desmosine as a marker of elastin degradation showed that excess elastin degradation could relate to cardiovascular comorbidities, atherosclerosis, arterial stiffness, systemic inflammation and mortality in COPD patients [115].

Vascular inflammation is a well-known manifestation in this cohort and there is strong associative evidence that the inflammatory cells and mediators in COPD are also relevant to the development of cardiovascular disease and cardiovascular complications [56, 112]. In one such study, Sin and colleagues studied around 6,000 participants and found that in the presence of both elevated high sensitive CRP and moderate or severe airflow obstruction, the risk of a cardiac injury was significantly higher in the COPD patients than in those without airflow obstruction and with low CRP, suggesting contributory effect of low grade inflammation on the risk of cardiac injury [112]. This may also explain the 'COPD effect' that contributes to increased cardiovascular complications as seen in this condition [56].

***Skeletal Muscle Dysfunction:*** One of the most striking systemic consequences of COPD is the reduction in peripheral muscle mass resulting in muscle wasting and dysfunction. Muscle dysfunction, with or without evidence of atrophy, can be defined physiologically as the failure to achieve the basic muscle functions of strength and resistance, the latter being inversely related to an increase in the fatigability of the muscle.

Inflammatory mediators such as TNF-α as well IL-1β and IL8 have been implicated in these observed changes [44, 93, 94].

Reduced quadriceps strength in COPD is associated with reduced exercise capacity [116, 117], compromised health status [118], increased need for healthcare resources [119] and mortality and was found to be independent of airflow obstruction [120]. Skeletal muscle weakness, particularly quadriceps weakness, has also recently been shown to be a feature of early disease [121], and its development is likely to be multifactorial with inflammation and oxidative stress [122] being the predominant factors, coupled with physical inactivity [123, 124]. Several other factors, such as protein synthesis/degradation imbalance and hypoxia, have also been postulated to explain the initiation and the progression of this muscle wasting in COPD [117,

125]. Studies also show that up to one third of COPD patients may present with net loss of muscle mass, which is partly responsible for the weight loss in these patients [126]. However, muscle wasting can also be present in 6-21% of patients with normal weight [126]. Unintentional loss of muscle mass has also shown to have a significant impact on quality of life and is associated with premature death [127].

Skeletal muscle dysfunction has thus been linked to various poor outcomes in COPD, including mortality, and has a strong correlation with inflammation. Studies have shown that sarcopenia is very common in patients with stable COPD, and is associated with more severe dyspnoea scores, lower exercise tolerance and increased levels of inflammatory mediators [128]. Other studies have also shown these pro-inflammatory cytokines to be the key contributors to the loss of skeletal muscle mass and the deregulated skeletal muscle physiology as seen in COPD [129]. Apoptosis and an impaired regenerative potential of the muscle that is associated with a high degree of systemic inflammation have also been implicated as crucial factors in the loss of muscle mass and dysfunction as seen in COPD [125]. This is important as it helps us understand the inflammatory cascade in COPD better, and also provides insight into the potential role of rehabilitation strategies as well as novel anti-inflammatory agents (such as TNF-α inhibitors) to help reverse the observed muscle dysfunction in this cohort [129].

***Osteoporosis:*** This is another well-known association with COPD and the prevalence of osteoporosis in COPD varies between 4% and 59%, depending on the diagnostic methods used, the population studied and severity of the disease [130]. A recent systematic review calculated an overall mean prevalence of osteoporosis of 35% from 14 studies that measured bone mineral density (BMD) in COPD. The individuals in these studies had a mean age of 63 and a mean $FEV_1$ per cent predicted of 47% [130].

Over half of patients with COPD recruited for the large TORCH (Towards a Revolution in COPD Health) trial (6,000 patients) also had osteoporosis or osteopenia as determined by DEXA scan [131]. In another cross-sectional study, the prevalence of osteoporosis was 75% in patients with severe COPD patients and strongly correlated with reduced fat free mass [132]. The other remarkable finding from this study was that the prevalence rate was high for males and even higher for postmenopausal females.

Studies show that low-grade systemic inflammation, as can be observed in clinically stable COPD patients, could be the main underlying mechanism able to explain this relationship of low BMD and airflow obstruction in this cohort [133]. It has also been shown that using the plasma level of markers like CRP, IL-6 and TNF-α as surrogates of systemic inflammation, significantly higher levels of these cytokines were observed in the COPD patients who had abnormal BMD [134]. The role of low-grade systemic inflammation in COPD in causing this is still deliberated, but the significant BMD improvement one year after lung volume reduction surgery in severe emphysematous COPD patients, as compared with a similar control group of COPD patients treated with pulmonary rehabilitation, further corroborates the fact that mechanical derangement of lung structure because of air trapping and parenchymal destruction might be pathogenically relevant in sustaining an overall chronic inflammatory response and its consequences [134, 135].

The main determinant of this bone fragility could thus be the chronic inflammation, as shown by the interactions between the inflammatory mediators and the bone remodelling. The inflammatory disease activity consequently adds to the osteoporotic risk factors in these patients and potentially to the overall inflammatory burden of the disease [136].

## 1.5 Need for biomarkers of lung inflammation in COPD

COPD is thus a complex, multi-component, heterogeneous chronic inflammatory lung disease that has varied clinical, functional and radiological presentation amongst patients despite similar degrees of airflow limitation [32, 39]. The standard way of assessing COPD in terms of lung function, (e.g., $FEV_1$) by itself does not adequately describe the complexity of the disease, and thus cannot be used in isolation for optimal assessment and the management of the disease.

As discussed, inflammation has a central role in the pathogenesis of both the lung and systemic effects of COPD. Within the airway lumen in COPD, there are increased numbers of neutrophils and their activation results in secretion of cytotoxins including proteinases such as neutrophil elastase and oxidants [137].

Studies have also shown an association between airway neutrophil burden and disease severity and progression of airflow limitation [138].

Neutrophil elastase and reactive oxygen species have been shown to up-regulate epithelial mucin gene expression with consequent increased mucus production in COPD [137].

Understanding the role these various inflammatory cells play in COPD is difficult because of the heterogeneity of the disease. Nevertheless, inflammatory cells, including neutrophils and macrophages as well lymphocytes, have indeed been implicated in this process as they release proteolytic enzymes and generate oxidants which can cause tissue damage, as well as activate cytokines and chemokines, potentiating further inflammation and triggering an immune response [139, 140].

Lymphocytes have also been associated with emphysema severity as well as airflow limitation and are found in increased numbers in the sputum of COPD patients and may have an important role in the pathogenesis of COPD [141]. The ability to assess and monitor the inflammatory response in the lungs in COPD patients is therefore

important for understanding the pathogenic mechanisms, but also could provide a measure of the activity of the disease as well as provide means to assess the potential of the various novel anti-inflammatory therapies.

Also, the fact that 50% of drugs fail in Phase III trials due to lack of demonstrable efficacy and that respiratory drugs are often the most costly to develop, highlights the need for non-invasive, quantitative molecular biomarkers that guide the selection of therapeutic targets and assess the treatment efficacy of novel respiratory therapies [142].

### 1.5.1 Current ways of assessing lung inflammation

The development of novel biomarkers of lung inflammation in COPD is a major area of research interest. The traditional ways of assessing lung inflammation currently include measuring inflammatory cells and cytokines in sputum, as well as measurement of distal airspace inflammation involving bronchoscopy and bronchoalveolar lavage (BAL). Some of these techniques, like BAL, are invasive; sputum induction requires inhalation of a hypertonic saline, which may provoke bronchoconstriction in COPD patients. Furthermore, processing the sputum and BAL samples requires approximately 2 hours work by a well-trained person to obtain reliable measurements, which limit its use.

Some concerns regarding the viability and reproducibility of the results from these samples have also been reported, with erroneous results noted when the analyses have not been performed in the first few hours of obtaining the sample [143]. Sputum assessment reflects inflammation in the central airways [144], while the results of bronchoscopy and BAL vary according to the region of the lungs that is sampled [145]. Other non-invasive methods such as exhaled breath measures, particularly nitric oxide, carbon monoxide, volatile hydrocarbons and exhaled breath condensate, all hold promise as surrogate markers of inflammation in COPD but require further validation [146]. There is therefore a need for other validated

biomarkers of lung inflammation.

The clinical development of anti-inflammatory therapies for lung diseases is thus, to an extent, hampered by the lack of robust methods to measure the anti-inflammatory activity of novel agents, necessitating large expensive $FEV_1$ based studies. A robust method to measure lung inflammation potentially with validated and more reproducible and demonstrable methodologies using relatively non-invasive techniques like dynamic PET scanning would indeed enable, in the future, to assess better responses to therapeutic interventions in chronic inflammatory lung conditions like COPD.

### 1.5.2 $^{18}$FDG PET/CT scanning as a potential biomarker of lung inflammation

External imaging of intravenously injected radio-labelled markers of inflammatory processes has the potential to provide a non-invasive and repeatable method of monitoring inflammatory cell behaviour, allowing the whole lung to be studied in situ. In this context, imaging using $^{18}$fluorodeoxyglucose positron emission tomography-computed tomography ($^{18}$FDG PET-CT) holds great promise. Use of PET/CT provides images of the concentration of a radiotracer in the body at a spatial resolution of approximately 4-7mm and has been used to assess the metabolic activity of pulmonary inflammatory cells particularly neutrophilic activity [146, 147].

There is considerable evidence that neutrophils contribute primarily to the increased uptake of $^{18}$FDG in the lungs and that the FDG-PET signal correlates with the presence of activated neutrophils [147].

***Mechanism:*** Following injection $^{18}$FDG is transported to the cell by the same mechanism as glucose facilitated transport by glucose transporter GLUT-1 (K1). It is then phosphorylated by hexokinase to $^{18}$F-FDG-6 phosphate (Figure 1.4) and can neither undergo further metabolism nor diffuse out of cells. As the dephosphorylation (k4) reaction also occurs slowly, FDG-6-phosphate is trapped intracellularly and accumulates in proportion to the metabolic rate of the cell [148]. Hence $^{18}$FDG uptake in the lungs could be potentially used to measure the inflammatory activity of the neutrophilic cells in the region of interest.

A series of previous observational studies have suggested that PET CT could be a useful tool to assess the neutrophilic inflammatory burden in the lungs in conditions like cystic fibrosis, pneumonia, and experimentally-induced lung inflammation [147, 149, 150].

The advantages of PET imaging include its relative non-invasiveness, ease of quantification, and the ability to assess the entire lung. As it has been shown to generate both quantitative and spatial data of pulmonary glucose uptake, $^{18}$FDG PET-CT may therefore represent a non-invasive, repeatable biomarker of pulmonary neutrophilic inflammation in COPD patients.

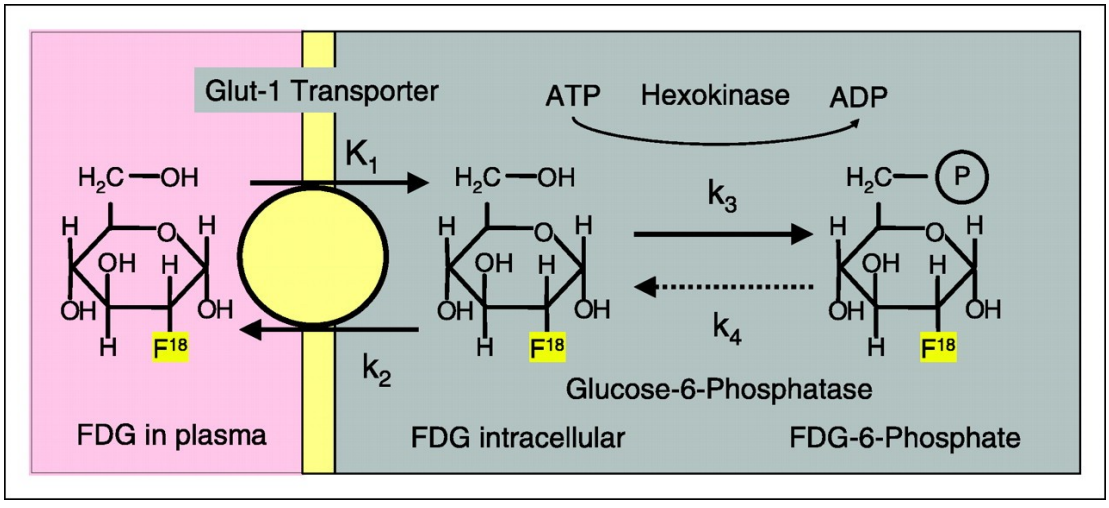


**Figure 1.4: Transport and metabolism of FDG.**

***Static vs dynamic imaging:*** A single static PET imaging technique is easier in a relatively fragile patient but may generate a weaker signal in the context of lung inflammation in COPD. The signal from static PET lung imaging is usually quantified by measuring the standardised uptake value (SUV). SUV is a simple and straightforward index of tracer uptake, but it introduces quantification bias since it is neither directly linked to any physiological process nor does it take account of blood flow and therefore might not relate to inflammation alone [151]. By contrast, dynamic PET studies offer the possibility of full kinetic modelling in real time and makes use of the time variable tracer uptake and radiotracer supply, thus potentially providing much more robust information on the metabolic activity of the tissues [152, 153].

Dynamic imaging therefore potentially allows a better quantitative description of tracer behaviour by taking into account the blood flow and the transportation rate constants between the blood and the tissue [154], which is particularly important in lung studies. This will be discussed more in detail in the methodology chapter.

### 1.5.3 Previous studies supporting the role of $^{18}$FDG PET/CT as a potential biomarker of lung inflammation

Some studies in the past have investigated the role of dynamic PET imaging using FDG as the surrogate with encouraging results. Parr and colleagues conducted a conventional voxel-based, dynamic PET CT image analysis in patients with COPD and healthy controls that quantified regional pulmonary uptake of $^{18}$F-FDG [152]. Plasma $^{18}$FDG activity was derived from venous blood sampling, performed at intervals during the scan. Quantification was determined by ratio of lung tissue PET signal to plasma radioactivity, basing it on a statistical analysis called the 3-dimensional Patlak analysis that will be discussed in detail in the methodology chapter. The study showed regional differences in pulmonary $^{18}$FDG uptake and, in patients with COPD, a correlation between $^{18}$F-FDG uptake rate (Ki) and clinical measures of disease severity. Uptake in the upper lobe of the lung was greater in

patients with COPD compared to the healthy control group and correlated with $FEV_1$% (p=0.001). In my study the aim was to test the Patlak analyses and also to take this a step further and assess the role of FDG as a radioactive tracer using conventional kinetic modelling analyses. This has also been discussed in more detail in the methodology chapter.

Harris *et al* studied pulmonary $^{18}$FDG uptake in patients with allergic asthma following a segmental allergen challenge, induced by bronchoscopic application of a pro-inflammatory substance (allergen extract from cat hair) in one segment of the lung [153]. Net $^{18}$FDG uptake in this study was again analysed by Patlak method.

Results showed increased tracer uptake in the allergen challenged segment consistent with increased inflammation in that segment. The study showed a linear relation between the numbers of inflammatory cells in BAL (performed 24 hours post challenge) from the allergen-challenged airway and the $^{18}$FDG uptake.

Jones and co-workers also showed that Streptococcus *pneumoniae-induced* pneumonia in rabbit lungs, which causes a profound inflammatory response lasting several days, produced pronounced FDG uptake 15 hours after the onset of inflammation with little uptake by 48 hours [154]. In the same study they also studied the bleomycin lung injury model, which progresses from an acute inflammatory stage to chronic inflammation, and scarring $^{18}$FDG uptake was detectable by PET for up to 21 days. These findings are again suggestive of the potential role of $^{18}$FDG as a biomarker of lung inflammation. The role of $^{18}$FDG has been investigated in idiopathic pulmonary fibrosis too and the uptake seem to be related to the lung density and ways to correct for this play an important role in interpreting the results [155]. This will be more extensively discussed in Chapter 4.

Chen *et al* also studied the role of $^{18}$FDG PET imaging as a biomarker of lung inflammation in a cohort of patients with cystic fibrosis and healthy volunteers [147]. The uptake of [$^{18}$F] FDG by the lungs was measured as in previous studies as

the net influx rate constant $K_i$ obtained from the Patlak analysis. Patients were stratified by rate of decline in pulmonary function into stable, intermediate, and rapidly declining groups. $K_i$ was compared between the groups and was correlated against neutrophil numbers in bronchoalveolar lavage. The study showed that the $K_i$ was significantly elevated ($p<0.05$) in patients with CF compared with healthy control subjects, particularly in patients with rapidly declining pulmonary function, suggesting potential relationship with disease activity. $K_i$ also correlated positively with the number of neutrophils present in the BAL fluid in this study.

All of these studies therefore provide support for a role for dynamic $^{18}$F FDG PET pulmonary imaging as a tool to assess the inflammatory burden in patients with chronic lung disease; to identify patients with more aggressive inflammatory diseases, and may be useful in monitoring changes in inflammation in response to novel therapies. However, none of these studies assessed both Patlak analyses and conventional compartmental modelling method [155] in the same cohort of study subjects.

In the current study, I thus aimed to compare the role of FDG PET as an inflammatory biomarker using the compartmental method of analysis as well, which is a mathematical framework commonly applied to estimate PET tracer kinetics. A compartmental model requires a plasma input, referred to as an input function (IF) and contains a series of compartments which each represent a simplified component of the radiotracer transport and binding process [155]. This has the potential benefits of better correction for the tissue fraction effect [TFE] (correction for the effect of air and blood in the highly vascular lung) and is discussed in more detail in the methodology chapter.

## 1.6 Study hypotheses and aim

A protocol for dynamic $^{18}$FDG-PET imaging enhanced by co-registering FDG-PET with quantitated pulmonary CT, enabling measurement of the extent of emphysema,

has thus been used to assess lung inflammation using $^{18}$FDG-PET in COPD patients [152]. Further validation of this methodology; including assessment of the reproducibility technique in COPD patients and then comparing the results with some healthy controls, were the main aims of this study.

***Hypothesis*** of this study was thus that combined $^{18}$FDG-PET/CT with focus on specific lung regions may provide a quantitative, reproducible assessment of lung inflammation in COPD patients, capable of detecting changes with future anti-inflammatory therapeutic interventions.

## Specific aims of the study were as follows:

1. To establish an optimum and validated local protocol for focused $^{18}$F FDG-PET/CT imaging of lung inflammation in COPD patients.
2. To study reproducibility of $^{18}$FDG-PET/CT in this cohort.
3. To relate $^{18}$FDG-PET imaging with lung structure (assessed as emphysema by CT scanning) and to lung inflammation.
4. To compare various methodologies of PET CT scan to measure lung inflammation (static vs dynamic scan including Patlak analyses and compartmental modelling technique).
5. To compare $^{18}$FDG-PET/CT imaging between the COPD cohort and age matched healthy volunteers.
6. Assess for vascular inflammation in COPD patients compared with health controls.

# Chapter 2. Methodology

## 2.1 Overview of methodology

This was a single centre, open label exploratory study to investigate the role of dynamic FDG PET scanning technique as a potential non-invasive biomarker of lung inflammation in COPD patients.

The study was divided into **three phases**:

**Feasibility phase**: To develop a protocol for dynamic FDG PET scanning and to assess different modes of analysis. In this phase six stable COPD patients with mild to moderate airflow limitations underwent FDG PET scanning.

**Reproducibility phase:** This was to test the reproducibility of the methodology over time. In this phase of the study 20 COPD patients were scanned twice 4 weeks apart. These patients were divided into groups of ex-smokers (n=15) and current smokers (n=5 patients) to compare potential differences in the inflammatory signals between these two subgroups in addition to assessing reproducibility.

**Comparative phase:** In the final phase I scanned 5 healthy controls (non-smokers with normal PFTs) and compared the results with those of the COPD patients.

Figure 2.1 summarises the experimental plan of these three phases.

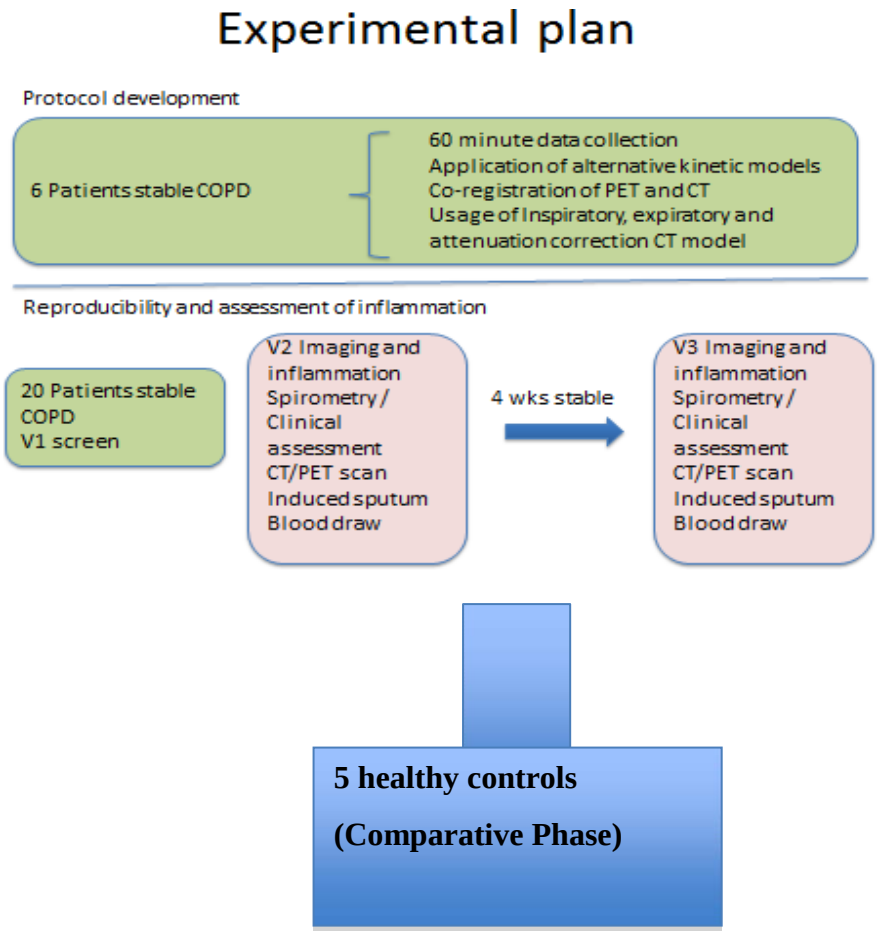


**Figure 2.1: Experimental plan of the study.**

## 2.2 Recruitment of participants

***Recruitment source:*** The patients were mainly recruited from the respiratory outpatient clinics and in-patients of the Royal Infirmary of Edinburgh (RIE). Some patients were also recruited from primary care through the Scottish Primary Research Network (SPCRN).

An invitation with information about the study was sent out to all potentially eligible patients. An 'expression of interest' form was also provided with a stamped addressed envelope so that interested patients could respond to the research team with their contact details. Unless the patient had been seen in the hospital clinic very recently, the patient's CHI number was used on the NHS database to check that the

patient had no major medical or social reasons why it would be inappropriate to send an invitation.

When primary care patients were recruited, GPs were asked to send out a postal invitation to patients on their COPD register, enclosing information about the study and the 'expression of interest' form to be returned to the research team.

***Consenting Process:*** Potential participants received a letter of invitation from their clinician (the consultant or GP as appropriate), enclosing an information sheet to enable them to decide if they would be interested in participating. If they wished to express interest they were asked to complete the 'expression of interest' form, which included basic demographic information (age, gender) and their preferred contact details. The completed from was returned to the clinical research fellow who contacted the patient, answered any questions and, if the patient was still interested, an appointment was arranged for a clinical assessment. Informed consent was obtained after the potential participants read the detailed study information booklet and discussed any questions in person.

## 2.3 Study outline

### 2.3.1 Combined $^{18}$F FDG PET/CT protocol development (Feasibility Phase) phase

The following were the objectives for this phase of the study:

- ☐ To test if a previously developed protocol for combined $^{18}$F FDG PET/ CT dynamic imaging could be validated in the COPD cohort [154].
- ☐ To compare different input functions (venous blood vs. arterial blood sampling vs. image derived techniques), to determine whether or not an arterial input function derived from the dynamic PET images is comparable to the blood derived methods [156].
- ☐ To analyse if $^{18}$FDG kinetics in the lungs using the Patlak analysis method,

and more complex kinetic models in the COPD cohort, could be used as markers of lung inflammation [157].

- To use simultaneous acquisition of CT with FDG-PET to enable co-registration of PET with CT images, which would allow quantification of emphysema to potentially increase the sensitivity of the PET signal [158].

### 2.3.2 Reproducibility and comparative phase

- The reproducibility of the measurements made on dynamic FDG PET scanning were assessed by scanning 20 stable COPD patients on two occasions twice 4 weeks apart.
- The reproducibility phase compared the various parameters obtained from analysis of dynamic FDG PET lung scanning (Patlak analyses and compartmental modelling analysis) to determine comparable results were obtained or not between the two visits of COPD patients.
- The comparative phase related the results obtained from analysis of dynamic FDG PET lung scanning in healthy controls (n=6) and the COPD patients (n=20).

***Study outline:***

- Twenty clinically stable COPD patients with moderate-severe disease using a spirometric classification ($FEV_1$ 30-79% predicted, post bronchodilator $FEV_1/FVC$ ratio <0.7) were studied.
- $^{18}$FDG PET/ CT scan was repeated on the same study cohort after 4 weeks.
- Patients were assessed and examined clinically together with measurements of $FEV_1$ to ensure clinical stability.
- Induced sputum (when possible) and blood sampling was carried out using standardized protocols. Sputum and blood samples were processed for differential cell counts and sputum supernatant and serum used in the analysis

of inflammatory markers.

- Concentrations of sputum inflammatory biomarkers IL-6, IL-8, eosinophil cationic protein, and alpha-2-macroglobulin were measured in sputum using validated ELISA assays (Abcam Inc, Cambridge UK).
- In the serum, concentrations of the cytokines IL-6, IL-8 (Abcam Inc.) and Fibrinogen and high sensitivity CRP were determined using standard ELISA laboratory assays.

### 2.3.3 Safety monitoring of patients

- Patients were observed for 2 hours post scanning to monitor for any clinical side-effects. A check phone call was made on the day following the scan to ensure the patient's wellbeing.
- Any incidental findings on the scan were reported to the patient and the GP and appropriate referral to specialties made if needed.

### 2.3.4 Dose calculation and risk assessment

A total dose of 14 milisieverts (mSv) (feasibility phase) or 28 mSv (reproducibility phase) was used in this study.

The estimated associated risk of developing fatal cancer is proportional to dose. Using a risk of 5% per Sv in a healthy adult population, the estimated associated risk of developing fatal cancer as a result of this exposure is in the region 1 in 700 (1 in 1400*). These risks were therefore classified as low. This assessment was performed with the assistance of Dr Alison Fletcher, Principal Medical Physicist, based at the Royal Infirmary of Edinburgh **(alison.fletcher@ed.ac.uk).**

*Denotes the dose for the feasibility phase of the study as these patients were only scanned once.

The following tables show the breakdown of the proposed radiation dose in this study.

| **Type** | **PET/CT** |
|---|---|
| Radionuclide | $^{18}F$ |
| Chemical Form | FDG |
| Activity | 200MBq |
| Route | IV |
| Administrations[1] | 1 |
| Effective dose per administration | 4 mSv[2] |

1. Number in parentheses indicates number of administrations for subjects in protocol development part of study
2. ARSAC Notes for Guidance 2006 Appendix V11

| **Procedure** | **No of procedures[4]** | **Estimated procedure dose (mSv)[1,2]** |
|---|---|---|
| High-resolution Chest CT on inspiration | 1 | 5 mSv |
| High-resolution Chest CT on expiration | 1 | 2 mSv |
| CT attenuation correction scan for dynamic lung PET[3] | 1 | 3 mSv |

[1]Using ICRP103 tissue weighting factors and scanner-specific DLP to effective dose conversion factor
[2]Dose for a standard sized patient based on phantom measurements.
[3]Modified protocol with fixed tube current (effective mAs 63, CTDIvol 4.2 mGy)
[4]Number in parentheses indicates number of procedures for subjects in protocol development part of study

### 2.3.5 Patient characterisation

***Inclusion criterion for COPD patients:***

- Stable COPD patients with moderate to severe air flow limitation $FEV_1$ 30-79% predicted with a post bronchodilator (2.5 mg of nebulised salbutamol) $FEV_1/FVC$ ratio <0.7.
- Smoking status: ex-smokers (n=5 in the feasibility phase and n=15 in the reproducibility phase) and current smokers (n=5 for the reproducibility phase).

In order to study COPD patients who were most likely to have chronic lung inflammation I included:

- Patients who had at least one exacerbation of COPD in the preceding 12 months prior to the study recruitment.
- Patients with symptoms of chronic bronchitis, defined by the MRC criteria (cough and sputum production for at least 3 months for 2 consecutive years) [159].

***Exclusion criterion:***

- Post-bronchodilator FEV1 <30% of predicted value. (We excluded these very severe COPD patients as we anticipated they would find it difficult to lie flat on the scanner for an hour, potentially therefore adding to the burden of movement artefacts.)
- Age <35 or >85 years.
- History of previous lung transplant.
- Any lung surgery within the past 2 years.
- On any thoracic surgery waiting list.
- Severe concomitant disease (e.g., serious malignant disease, congestive heart failure, NYHA III/IV, clinical significant pulmonary fibrosis, life expectancy <2 years).
- Women of childbearing age not on any long-term contraception.
- Pregnant or lactating women.
- Participation in another clinical treatment trial within 30 days prior to inclusion at baseline.
- Subjects who have previously had 3 or more CT scans.
- History of diabetes.
- Active pulmonary infection/exacerbations within the preceding 8 weeks.

***Definition of clinical stability:***

To ensure that the study patients were all clinically stable at the time of study:

- Patients had no exacerbation in the 4 weeks prior to commencing the study.
- No exacerbations in 4 weeks between the two visits for the reproducibility phase. If an exacerbation occurred during this period, the second scan was postponed for a 4-week exacerbation-free period.
- ***Spirometric stability*** between the 2 visits in the reproducibility phase with a post-bronchodilator $FEV_1$ variability was ensured with a variation of less than 200ml over the 2 weeks prior to the first scan (consenting visit) and between the day of the first scan and on the day of the second scan. This was achieved on all patients. The 200 ml cut-off was decided based on a previous study [152].
- For the feasibility study, post-bronchodilator spirometry was assessed on the screening visit day and the day of the scan, and the scan was performed if variability in $FEV_1$ between each measurement was less than 200ml.

**Healthy controls:** All healthy subjects were between 40-65 years of age, no previous history of any medical illnesses and were non-smokers with normal pulmonary function tests.

### 2.3.6 Patient preparation on the scan day

The following measures were followed for every COPD patient scanned in this study. Steps:

1) Medications: All patients were receiving inhaled corticosteroids and long-acting bronchodilator(s). Patients were allowed to take their inhalers as per their normal schedule, other than withholding the ICS on the morning of the scan. All patients were given 2 puffs of their inhaled short-acting beta agonist inhaler 10 minutes prior to the scan. Other medications were allowed as per normal.

2) Patients were fasted from midnight the previous day prior to the scan.

3) A large bore cannula intravenous was inserted into an arm vein, flushed with 0.9% saline and used for FDG injection.

4) Another venous (at least 18 gauge) cannula was inserted into the patient's other arm. A 3-way tap with 15 cm tubing was then attached. A drop of blood was withdrawn and used to perform the first (baseline) blood glucose measurement. The cannula and tubing was then flushed with 0.9% sterile saline.

5) The aim was to keep the blood sugar level between 4-10 mmol/L prior to commencing the scan, since high blood sugar levels can compete with the FDG cellular uptake potentially giving false negative results.

6) All subjects were scanned supine.

7) Subjects were assessed for haemodynamic stability prior to the scan by recording blood pressure, heart rate, temperature and oxygen saturation (on room air).

8) An arterial cannula was inserted into the radial artery in the non-dominant arm under local anaesthetic (5ml of 2% lignocaine) using an aseptic technique to obtain the arterial blood samples. This was applied *only* to the first 6 patients as a part of the feasibility study.

Steps 2-7 were also followed when scanning the healthy controls.

## 2.4 Protocols for PET/CT Analysis

### 2.4.1 CT protocol and analyses

CT is an anatomical imaging method, which makes use of a rotating X-ray source to build a 3D image. This is attained through multiple quantification of attenuation through a plane of the body with finite thickness to attain attenuation values, which are then converted to produce images in terms of CT-numbers known as Hounsfield Units (HU) [160].

All subjects in this study were scanned using a Siemens Biograph CT, (Siemens Medical Systems, Erlangen, Germany). A full ***inspiratory CT scan*** was performed initially prior to commencing the dynamic PET scanning, followed by a full ***expiratory scan*** (only on visit 1).

Reconstruction parameters were used as per the COPDGene study [161]. This was then followed by an attenuation correction CT (ACCT) scan (relaxed expiration phase) which was matched to the PET bed. The full inspiration HRCT and whole lung relaxed expiration CT was registered to ACCT, matched to PET using advanced normalization tools (ANTS) [http://www.picsl.upenn.edu/ANTS/], and lung regions transferred to PET using the same transformations.

Analysis of full inspiration and expiration CT of whole lung were done using Vida Apollo software (Vida Diagnostics, Coralville, USA), as used by COPDGene Study as well, to generate lobar regions of interest [161].

***Need for attenuation correction scan (ACCT):*** The body attenuates the majority of the emitted photons, and attenuation correction (AC) is therefore essential for

accurate quantification of the emitted signal. Attenuation correction is thus intended and imperative for use in a single scanner that combines volume-imaging (3D) PET with x-ray computed tomography (CT) for the purpose of providing accurately registered anatomical localization of structures seen in the PET image.

***Reconstruction details*** for the CT scans were as follows:

For the **inspiratory CT scan:** 64x0.6mm collimation, 120 kV, 125 effective mAs, pitch 1.1, 0.75mm thickness, 0.5mm slice interval, rotation time 0.5 s, B31f and B46f reconstruction filters were used.

For the **expiratory CT scan:** 64x0.6mm collimation, 120 kV, 31 effective mAs, pitch 1.1, 0.75mm thickness, 0.5mm slice interval, rotation time 0.5 s, B31f and B46f reconstruction filters were used.

For the **ACCT**: 64x0.6mm collimation, 120 kV, 63 effective mAs, pitch 1.1-rotation time 0.5s. For lung analysis recons: 0.75mm thickness, 0.5mm slice interval, B31f and B46f reconstruction filters were used. For attenuation correction recon: 780mm FOV, 5mm thickness, 3mm slice interval, B19f filters were used.

Slides were reconstructed at 3mm and 1.5mm slice separation (with use of Vida Apollo software) to analyze the attenuation correction CT.

***Correction for BMI was applied as follows:*** Relative scaling of effective mAs setting to correct for BMI was used, ie:
BMI<20: Inspiration 90 eff mAs, expiration 23 eff mAs, and attenuation correction eff 45 mAs
BMI 20-30: Inspiration 125 eff mAs, expiration 31 eff mAs and attenuation correction eff 63 mAs
BMI>30: Inspiration 175 eff mAs, expiration 44 eff mAs, and attenuation correction eff 88 mAs
**Quantification of emphysema** was measured on the full inspiratory by measuring the % of low attenuation areas (voxels) with Hounsfield units (HU) <-950 HU

investigated by the following procedure (figures 2.2 a-c):

- Areas of emphysema were transferred from HRCT full inspiration using the lung mask technique, defined by areas below -950 HU [160, 162].
- Non-rigid registration of HRCT full inspiration to attenuation-correction CT (at defined level of inspiration) with lung mask defined in attenuation-correction CT using Elastix software (http://elastix.isi.uu.nl) which was also used for similar registration in lung lobar analysis). Emphysema masks were transferred using the same registration parameters
- To investigate if removal of emphysema had an effect on the PET signal, I used a protocol for removing emphysema in lung voxels of interest (VOIs) containing tissue with Hounsfield Unit below -950 HU on the full inspiration CT (corresponding to the relative area -950 [RA -950] standard) and subsequently non-rigidly transforming these volumes of interest (VOI) to match the ACCT and PET data [162].

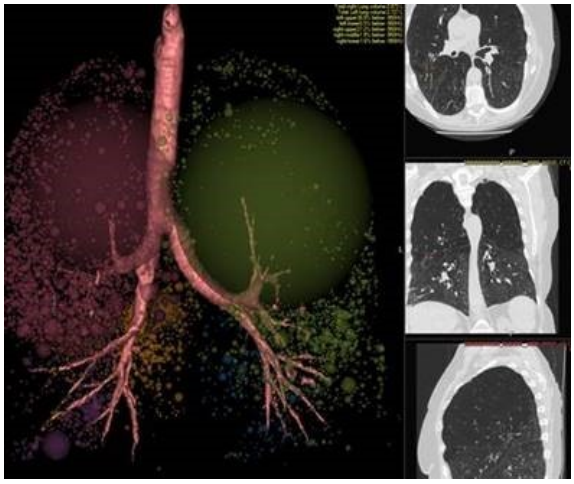

**Figure 2.2a: shows an example of a severe COPD patient with defined areas of emphysema according to lobes using VIDA software, the spheres are used in VIDA to represent the size of contiguous areas below -950 HU in a 3D display with the colours representing different lobes.**

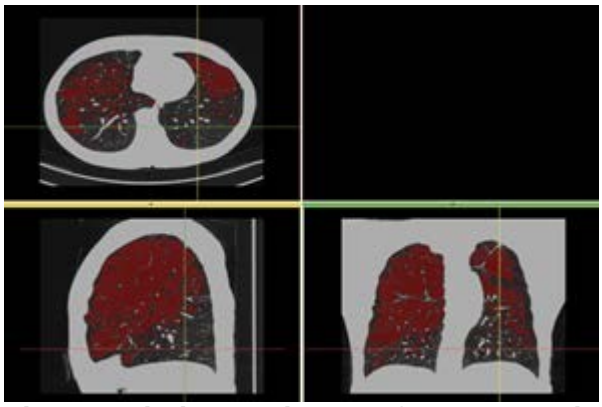

**Figure 2.2b: is a CT image of a COPD patient showing emphysema areas below -950 HU in full inspiration.**

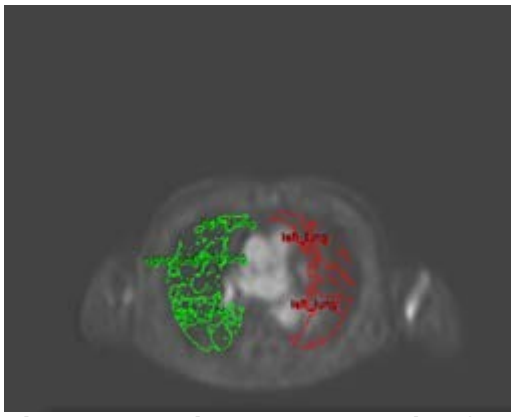

**Figure 2.2c: shows an example of a FDG time activity curves after removal of areas of emphysema in a COPD patient.**

### 2.4.2 PET protocol and analyses

PET is a technique that utilises molecules labelled with positron emitting radionuclides (radiotracers like $^{18}$F FDG) to image physiological and molecular function. The main advantage of combining this with CT scan lies in the fact it allows determination of both anatomical and functional information in one clinical session, also allowing for a fast attenuation acquisition for correction of the PET images [155].

In my study, the PET data was captured with the patient in free breathing during 60-minutes acquisition, and was therefore assessed at an average level of

inspiration. It was assumed that the ACCT at relaxed expiration matches the average PET. The full inspiration CT was registered to 1mm slice thickness relaxed expiration ACCT covering the full lung using non-rigid transformations (ANTS, PICSL, UPenn), and then full lung 1mm slice thickness ACCT was registered rigidly to 3mm ACCT matched to the full range of PET. Volumes of interest (VOIs) for lungs and lobes were segmented in the full inspiration HRCT and whole lung relaxed expiration ACCT using Apollo software (Vida Diagnostics, Coralville, USA), and transferred to PET using the previously calculated transformations. VOIs were further processed by morphological erosion to reduce interference from the myocardium and liver (Figure 2.3).

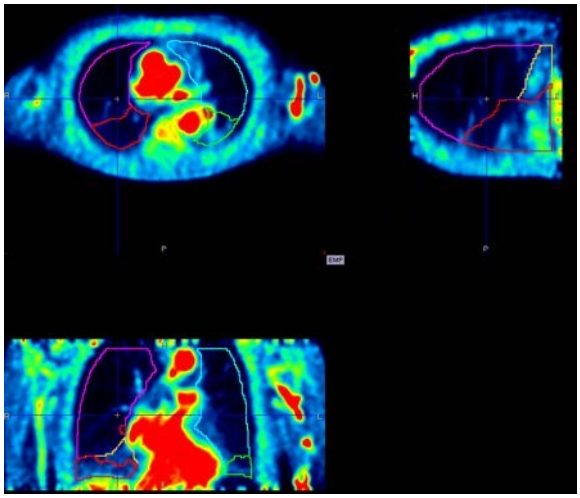

**Figure 2.3: A single frame from dynamic PET acquisition showing lung lobes outlined with morphological erosion from the myocardium.**

***PET imaging protocol:*** During each study experiment, the following sequence was followed:

1. Confirm availability of ligand and PET scanner.
2. Ensure subject is accurately briefed, is happy to proceed and has had the opportunity to pass urine.
3. Obtain reliable venous and radial arterial access (venous access first) whilst the subject is in the scan room and do so only after first ensuring that the equipment and ligand are functional and available.

4. Position subject in the scanning position and ensure they are comfortable.

5. Remove three-way tap with extension from art-line and attach PTFE tubing.

6. Baseline blood sample (aspirate until pure blood, take sample and then flush with heparinized saline.

7. Attenuation correction CT (one PET 'bed' coverage 22cm positioned over lungs).

*When all team in place:*

8. Start PET and inject 200MBq FDG 2 seconds after PET start, as a fast bolus.

9. Start 60-minute PET LM acquisition simultaneously with injection.

10. Blood samples at time points 0, 1.5, 3, 5, 7, 10, 12.5, 15, 20, 25, 30, 40, 50, 60 minutes). The arterial samples (only during the feasibility phase) were also taken at the same time points.

11. End of scan.

12. Specimens transported to nuclear medicine for whole blood count, centrifugation and plasma count.

13. Dispose of consumables appropriately.

14. Following the scan, subject was observed for 2 hours and if stable was discharged home later that day.

***Measurement of [$^{18}$F] FDG activity in whole blood and plasma:*** Whole blood and plasma radioactivity were measured for each blood sample using a Packard Cobra II Auto-Gamma counting system (GMI Inc., Ramsey, MN, USA). The radioactivity of each aliquot of whole blood was counted over 1 minute. The blood samples were then centrifuged (300g, 20°C, for 10 minutes) and the plasma extracted into separate, labelled tubes. The radioactivity of each aliquot of plasma was counted over 1 minute. The radioactivity counts for whole blood and plasma samples were then individually corrected for sample weight, background radioactivity (calculated from an empty control tube) and decay time to give decay-corrected whole blood or

plasma activity (Bq/ml).

For each subject, the $^{18}$FDG activity in lung tissue and in plasma was used to generate time-activity curves and calculate influx constant (Ki) as described below.

## 2.5 Methods for analyses of pulmonary uptake of FDG from combined PET/CT data

Pulmonary uptake of FDG was quantified using the following methods:

1. **Patlak analyses**: Arterial input functions (AIFs) were derived from either blood samples or image-derived from the lumen of the aortic arch or descending aorta (Figure 2.4). Patlak compartmental analysis [157] was performed on these input functions. Estimates of Patlak slope (influx constant Ki) and intercept (initial volume of distribution) were calculated from the time-activity curves for the volumes of interest (VOIs) previously segmented and registered to PET using PMOD (PMOD Technologies Ltd, Zurich, Switzerland) [163]. This is explained in detail in section 2.5.1.

2. **Kinetic modelling analyses**: The kinetics of $^{18}$F-FDG uptakes in the lungs were also analysed with the conventional standard compartmental modelling method. This is explained more in detail in section 2.5.2.

3. **Standard uptake value (SUV)** analysis using data acquired between 50-60 minutes post-injection. This is explained in detail in section 2.5.3.

### 2.5.1 Patlak analyses

In quantitative dynamic PET studies, compartment modelling with a plasma input is usually considered as the standard approach for a full analysis of tracer kinetics. A compartmental model is usually described by a number of differential equations and

parameters for tracer kinetics in vivo [155]. The parameters of a compartmental model are commonly estimated by fitting the measured plasma input to the measured tissue time activity curves (TACs) using nonlinear or linear regression. The selection of a specific compartment model requires knowledge of the in vivo tracer and the biochemical and physiological attributes of the model evaluated. By focusing on the macro-parameters of tracer kinetics, such as uptake rate constant and total distribution volume, the laborious and complicated procedure of the classical compartmental modelling technique can be remarkably simplified by graphical analysis methods such as using the ***Patlak analysis technique***.

Patlak analysis is a series of 3 dimensional graphical analyses where the radioactive tracer undergoes a transformation and is then plotted against normalised time [157]. It is therefore a graphical analysis technique based on the principle of a compartment model that uses linear regression to identify and analyze pharmacokinetics of tracers with irreversible uptake, as is in the case with FDG.

The method is less model-dependent because it does not depend on any specific configuration for the tracer, the minimal assumption being that the behaviour of the tracer can be approximated by the same concept as the two-compartment modelling hypothesis – a "central" (or reversible) compartment that is in rapid equilibrium with plasma, and a "peripheral" (or irreversible) compartment where tracer enters without ever leaving during the time of the measurements.

This graphical tool therefore analyses the uptake of a radioactive tracer in a two-compartmental model, with plasma representing the reversible compartment (Figure 2.4). Upon cellular uptake (for example, within the lungs), $^{18}$F FDG becomes phosphorylated by hexokinase and is irreversibly trapped. After sufficient time has elapsed to create equilibrium between the two compartments, the curve of the Patlak plot becomes linear, where the ***slope*** is equivalent to Ki (uptake rate constant) and the ordinate ***intercept*** indicates the distribution volume.

The Patlak analysis thus depends on some assumptions, including equilibrium being achieved between the blood and tissue compartments and complete entrapment of the tracer without loss (in the case of FDG, by de-phosphorylation) from the tissue region of interest during the scan period.

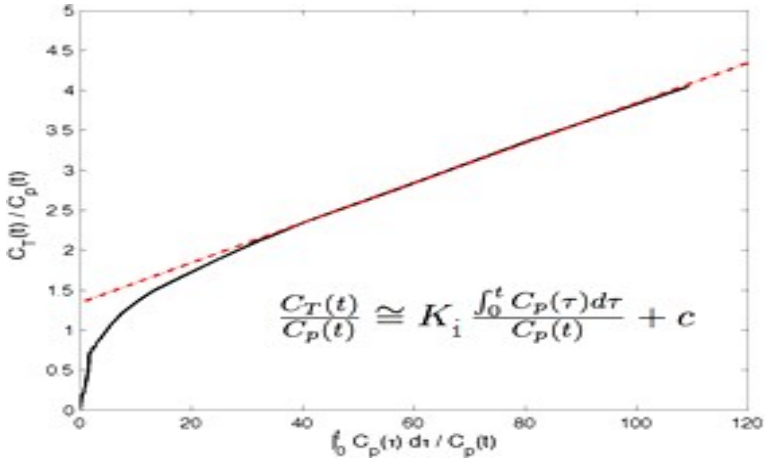


**Figure 2.4: showing a graphical representation of Patlak analyses.**

The Patlak 2-tissue compartment method therefore is an irreversible model of FDG activity in lung that is corrected by FDG activity in blood plasma to give an influx constant (***Slope***).

Figure 2.4 shows a typical example where:

Y-axis is FDG activity in ROI normalised to plasma activity.

X-axis is integral of plasma activity in time normalised to plasma activity.

Net uptake rate of FDG in tissue under study is the slope of straight portion of the curve.

The amount of tracer in the ***region of interest*** is expressed according to the equation:

$$R(t) = K \int_0^t C_p(\tau)\, d\tau + V_0 C_p(t)$$

Where t represents time after tracer injection, R(t) is the amount of tracer in region of interest, $C_p(t)$ is the concentration of tracer in plasma or blood, K is the clearance determining the rate of entry into the peripheral (irreversible) compartment, and $V_0$ the initial volume of distribution of the tracer in the central compartment, also known as the intercept**.** The first term of the right-hand side represents tracer in the peripheral compartment, and the second term tracer in the central compartment.

The Patlak plot is therefore expressed by the equation [157]:

$$\frac{R(t)}{C_p(t)} = K \frac{\int_0^t C_p(\tau)\, d\tau}{C_p(t)} + V_0$$

This means that the measured PET activity is divided by plasma activity, and plotted against a "normalized time" (integral of input curve from injection divided by instantaneous plasma activity). For systems with irreversible compartments this plot will result in a straight line after sufficient equilibration time.

Patlak analysis is thus only applied to timepoints where equilibrium has been reached and is therefore less accurate than using the appropriate compartmental model to analyse the complete time activity curves. However, where the correct model is uncertain, the Patlak model can be exploited as it has the advantage of being model-independent as well as fast, less sensitive to noise, and has the ability to produce parametric images (parameter estimates on a voxel basis) [163].

In my study the Patlak analysis was performed using arterial input functions (AIFs) derived from either venous or arterial blood samples (only during the feasibility phase) as well as image-derived modality. As a part of the feasibility phase time, activity curves derived from all 3 modalities (image derived/arterial as well as venous sampling methods) were compared. An image derived AIF was obtained by placing regions of interest (ROIs) on vascular structures in dynamic PET images (drawn over the lumen of blood vessels [eg, the aortic arch or descending aorta]), and thus exclude the need for manual blood sampling. This method has been validated for some large vascular structures such as cardiac cavities or aortic arteries [164].

### 2.5.2 Compartment kinetic modelling analyses

The kinetics of $^{18}$F-FDG uptake in the lungs were also analysed using the conventional standard compartmental modelling method.

***Need for compartmental analyses:*** In the lung, the average size of an alveolus is approximately 0.008mm$^3$, 6000 times smaller than the typical PET voxel [163, 165]. Consequently, a single voxel will contain air and multiple tissue components including blood and parenchyma. The $^{18}$F-FDG signal within each PET voxel or predefined region of interest (ROI) in the lungs represents the contribution of activity in parenchymal (ie alveolar), airway wall, vascular wall (e.g. endothelial cells) and immune cells, as well as blood, and water (i.e. extracellular fluid). A number of factors can degrade the lung cells' signal within each voxel, including normal respiratory motion and the presence of air that causes partial volume averaging within each voxel. Furthermore, the contribution of a signal from compartments without specific binding, such as blood or water in the lungs, further reduces the signal specificity [155]. The voxel value will therefore then be an

average of the tracer concentrations within that voxel and not the signal from the parenchyma alone.

A majority of the lung parenchyma is also blood and therefore correcting for this blood volume fraction should be important [155]. One such study by Holman and colleagues included the blood component and also investigated the effect of air content in the lung that influences reconstructed image values the so called 'tissue fraction effect' (TFE) in dynamic imaging [155].

Different approaches have therefore applied to reduce the contribution of background $^{18}$F-FDG signal from blood and water as well as reduce partial volume averaging from air in the ROI so that the lung cell signal can be specifically quantified. Kinetic modelling of dynamic PET data can thus help determine the fractional blood volume, **($V_b$)** and CT images have been used to estimate the regional air fraction **($V_a$)**. Using these fractional volumes, the $^{18}$F-FDG uptake in everything that is not air and blood (ie lung cells and water), can therefore be measured.

Accurate estimation of tissue density is also essential for accurate attenuation correction of PET images and any spatial mis-registration of the measured attenuation map and PET activity distribution will result in artefacts [142]. Additionally, increased density alone, whether due to pathologic processes (infection, malignancy etc) or increased physiological atelectasis at end-expiration or denser lungs as potentially observed in healthy individuals, can lead to an increase in the observed $^{18}$F-FDG signal within a PET voxel. Therefore, changes in lung density related to normal respiration can not only lead to large attenuation correction errors, but can also introduce additional variability to serial measurements over time and limit accurate assessment of the entire lung volume. Since the molecular processes of interest are generally within the lung tissue, accounting for the underlying causes of density variations within the lung have been used to obtain more accurate measures of $^{18}$F-FDG uptake, specifically in the lung tissue.

***Analyses Technique:*** As another form of analysis to correct for this blood volume fraction and air fraction effect, the compartment model analyses were explored. This is important as blood volume (Vb) is a large component of the lung voxel (~20%) and adds to the PET signal [166]. It affects voxel concentration of the tracer and must therefore be taken into account. This is thus important as it gives an opportunity to investigate any potential errors if the air and blood components of the TFE are not accounted for, as can happen in Patlak analysis.

The **Sokoloff method** for quantifying $^{18}$F-FDG uptakes has served as the basis from which all currently used kinetic quantification approaches are derived (142, 163, 167, 168). Figure 2.5 illustrates the three-compartment model and its associated equation. The method was originally developed to measure brain glucose metabolism, and one of the key underlying assumptions was that the blood volume was small enough that it contributed a negligible signal compared to the brain parenchyma. This was recognized as a limitation for applying the method for brain tumours, which contain much higher relative blood volumes than normal brain, necessitating the addition of a blood volume component to the model [169]. This is even more important in the lungs than the brain because the lung is a significantly more vascular organ where Vb has been reported at approximately 0.16 and the air fraction of approximately 0.74, implying that the blood activity contributes substantially to the overall signal.

**Figure 2.5:** Explains the kinetics of the 2-compartment model: A conventional standard compartmental model using nonlinear regression [170, 171], where K1 is the forward rate constant (influx) between the blood and tissue compartment, k2 is the reverse rate constant (efflux) between the same 2 compartments, and k3 is the

rate constant representing trapping of $^{18}$F-FDG intracellularly after phosphorylation by hexokinase and k4 is the dephosphorylation rate of the glucose analogue.

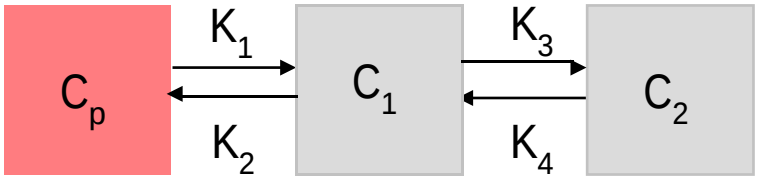


The typical interpretation is that $C_1$ represents free and non-specifically bound tracer in tissue (non-displaceable compartment), and $C_2$ represents specifically bound tracer.

**The Sokoloff Equation is expressed as follows:**

$$\mathbf{C_M(t)=V_A C_A(t) + V_B C_B(t) + (1-V_B-V_A)C_r(t)}$$

where $C_M(t)$ is the measured radioactivity concentration, $C_B(t)$ is the radioactivity concentration in blood, $C_r(t)$ is the radioactivity concentration in tissue, $C_A(t)$ is the radioactivity concentration in air, $V_A$ is the fraction of air in the region of interest (ROI) and $V_B$ is the fraction of blood in the ROI. For radiotracers administered intravenously like $^{18}$F-FDG, the radioactivity concentration in air ($C_A(t)$) can be considered negligible in an organ like brain and so the first term of the above equation is zero. Nevertheless, the volume of air is still present in the equation as a weighting factor of the radioactivity concentration in tissue, when the ROI is in an organ like the lungs.

The Patlak analysis, as mentioned previously, has been developed for systems with irreversible trapping (where $k_4$ equals to zero). The $k_4$ is assumed to be zero as it is presumed that dephosphorylation in the lungs is negligible over the one-hour scanning period.

***The Patlak parameters in terms of 2 compartment rate constants therefore can be summarised as***:

The Patlak graphical analysis is derived from the general compartment model for tracers that are irreversibly trapped in the target tissue. A prerequisite thus for the use of a Patlak plot is an irreversible trapping compartment of the tracer, as in the case of FDG [142].

The slope (Ki) and the intercept (Vo) can be interpreted according to the underlying compartment model theory with the assumption that FDG is a two-tissue compartment irreversible model. The slope thus equals K1*k3/ (k2+k3) (in terms of the microparameters of the equivalent two tissue compartment model) and represents the influx, while the intercept (Vo) is equivalent to the distribution volume and equals k1*k2/ ((k2+k3)*(k2+k3)). These are summarised in the following 2 equations.

**Slope Ki = k1*k3/(k2+k3)**

**Intercept = k1*k2/((k2+k3)*(k2+k3))**

***Indices used in the kinetic model analysis in my study:***

To correct for the air volume fraction (Va) derived from CT density and the blood volume fraction (Vb), two methods have been used in my study to calculate influx rate parameter Ki and they are [155]:

1. **Retrospective correction of Ki [=K1*k3/ (K2+k3)] using (1-Vb)/ (1-Va-Vb) [Method 1].** This generated the parameters, **KiAoVb** and **KiPulmVb** = Ki data from aorta (KiAoVb) and pulmonary artery (KiPulmVb).
2. **Direct estimation of Ki and Vb (Cv = VbCb+(1-Vb-Va)Cpa[K1,k2,k3] ) [Method 2].** This generated the following parameters: **KiAoVbVa and** KiPulmVbVa: Ki data from aorta (KiAoVbVa) and pulmonary artery (KiPulmVbVa).

Method 1 could be implemented using PMOD or MIAKAT software, but Method 2 requires custom modifications to open source software such as MIAKAT (Imanova) validated with simulated data [171].

This will all be discussed further in the results and discussion chapters.

### 2.5.3 Standardised uptake value (SUV)

This is the static way of measuring lung inflammation using PET methodology.

The standardised uptake value (SUV) is the concentration measured within a region or voxel normalized to the patient's weight and the injected activity and thus will reflect the contribution of all components of the lungs (lung cells, blood, and water). This is the most common parameter measured clinically for PET assessment due to its simplicity, despite its dependency on metabolism in other organs, body mass and other confounding factors [172].

SUV is therefore a semi-quantitative ratio of tissue radioactivity ($^{18}$F FDG uptake) within the region of interest to the injected tracer activity, adjusted for lean body weight and the dose of the FDG injected [173].

The basic expression of SUV is:

$$SUV\,(t) = \frac{c(t)}{injected\ activity\ (t)\ /body\ weight}$$

where c is the tissue radioactivity concentration (eg in MBq/kg = kBq/g) at time point t.

The use of SUVs as a measurement of relative tissue/organ uptake facilitates comparisons between patients, and has been suggested as a basis for diagnosis. However, measured SUVs may have a large degree of variability due to physical and biological sources of error, as well as inconsistent and non-optimized image acquisition, processing and analysis [173].

For this study the mean standardised uptake values (SUVs) were calculated from the PET images obtained during the final 10-minute frame from regions of interest in the lung parenchyma as delineated using the PMOD software. The SUV was measured as the maximum pixel signal within the ROI, which is termed the maximum SUV [SUVmax] [174]. SUVmax has several attractive features, including the fact that it reflects the most metabolically active, and possibly most clinically significant, part of the ROI.

The SUV measurement is still a semi-quantitative way of measuring FDG activity and may give variable results depending on the following factors:

- Scatter correction
- Respiratory motion
- Partial volume effect
- Tomographic reconstruction (noise, spatial resolution in the reconstructed images)
- Measurement method
- Post-injection PET scan time
- Attenuation correction

These factors will be discussed further in the discussion chapter.

## 2.6 Measurement of vascular inflammation

The association between COPD and cardiovascular disease, as discussed before, results in a poorer clinical outcome in COPD patients, and is believed to be mediated; at least to an extent through vascular inflammation [92]. As a sub-study I therefore also aimed to quantify vascular inflammation in the COPD patients and the healthy controls using combined $^{18}$F-FDG PET/CT scan technique.

For this sub-analysis I hypothesised that COPD patients would have increased inflammation in systemic arterial walls.

**The aims of this sub-study were therefore:**

1. To compare aortic inflammation in ex-smokers with moderate or severe COPD, versus healthy individuals using static reconstructions of dynamically acquired 18F- FDG PET/CT scans.
2. To determine the relationship between aortic and systemic inflammation.

**Indices measured:** To quantify vascular inflammation in the COPD cohort, the PET signal from regions of interests (ROIs) drawn around the aorta and the mean and maximum aortic **standardised uptake values** (SUVs) were obtained from the pixel activity within each ROIs at 50-60 minute scan time period. Three ROIs were drawn in this study for each subject in the ascending, descending and the arch of the aorta. The mean SUV values obtained were also divided by the mean SUV in the superior vena cava (SVC) to obtain a blood-corrected arterial SUV, also known as **target-to-background ratio** [Figure 2.6] (TBR) [175]. These were the two indices that I used to assess the vascular inflammation in my study.

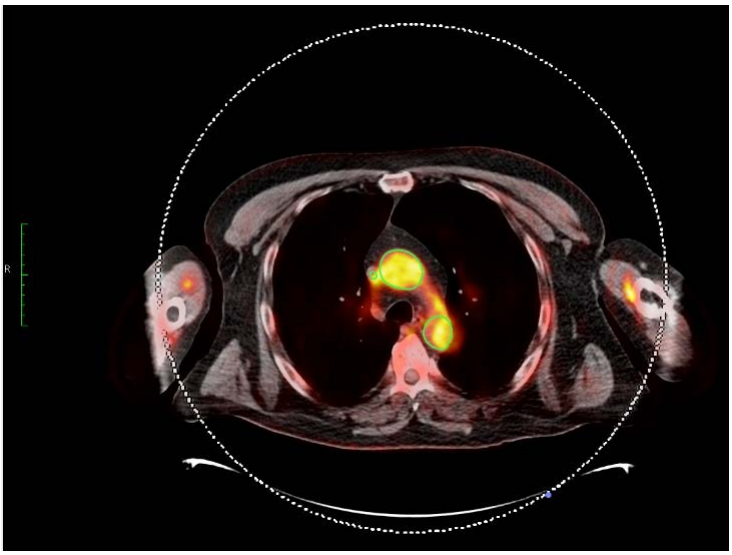

**Figure 2.6: shows circular ROIs on the ascending aorta, descending aorta and the superior vena cava (SVC). This technique is standardised and utilised on every 3mm slices of trans-axial PET/CT images.**

## 2.7 Measurement of systemic markers of inflammation

To assess systemic inflammation, I measured the following inflammatory markers: Blood: White cell count, fibrinogen, C Reactive protein (CRP) (by conventional ELISA techniques).

I also assessed the following cytokines from stored serum samples in COPD and the healthy controls: Interleukin 6 (IL6), Interleukin 8 (IL8), Alpha 2 macroglobulin (A2MG) and myeloperoxidase (MPO). Standard enzyme-linked immune sorbent assay (ELISA) techniques were used to assess the cytokines. The principle of the ELISA methodology followed in this study has been added as a supplement in the appendix section.

Induced sputum from the COPD patients who could produce a sample were also analysed to assess the above cytokines as a measure of airway inflammation. The technique followed to process the induced sputum has also been added as a supplement in the Appendix section.

## 2.8 Statistical analyses

All data were expressed as mean±SEM (standard error of the mean). Normality was tested using Shapiro Wilk and Kolmogorov Smirnov tests.

Comparisons between COPD and controls were performed using student t test or wilcoxon signed-rank test for non-normally distributed variables.
Comparison between COPD smokers, COPD ex-smokers and controls were conducted using ANOVA with Student-Newman–Keuls as a post hoc test or the Kruskall–Wallis equivalent with Dunn's test as a post hoc test for non-normally distributed variables.

Correlations were calculated as Pearson's correlation coefficient or Spearman's correlation coefficient for non-normally distributed variables.

Analyses were conducted using the SAS Version 9.3 (SAS Institute Inc, Cary, NC, USA).

The histograms were drawn using Graphpad Prism (www.graphpad.com).

## 2.9 Power calculation

One of the objectives of this study was to develop a protocol to use dynamic FDG PET scanning as a marker of inflammation with a view to trial novel anti-inflammatory drugs subsequently in the COPD patients. The requirements for conducting a drug study using the type of biomarker developed here is to estimate the number of subjects that would be required to detect a specific change.

For the reproducibility phase, using 80% Power, one-sided alpha of 0.1 and a correlation = 0.52 and a percentage allowed change of 15% in the slope I needed

around 20 patients. Hence, I decided to go for this number in the reproducibility phase. To compare this data with the normal subjects without exposing too many healthy controls to the radiation I decided on six healthy subjects to complete the study. The study was therefore underpowered as has been discussed in more detail in Chapter 4.

# Chapter 3. Results

## 3.1 Demographics

Six patients were scanned in the **feasibility phase** and 20 patients during the **reproducibility phase**. Table 3.1 shows the comparative demographics between the COPD patients (combined feasibility and reproducibility phase) and the healthy controls for their age, spirometry, symptom scoring (COPD Assessment Test (CAT) score, St Georges respiratory questionnaire, modified MRC (mMRC) score as well as systemic inflammatory biomarkers (serum, white cell count (WCC), C reactive protein (CRP) and fibrinogen and cytokines as described in the methodology chapter). Out of the 20 patients scanned during reproducibility, three visit 2 scans could not be assessed (two patients dropped out, one scan was done with wrong settings).

| Variables | Mean | SEM | Mean | SEM | p value |
|---|---|---|---|---|---|
| | COPD (n=26) | | Controls (n=6) | | |
| **Age (years)** | 66.3 | 1.5 | 58.3 | 5.1 | 0.12 |
| **FEV1 (L)** | 1.3 | 0.1 | 3.1 | 0.3 | <0.0001 |
| **FEV1 pp (%)** | 48.4 | 3.3 | 95.1 | 4.1 | <0.0001 |
| **FVC (L)** | 3.2 | 0.1 | 4.2 | 0.1 | 0.14 |
| **FVCpp (%)** | 90.7 | 3.1 | 99.0 | 8.7 | 0.28 |
| **FEV1/FVC ratio** | 0.4 | 0.02 | 0.80 | 0.3 | 0.04 |
| **CRP (mg/L)** | 4.9 | 0.01 | 2.5 | 0.02 | 0.28 |
| **Fibrinogen (g/L)** | 3.1 | 0.1 | 2.2 | 0.2 | <0.0001 |
| **WCC ($x10^9$)** | 8.2 | 0.6 | 5.3 | 0.3 | <0.0001 |
| **SGRQ total score** | 58.0 | 4.13 | 0 | 0 | <0.0001 |
| **CAT score** | 21.5 | 1.48 | 0 | 0 | 0.04 |
| **mMRC dyspnoea score** | 1.9. | 0.23 | 0 | 0 | 0.04 |
| **neutrophil count ($x10^9$)** | 5.1 | 0.51 | 2.8 | 0.2 | 0.28 |
| **Serum MPO (ng/ml)** | 195.1 | 18.3 | 126.5 | 6.2 | 0.06 |
| **Serum IL8 (pg/ml)** | 107.6 | 23.0 | 59.1 | 10.0 | 0.29 |
| **Serum IL6 (pg/ml)** | 12.1 | 4.9 | 4.3 | 1.3 | 0.06 |

**Table 3.1: shows comparative demographic characteristics of the COPD cohort (n=26) and the controls (n=6) with the respective values.**

## 3.2 Normality distribution

A normality distribution was performed to determine if it was appropriate to use parametric or non-parametric statistical analysis techniques. The distribution of both the groups (combined) in terms of demographic characters and the PET parameters were found to follow a non-normal distribution: hence I have used non- parametric techniques for all further statistical analyses.

## 3.3 Patlak analyses

### 3.3.1 Feasibility study

The feasibility phase was performed initially with six stable COPD patients to validate and standardise methods of FDG analyses, and was also used to compare the various methods of assessing the input function (arterial, venous and image derived techniques).

### 3.3.2 Comparison of various input functions (arterial, venous and image derived techniques)

One of the primary aims of the feasibility phase of the study was to validate and standardise the PET scan protocols and then to evaluate whether time activity curves as generated by all three input functions (arterial blood, venous blood and image derived techniques) were comparable. As described in the Methods chapter, analyses were performed with arterial input functions (AIFs) derived from either the blood samples (plasma and whole blood) or the image-derived techniques derived from volumes of interest (VOI) drawn in the blood vessels (eg lumen of the aortic arch or descending aorta) in the dynamic PET images of the six COPD patients.

Estimates of Patlak slope (influx constant Ki) and intercept (initial volume of distribution) were calculated using the PMOD software from the time-activity curves for the volumes of interest (VOIs) previously segmented and registered to PET. Figure 3.1 shows a typical example of full inspiratory CT PET images in various lung lobes with respective time activity curves (Figure 3.2 colour coded according to the lobes).

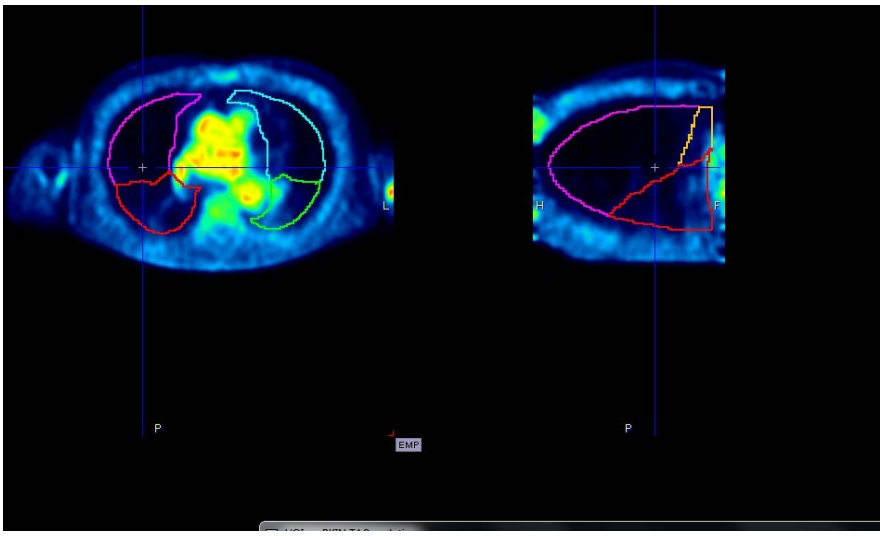

**Figure 3.1: Frames from a dynamic PET scan showing the lobar demarcation.**

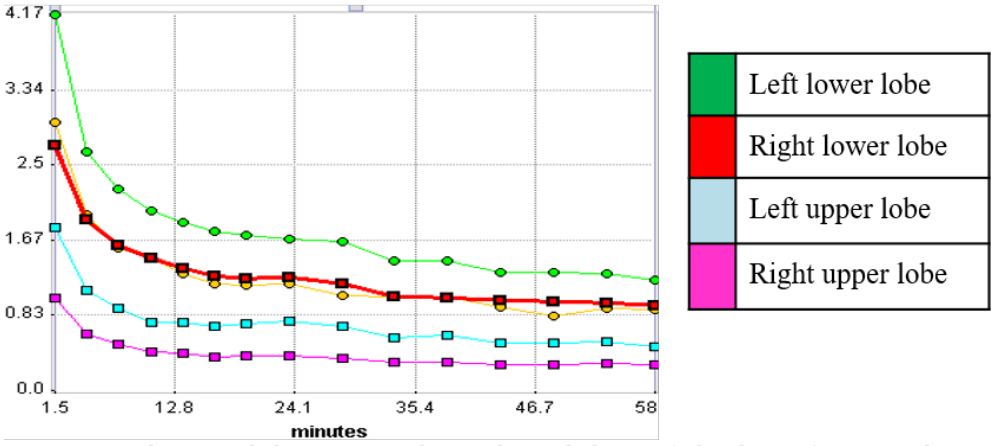


**Figure 3.2: Time activity curves in various lobes of the lung from an image derived input functioning. [Note the yellow line denotes the mean time activity curve for the whole lung].**

The time activity curves generated from all three input functions were found to be similar. Figures 3.3a and 3.3b show a typical example in one such COPD patient.

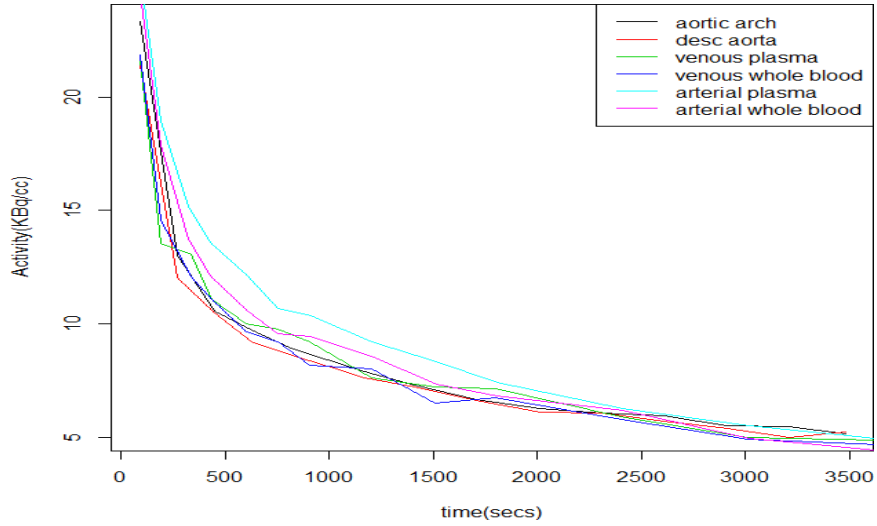


**Figure 3.3a: Time activity curves from venous and arterial blood (whole blood and plasma) and image-derived techniques in one subject.**

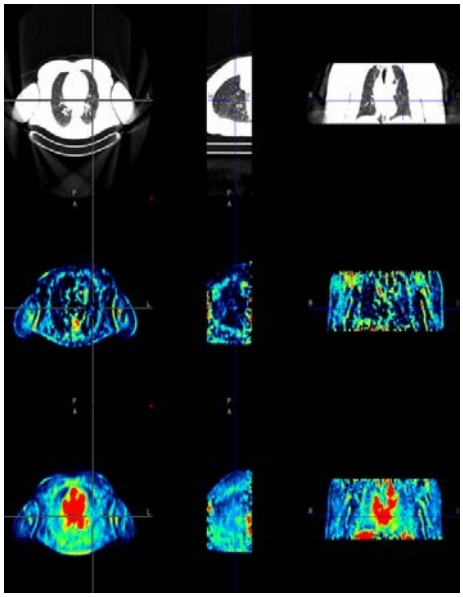

**Figure 3.3b: Patlak image from venous plasma CT (upper row), slope (middle row) and intercept (lower row).**

There was in general a good correlation demonstrated between both blood and image derived techniques.

These correlations were performed using the image derived and blood-derived data from the first six COPD patients in the feasibility phase of the study. Figures 3.4 a-d summarise these observations.

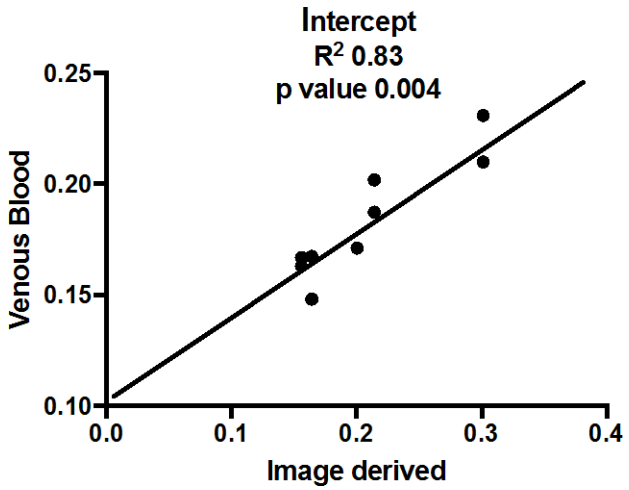


**Figure 3.4a: Relationship between Patlak intercept derived from venous blood vs image derived AIFs.**

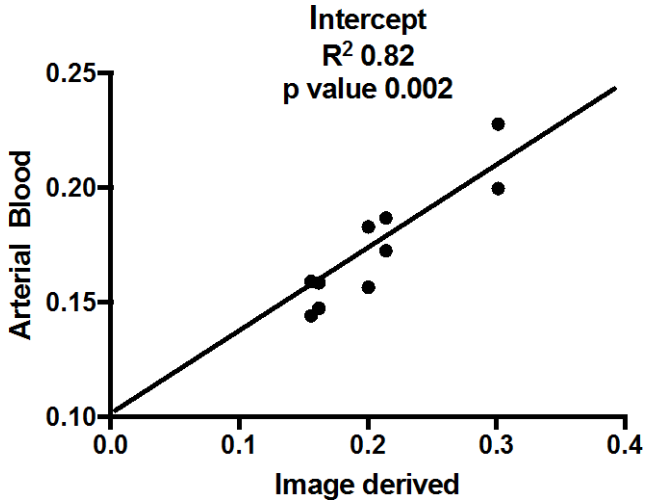


**Figure 3.4b: Relationship between Patlak intercept derived from arterial blood vs image derived AIFs.**

Figure 3.4c and 3.4d show these respective comparative data in column statistics. Some of the detailed statistical analyses between COPD and controls for all further comparisons have been added as supplemental tables in the Appendix section.

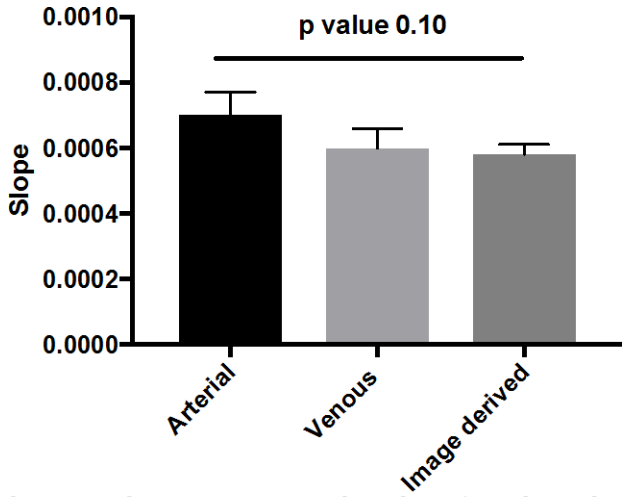


**Fig 3.4c shows comparative data for slope between all three modalities of AIF with no significant statistical difference (Histograms denote Mean and the bars the SEM. p=0.10).**

Similar non-significant results were shown when an analysis was made using all three input functions to measure the intercept (p value 0.35). Figure 3.4d summarises these results.

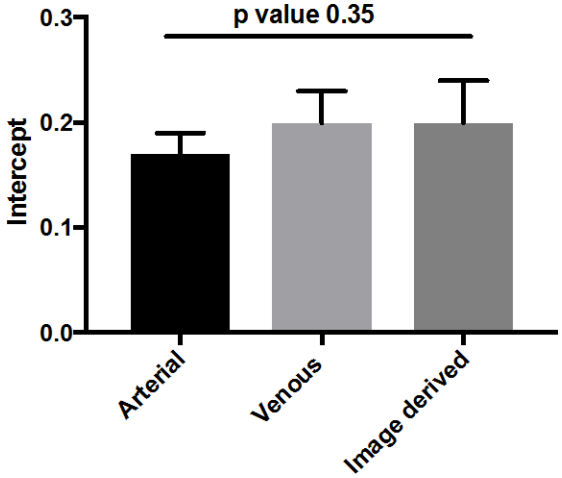


**Fig 3.4d shows these comparative data for intercept between all three modalities of AIF with no significant statistical difference (Histograms denote Mean and the bars the SEM, p=0.35)**

Since there were no significant differences between the results for slope and intercept for these three methods of deriving the input function, for all the subsequent data analyses I used the image derived input functions.

### 3.3.3 Summary inferences from feasibility phase

The feasibility study thus helped us to optimise the PET/CT protocol using the first six patents. It also showed similar results between all three methods of deriving the input function.

## 3.4 Reproducibility study

The next phase of the study was to determine if the results from data from all the parameters derived using the Patlak analysis was reproducible across time between the two visits in the COPD patients, which was assessed using Bland-Altman plots.

Tables 3.5 and 3.6 show the mean and the SEM of the Patlak data available from visits 1 and 2.

| Variable | Mean | SEM | N |
|---|---|---|---|
| Slope<br>Intercept | 0.0004<br>0.18 | 0.00006<br>0.01 | 20<br>20 |

**Table 3.5: Mean and SEM of COPD patients for the Patlak parameters slope and intercept from visit one.**

| Variable | Mean | SEM | N |
|---|---|---|---|
| Slope<br>Intercept | 0.0004<br>0.15 | 0.00005<br>0.009 | 17<br>17 |

**Table 3.6: Mean and SEM of COPD patients for the Patlak parameters slope and intercept from visit two.**

### 3.4.1 Reproducibility of slope

The data between visits one and two were found to be reproducible with all data points within two standard deviations in Bland-Altman plots (Figure 3.7a).

Figure 3.7b shows the mean plus SEM data for slopes between visits 1 and 2 of the COPD patients and, although not a measure of reproducibility, the similar results are reassuring to observe.

**Slope**

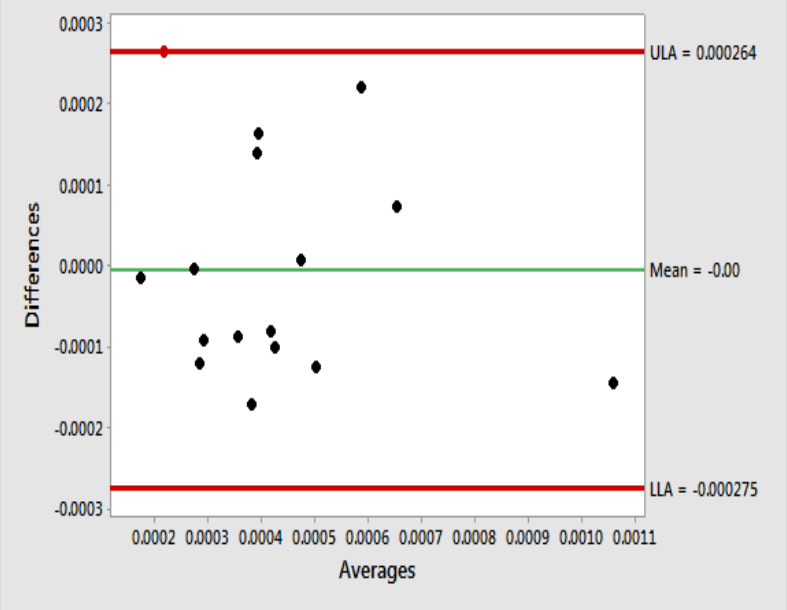


**Figure 3.7a: Bland Altman Plot analyses for slope showing acceptable reproducibility between the two visits.**

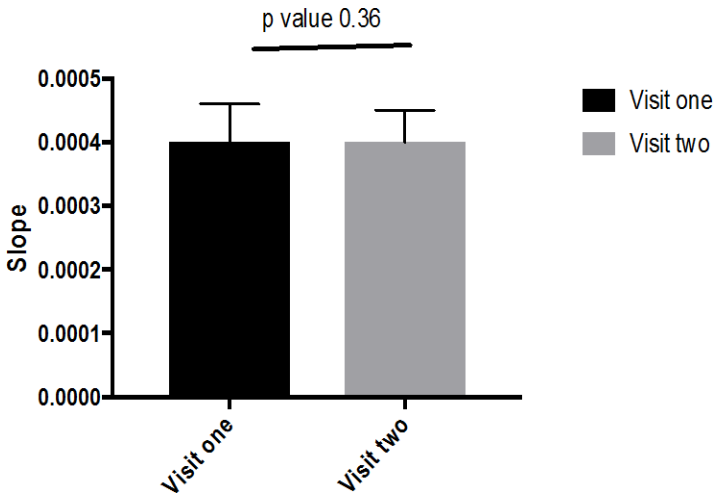


**Figure 3.7b: Mean and SEM of slope between two visits of COPD (Histograms denote Mean and the bars the SEM. p=0.36).**

### 3.4.2 Reproducibility of intercept

Similarly, the data for intercept between visits 1 and 2 were found to be reproducible with all data points within two standard deviations in Bland-Altman plots (Figures 3.8 and 3.9).

Figure 3.8: Patlak intercept data in COPD patients between two visits is reproducible using B-A plot analyses.

Figure 3.9: shows the mean plus SEM data for intercept between visits 1 and 2 of the COPD patients and, although not a measure of reproducibility, these similar results are reassuring to observe.

## Intercept

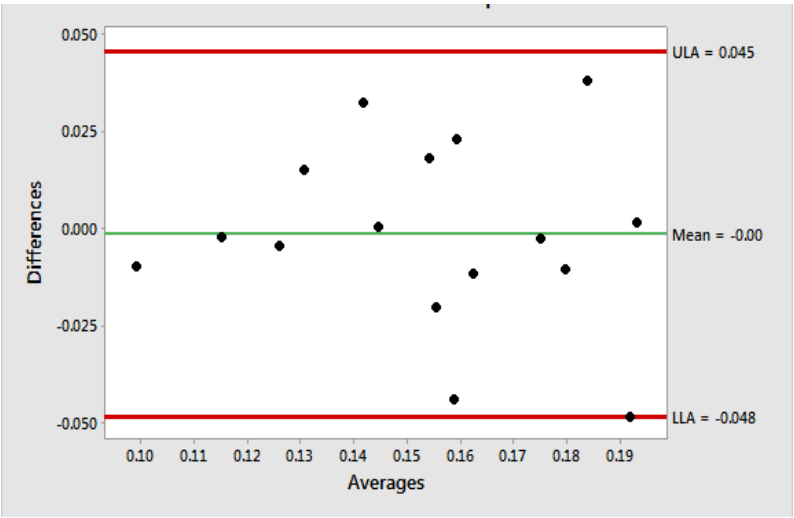


**Figure 3.8: Bland Altman Plot analyses for intercept showing acceptable reproducibility between the two visits.**

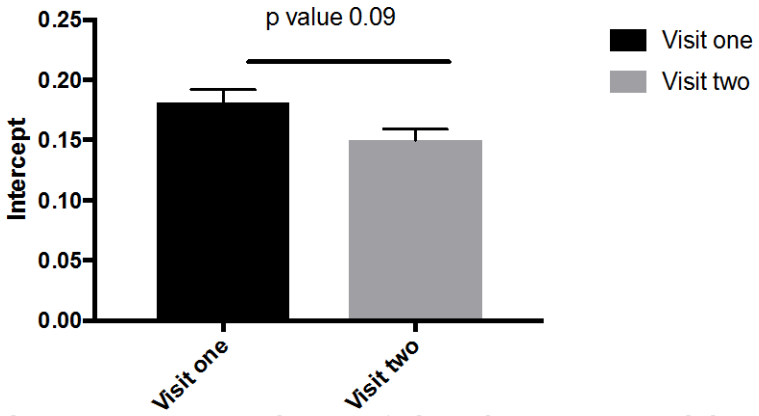


**Figure 3.9: Mean and SEM of slope between two visits of COPD (Histograms denote Mean and the bars the SEM, p=0.09).**

## 3.5 Comparison between COPD and controls (comparative phase)

### 3.5.1 Comparison of slope and intercept between the COPD and the controls

When these parameters were compared between the COPD patients and the healthy control, the intercept particularly was found to be higher in the controls compared to the COPD patients. Figures 3.10 and 3.11 demonstrate these findings.

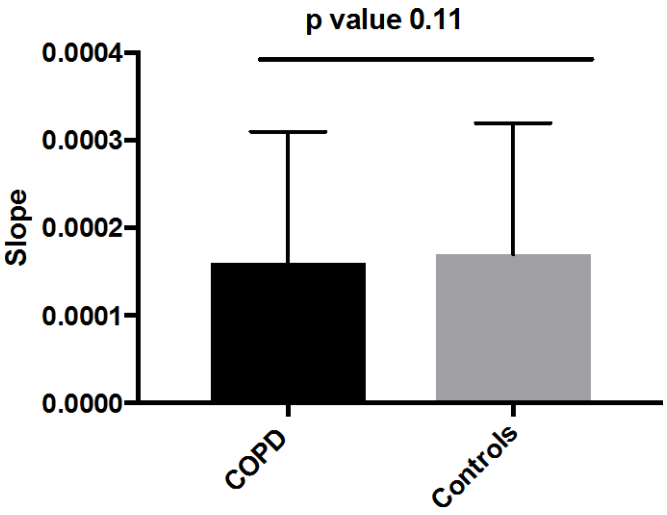


**Figure 3.10: shows the data from COPD patients (n=20) and healthy controls (n=6) for the slope. (Histograms denote mean and the bars the SEM, p=0.11).**

Figure 3.11 shows the data from COPD Patients (n=20) and healthy controls (n=6) for the intercept and was significant with higher values observed in the controls.

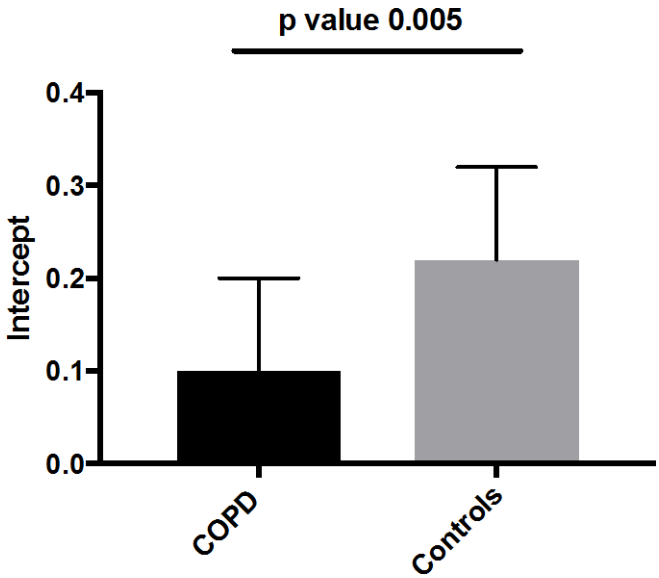


**Fig 3.11: Comparison of Patlak intercept in COPD patients and the controls. (Histograms denote mean and the bars the SEM, p=0.005).**

***Density effect:*** To explore the reason for the higher values of the intercept in healthy controls, I postulated that this may be an effect of lung density since healthy

controls have more lung tissue than COPD patients, who would have variable degrees of emphysema, resulting in higher lung density in the control subjects and hence greater volume of distribution (intercept), therefore resulting in a greater uptake when compared to the COPD patients.

In this context I found a very strong correlation between the CT lung density measurements and the intercept ($R^2$ 0.78, p value 0.01) (Figure 3.12a).

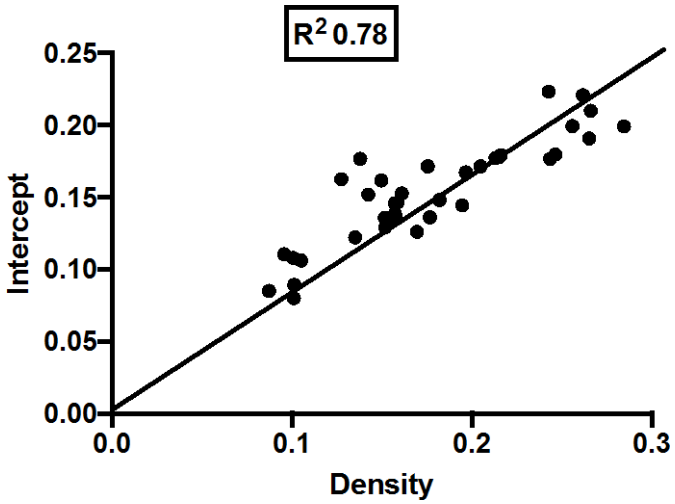


**Fig 3.12a: Shows good correlation between Patlak intercept and CT lung density ($R^2$ value 0.78, p=0.01).**

Since there was a very good correlation between the intercept and lung density, it would seem appropriate to correct for lung density with a view to potentially improve the inflammatory signal. One way of doing this would be to divide the slope by the intercept to generate a corrected Ki.

I also investigated the relationship between slope/intercept with lung CT density and found no significant correlation (Figure 3.12b, $R^2$ =0.19, p value 0.68) suggesting that this index perhaps corrects for the lung density effect (as measured on CT) at least to an extent.

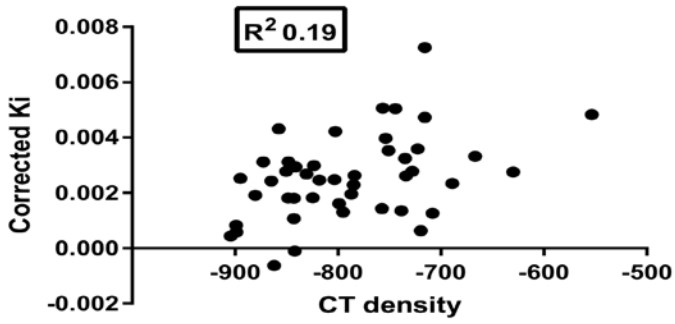


**Figure 3.12b: shows poor correlation between CT lung density and slope/intercept ($R^2$ 0.19, p=0.68).**

### 3.5.2 Comparison of slope/intercept between COPD and controls

A comparison was also therefore made between the COPD and the controls for this corrected Ki value (slope/intercept).

Figure 3.13 shows the results of slope divided by intercept, which showed no difference between the groups.

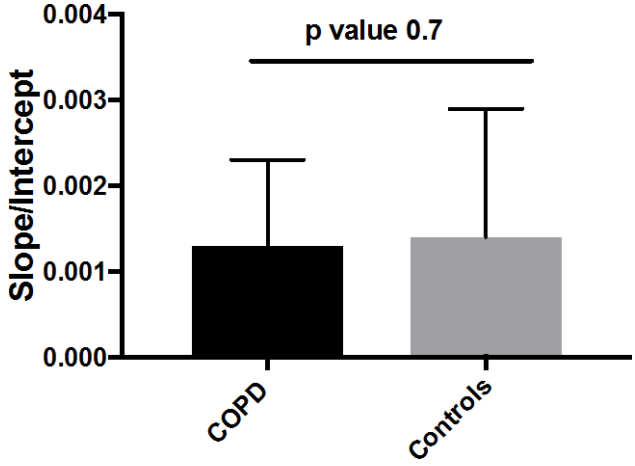


**Figure 3.13: the results of slope divided by intercept for COPD and controls. (Histograms denote mean and the bars the SEM, p=0.7).**

The values were reproducible with all data points within two standard deviations in Bland-Altman plot analysis (Figure 3.14).

Figure 3.15 shows the mean plus SEM data for slopes divided by intercept between visits 1 and 2 of the COPD patients and, although not a measure of reproducibility, the similar results are reassuring to observe.

## Slope/Intercept

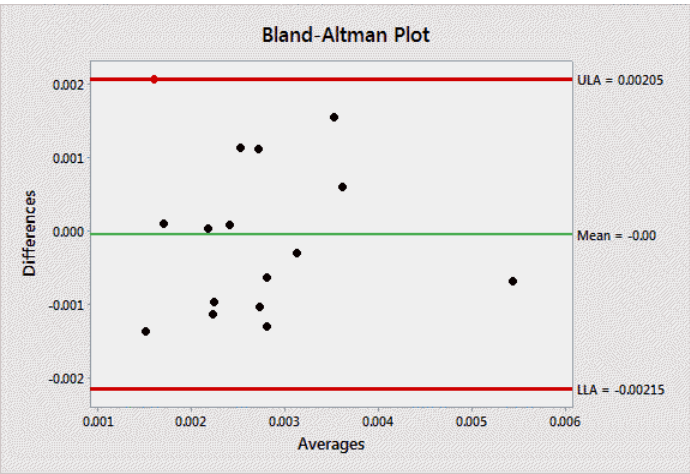


**Figure 3.14: Bland Altman Plot analyses for slope/intercept showing acceptable reproducibility between the two visits.**

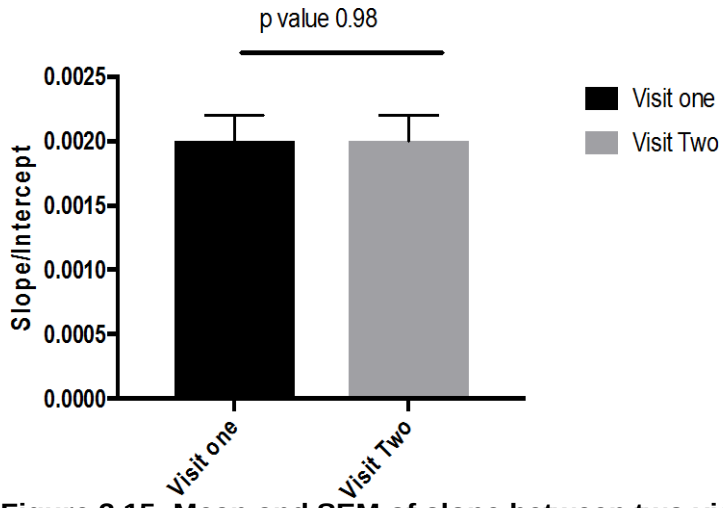


**Figure 3.15: Mean and SEM of slope between two visits of COPD (Histograms denote Mean and the bars the SEM, p=0.98)**

### 3.5.3 Comparison between subgroups of COPD and controls

A sub-analysis was also performed of the slope divided intercept data comparing by groups between the ex-smoker and smoking COPDs and the controls. There was a higher numerical value of slope/intercept in the current smoker COPD subgroup when compared to the others, but this failed to reach statistical significance (p value 0.14). Figure 3.16 summarises these observations.

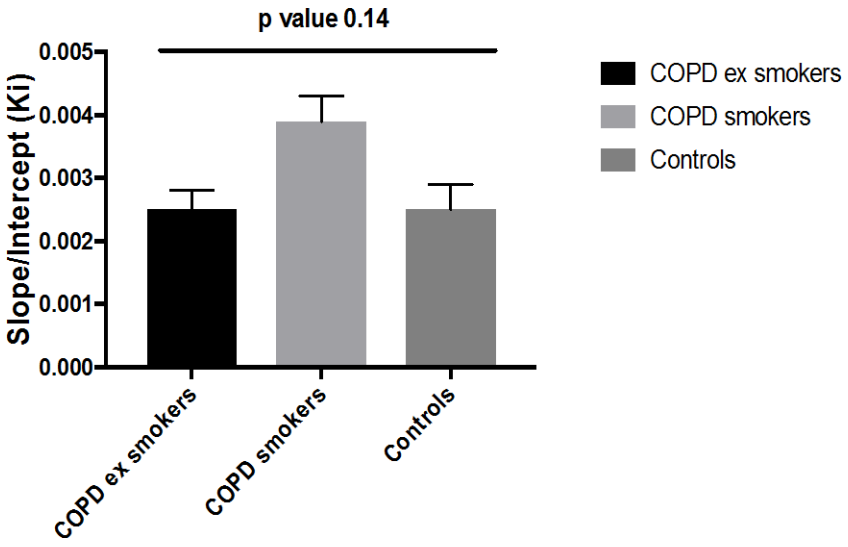


**Figure 3.16: shows comparison of slope/intercept between COPD ex-smokers, smokers and the healthy controls. (Histograms denote Mean and the bars the SEM, p=0.14)**

### 3.5.4 Removal of areas of emphysema

Since areas of emphysema in the lungs of COPD patients would contain little lung tissue, and hence may dilute any inflammatory signal, I also explored the possibility that removal of emphysematous voxels (areas with Hounsfield Units ≤ -950 on a full inspiration CT scan) would improve the signal obtained. This however did not show any difference in the slope between COPD and controls (Figure 3.17).

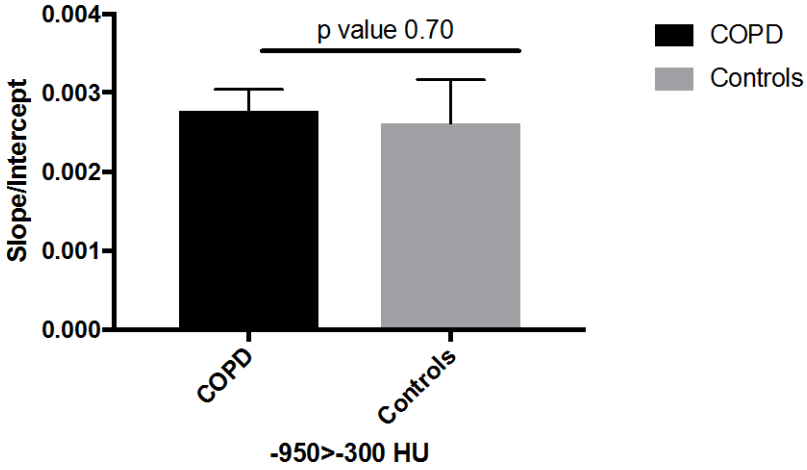


**Figure 3.17: shows the slope divided by intercept corrected for emphysema (areas with Hounsfield Units ≤ -950 on a full inspiration CT scan) between the COPD and the controls. (Histograms denote Mean and the bars the SEM, p=0.70)**

These data were also reproducible with all data points within two standard deviations in B-A analyses as shown in Figure 3.18a. Figure 3.18b shows the mean plus SEM data for this slope divided by intercept corrected for emphysema between visits 1 and 2 of the COPD patients and, although not a measure of reproducibility, these similar results (p value 0.98) are reassuring to observe.

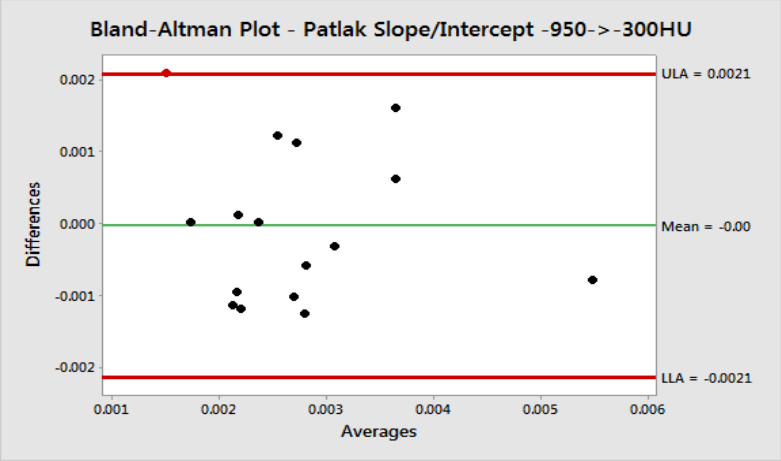


**Figure 3.18a: Bland-Altman plot of the slope divided by intercept corrected for emphysema in COPD patients between visits 1 and 2.**

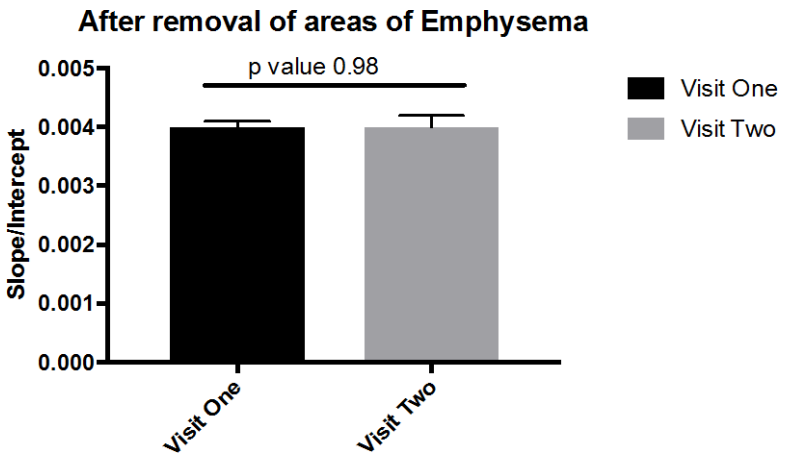


**Figure 3.18b: shows no statistical difference of mean and SEM between the two visits for this data (histograms denote mean and bars the SEM, p=0.98).**

***Comparison of slope/intercept corrected for emphysema between subgroups of COPD and controls:*** The slope/intercept data corrected for emphysema between the subgroups (COPD ex and current smokers and controls) was also assessed and, although higher numerically in COPD current smokers, this difference was not statistically significant (p=0.23) (Figure 3.18c).

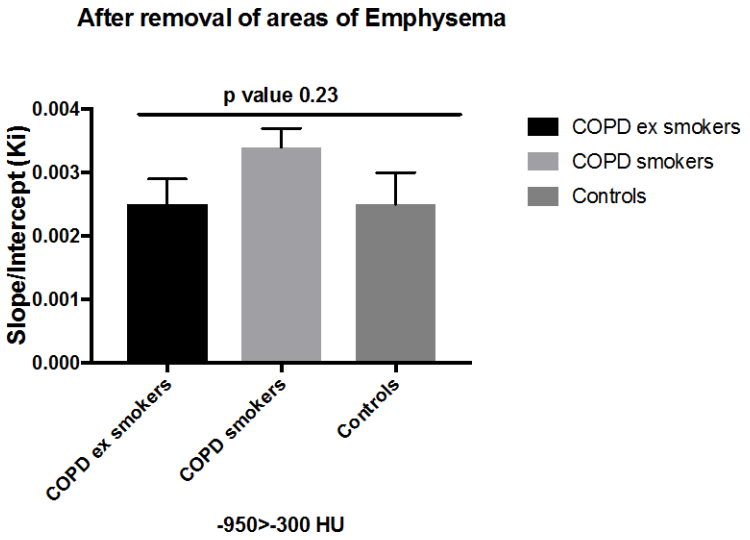


**Fig 3.18c: comparison of slope/intercept corrected for emphysema between COPD ex- smokers, smokers and the healthy controls (Histograms denote Mean and the bars the SEM, p=0.23).**

## 3.6 Lobar data analyses

The lobar variation in Patlak corrected Ki (slope/intercept) was also investigated as a part of this study. Tables 3.4, 3.5 and 3.6 respectively show the mean and SEM values of slope divided intercept (Ki) for the various lobes between COPD (visits 1 and 2) and controls. (Note: RUL = right upper lobe, LUL = left upper lobe, RLL = right lower lobe, LLL = left lower lobe).

**Table 3.4: COPD Visit=1 (Ki values)**

| Variable | Mean | SEM |
|---|---|---|
| RUL LUL RLL LLL | 0.003<br>0.004<br>0.004<br>0.003 | 0.0004<br>0.0006<br>0.0003<br>0.0002 |

**Table 3.5: COPD Visit=2 (Ki values)**

| Variable | Mean | SEM |
|---|---|---|
| RUL LUL RLL LLL | 0.003<br>0.003<br>0.004<br>0.004 | 0.0006<br>0.0007<br>0.0006<br>0.0007 |

**Table 3.6: Controls (Ki values)**

| Variable | Mean | SEM |
|---|---|---|
| RUL LUL RLL LLL | 0.002<br>0.002<br>0.004<br>0.003 | 0.0004<br>0.0005<br>0.0008<br>0.0008 |

The lobar data failed to reach any statistical significance between the two groups, although there was a trend for the upper lobe uptake to be greater in COPD compared with controls.

Figures 3.19 a-d show the comparative lobar data between the COPD and the controls with the corresponding p values.

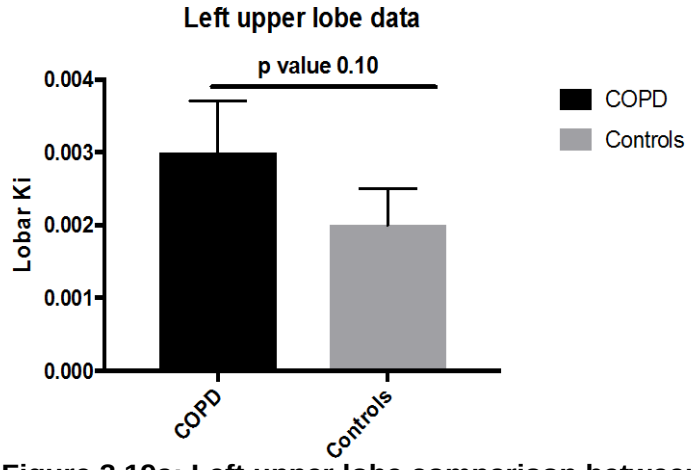


**Figure 3.19a: Left upper lobe comparison between COPD and controls. (Histograms denote Mean and the bars the SEM, p=0.10).**

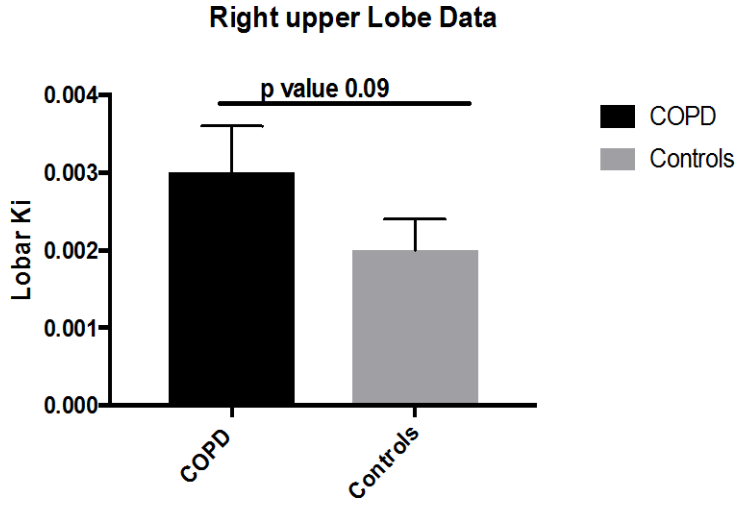


**Figure 3.19b: Right upper lobe comparison between COPD and controls. (Histograms denote Mean and the bars the SEM, p=0.09).**

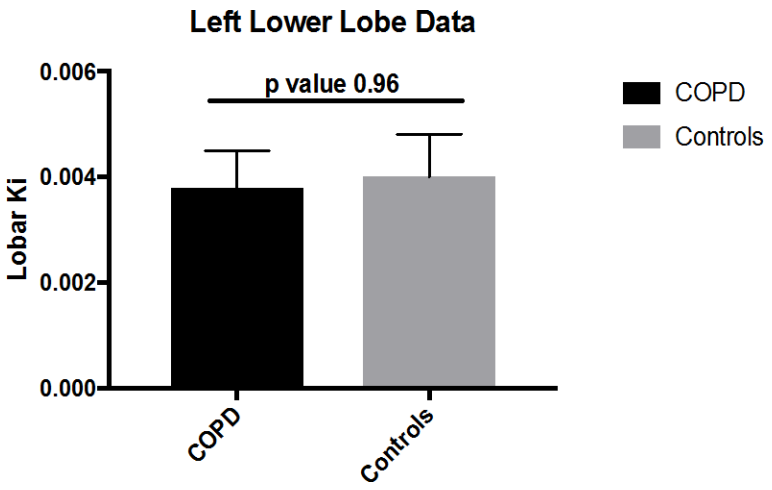


**Figure 3.19c: Left lower lobe comparison between COPD and controls. (Histograms denote Mean and the bars the SEM, p=0.96).**

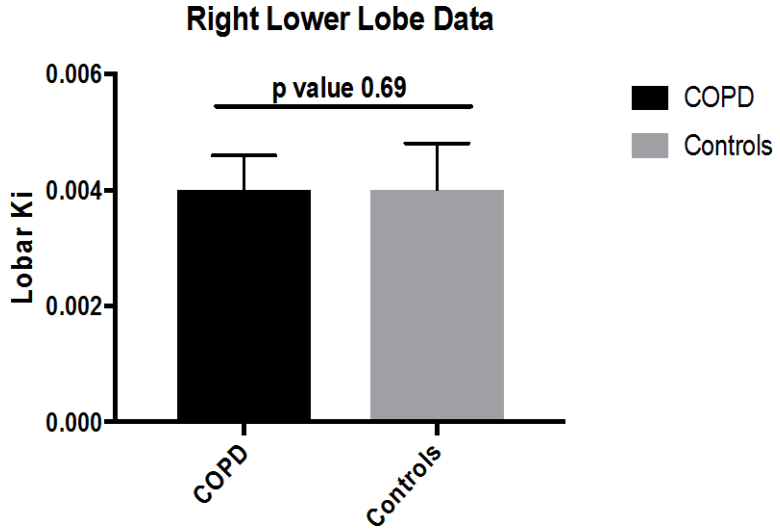


**Figure 3.19d: Right lower lobe comparison between COPD and controls. (Histograms denote Mean and the bars the SEM, p=0.69).**

To summarise, there was no statistically significant difference in the corrected Ki between the COPD and controls in the lobar data analyses. However, the upper lobe in COPD showed a trend to higher values (left upper lobe p value 0.1 and right upper lobe p value 0.09) compared to the lower lobe data when compared to the controls.

### 3.6.1 Lobar data analyses between subgroups of COPD and controls

I also compared the lobar data between the two subgroups of studied COPD patients (smokers and ex-smokers) with the healthy controls. The current smokers had higher numerical readings for all the lobes, more so with the upper lobes, when compared to both the ex-smoker COPD and the controls, but again failed to reach clinical significance (right upper lobe p value 0.14, left upper lobe p value 0.34, right lower lobe p value 0.5, left lower lobe p value 0.6).

Figures 3.20 a-d summarise these observations.

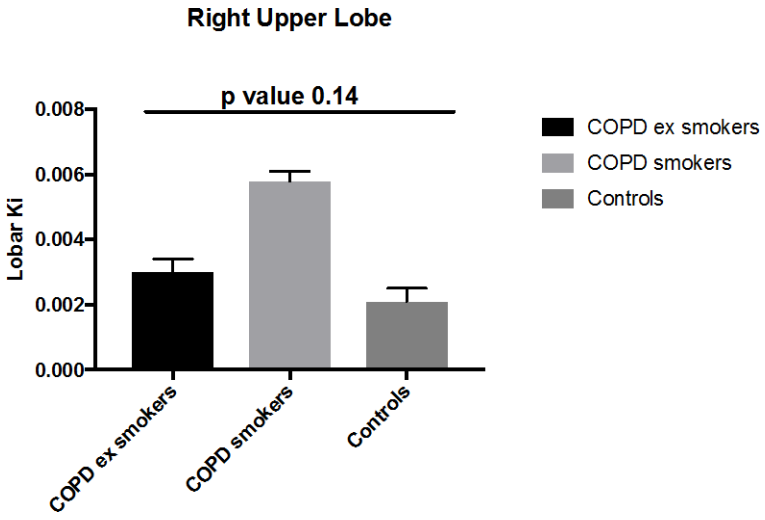


**Fig 3.20a: Comparison of lobar data (right upper lobe) between COPD smokers, ex- smokers and controls (Histograms denote Mean and the bars the SEM, p=0.14).**

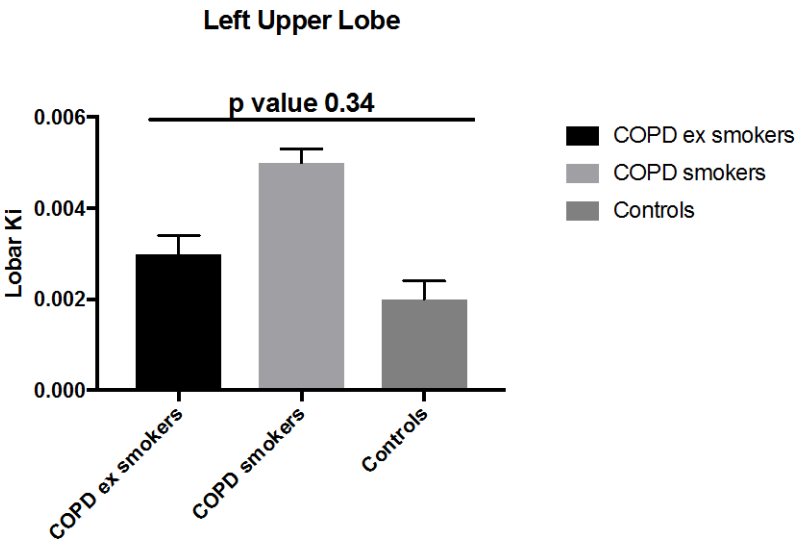


**Fig 3.20b: Comparison of lobar data (left upper lobe) between COPD smokers, ex- smokers and controls (Histograms denote Mean and the bars the SEM, p=0.34).**

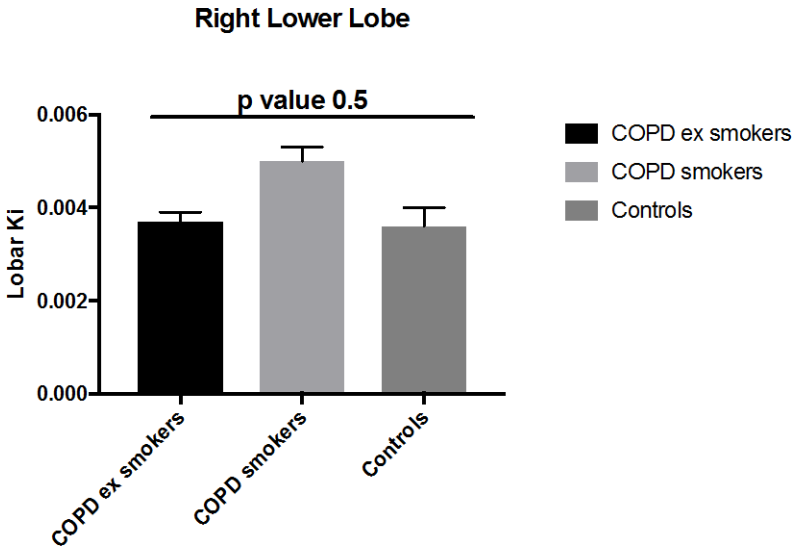


**Fig 3.20c: Comparison of lobar data (right lower lobe) between COPD smokers, ex- smokers and controls (Histograms denote Mean and the bars the SEM, p=0.5).**

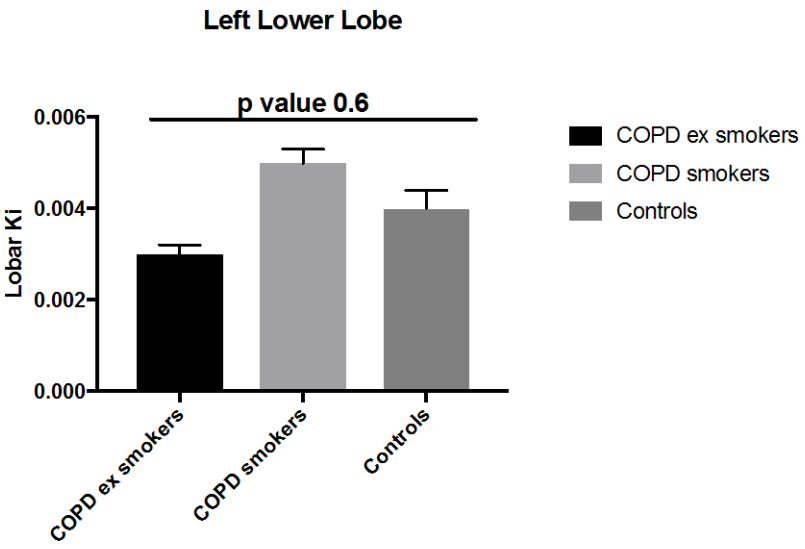


**Fig 3.20d: Comparison of lobar data (left lower lobe) between COPD smokers, ex- smokers and controls (Histograms denote Mean and the bars the SEM, p=0.6)**

## 3.7 Key summary points from the reproducibility and comparative analyses

☐ Patlak analysis of FDG PET scanning of the lung gives a reproducible signal of lung inflammation in COPD patients.

☐ There is a strong relationship between lung density and Patlak intercept, and dividing slope by intercept potentially could be a way to improve the inflammatory signal.

☐ My study however showed no significant difference in these parameters between the COPD and the healthy controls.

☐ The lobar data showed no significant difference either between the COPD and the controls. The upper lobe data uptake was, however, found to be higher but not statistically different in the COPD patients compared to the controls.

☐ Other modes of analysis to correct for the density effect were therefore warranted.

## 3.8 Kinetic modelling analyses

### 3.8.1 Parameters tested with the kinetic modelling

Having established a strong relationship between the FDG uptake in the lungs and lung density with the Patlak analyses, a kinetic modelling analysis (as discussed in the methodology section) was then performed as an alternative way of investigating the data to account for the air fraction (Va) and blood fraction (Vb) components in the estimation of metabolic rate constant Ki.

Table 3.8 summarises the mean and the SEM for the various parameters as measured by the kinetic modelling methods, described in the methods chapter. They are as follows:

**kiAoVb** and **kiPulmVb**: Ki data estimated from aorta (KiAoVb) and pulmonary artery (kiPulmVb) image-derived AIFs using method 1 (Method 1 applies correction factor (1-Vb)/(1-Va-Vb))

**kiAoVbVa** and **kiPulmVbVa**: Ki data estimated from aorta (kiAoVbVa) and pulmonary artery (KiPulmVbVa) image-derived AIFs using method 2 to include air fraction (Va) from CT directly in the kinetic model estimation of blood fraction (Vb) and Ki.

Table 3.7a shows the mean and the SEM for the various parameters as described in the kinetic modelling in COPD (visit 1).

| Variable | Mean | SEM |
|---|---|---|
| **kiAoVb kiAoVbVa** | 0.008 | 0.0007 |
| **kiPulmVb kiPulmVbVa** | 0.008<br>0.008<br>0.008 | 0.0008<br>0.0006<br>0.0007 |

**Table 3.7a: visit 1 COPD (Mean and SEM of kinetic model parameters).**

Table 3.7b shows the mean and the SEM for the various parameters as described in the kinetic modelling in COPD (visit 2).

| Variable | Mean | SEM |
|---|---|---|
| **kiAoVb kiAoVbVa** | 0.008 | 0.0008 |
| **kiPulmVb** | 0.008<br>0.008 | 0.0008<br>0.001 |
| **kiPulmVbVa** | 0.008 | 0.001 |

**Table 3.7b: visit 2 COPD (Mean and SEM of kinetic model parameters).**

Table 3.8 shows the mean and the SEM for the various parameters as described in the kinetic modelling in the healthy controls.

| Variable | Mean | SEM |
|---|---|---|
| **kiAoVb kiAoVbVa** | 0.008 | 0.001 |
| **kiPulmVb** | 0.006<br>0.005 | 0.0009<br>0.0005 |
| **kiPulmVbVa** | 0.005 | 0.0005 |

**Table 3.8: Controls (Mean and SEM of kinetic model parameters).**

### 3.8.2 Comparison of all kinetic model data between the two visits of COPD and reproducibility

All data were reproducible between the two visits for the COPD patients.

***KIAoVb:*** The values were reproducible with all data points within two standard deviations in a Bland-Altman plot analysis (Figure 3.21a). Figure 3.21b shows the mean plus SEM data for KiAoVb between visits 1 and 2 of the COPD patients and, although not a measure of reproducibility, the similar results are reassuring to observe.

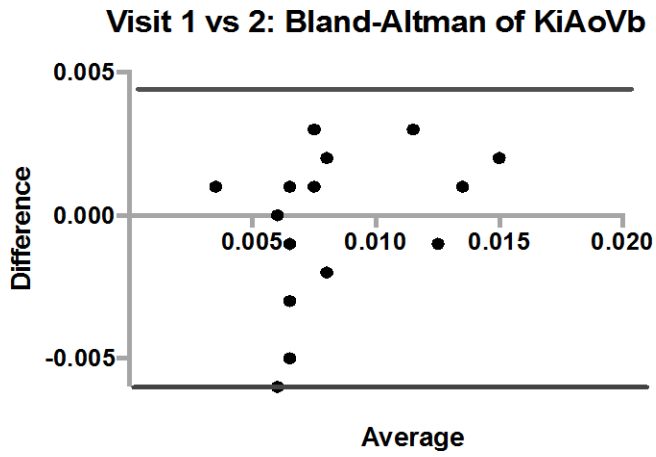


**Figure 3.21a: Bland-Altman plot of KiAoVb in COPD patients between visits 1 and 2.**

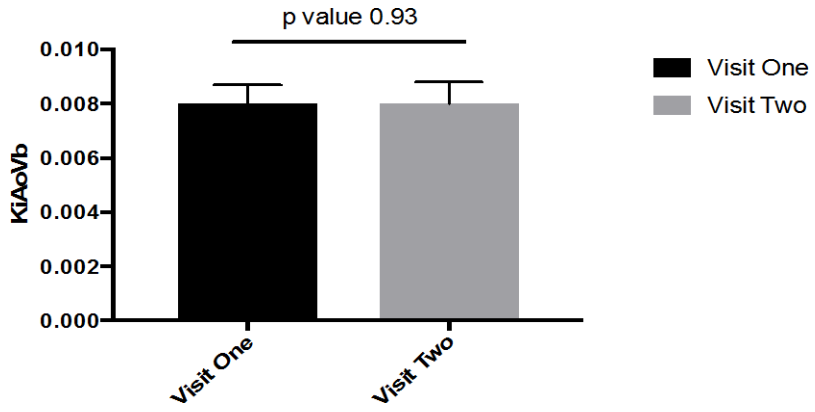

**Figure 3.21b: shows no statistical difference of mean and SEM between the two visits for this data (histograms denote mean and bars the SEM, p=0.93).**

***KiPulmVb:*** The values were reproducible with all data points within two standard deviations in a Bland-Altman plot analysis (Figure 3.21c). Figure 3.21d shows the mean plus SEM data for KiPulmVb ((Ki corrected for Vb and Va retrospectively based on pulmonary artery image-derived AIF) between visits 1 and 2 of the COPD patients and, although not a measure of reproducibility, the similar results are reassuring to observe.

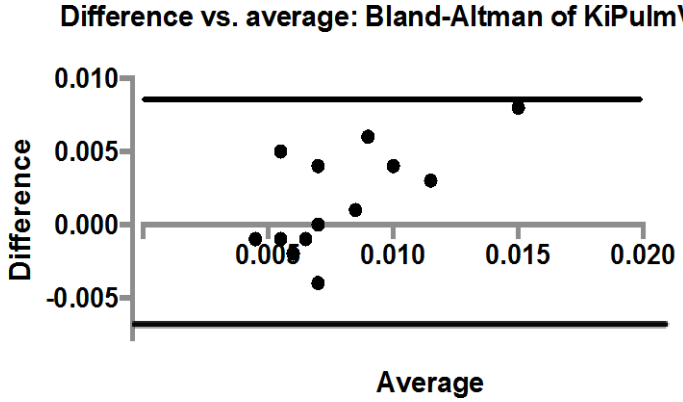


**Figure 3.21c: Bland-Altman plot of KiPulmVb in COPD patients between visits 1 and 2.**

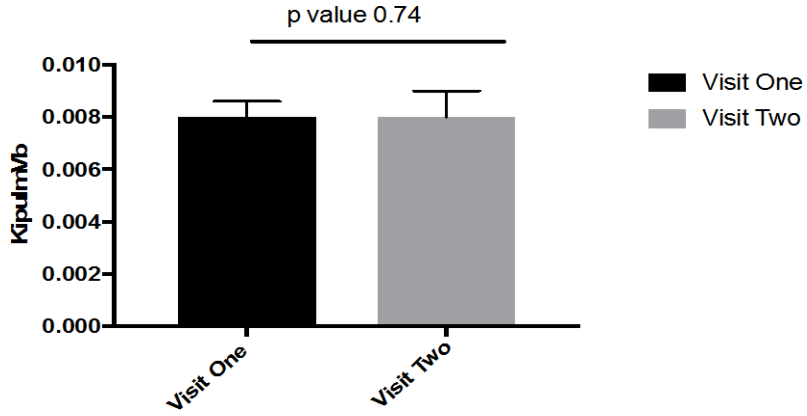


**Figure 3.21d: shows no statistical difference of mean and SEM between the two visits for this data (histograms denote mean and bars the SEM, p=0.74).**

***KiAoVbVa:*** The values were reproducible for KiAoVbVa with almost all data points within two standard deviations in a Bland-Altman plot analysis (Figure 3.21e).

Figure 3.21f shows the mean plus SEM data for KiAoVbVa (based on aortic image derived AIF) between visits 1 and 2 of the COPD patients and, although not a measure of reproducibility, the similar results are reassuring to observe.

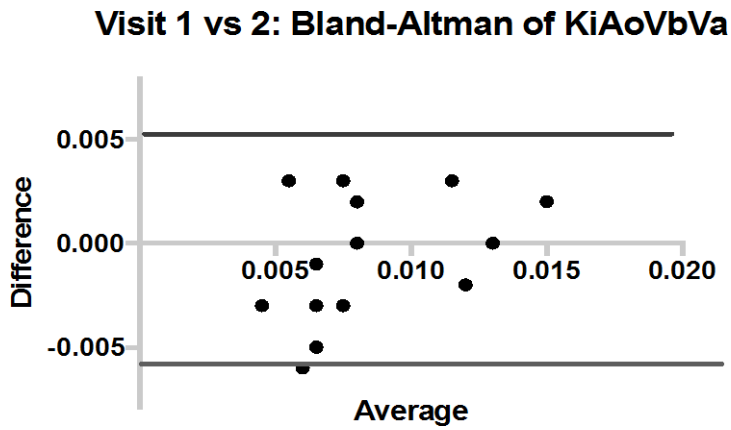


**Figure 3.21e: Bland-Altman plot of KiAoVbVa in COPD patients between visits 1 and 2.**

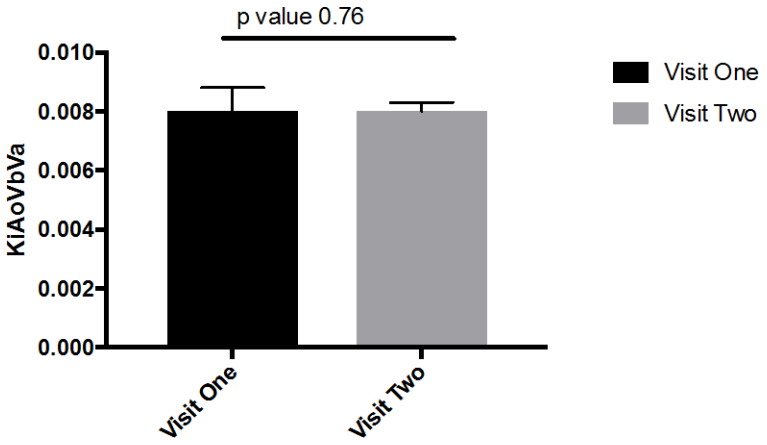


**Figure 3.21f: shows no statistical difference of mean and SEM between the two visits for this data (histograms denote mean and bars the SEM, p value 0.76).**

**KipulmVbVa:** The values were reproducible for KiPulmVbVa with all data points within two standard deviations in Bland-Altman plot analysis (Figure 3.21g). Figure 3.21h shows the mean plus SEM data for KiPulmVbVa (based on pulmonary artery image derived AIF) between visits 1 and 2 of the COPD patients and, although not a measure of reproducibility, the similar results are reassuring to observe.

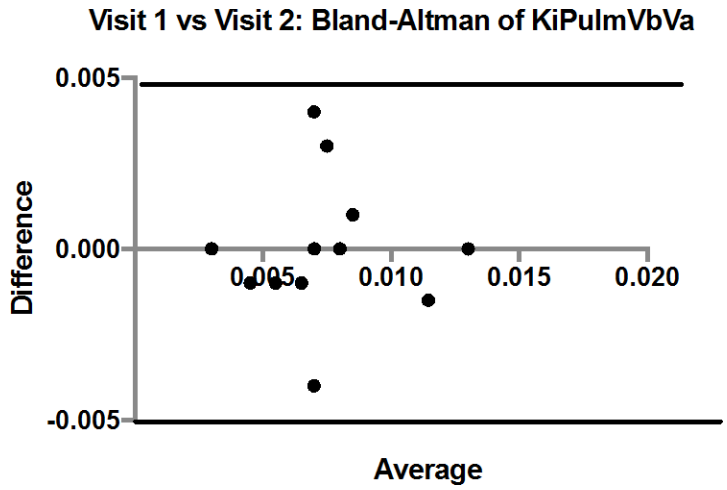


**Figure 3.21g: Bland-Altman plot of KiPulmVbVa in COPD patients between visits 1 and 2.**

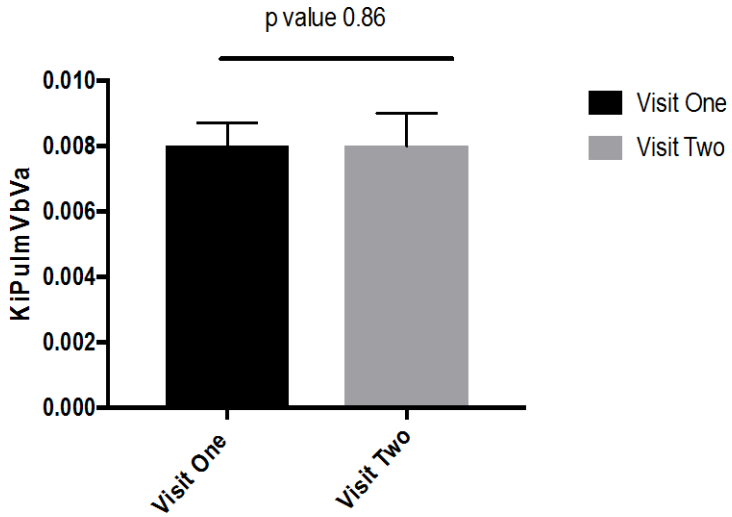


**Figure 3.21h: shows no statistical difference of mean and SEM between the two visits for this data (histograms denote mean and bars the SEM, p=0.86).**

### 3.8.3 Comparison of kinetic modelling data between the COPD and healthy controls

There was no statistical significance between the COPD as a whole group and the controls for **KiAoVb and KiAoVbVa** parameters. However, the parameters **KipulmVb** showed statistically significantly higher values in the COPD patients compared to controls (p value of 0.04), and the difference between COPD and controls just failed to reach statistical significance for **KiPulmVbVa** (p value 0.08).

These results are summarised in Figures 3.22 a-d.

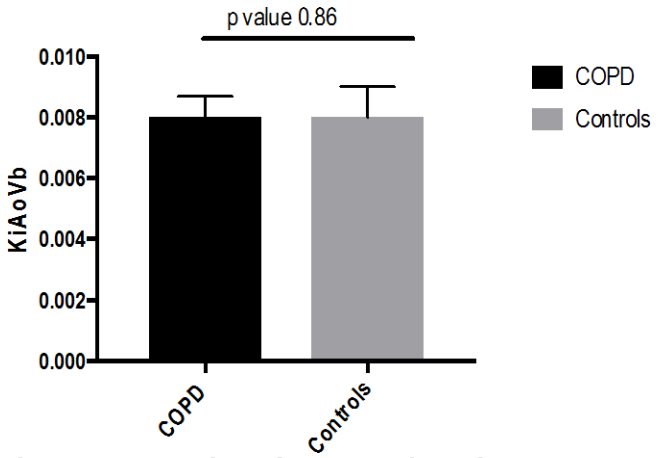


**Figure 3.22a: KiAoVb comparison between COPD and controls (Histograms denote Mean and the bars the SEM, p=0.86).**

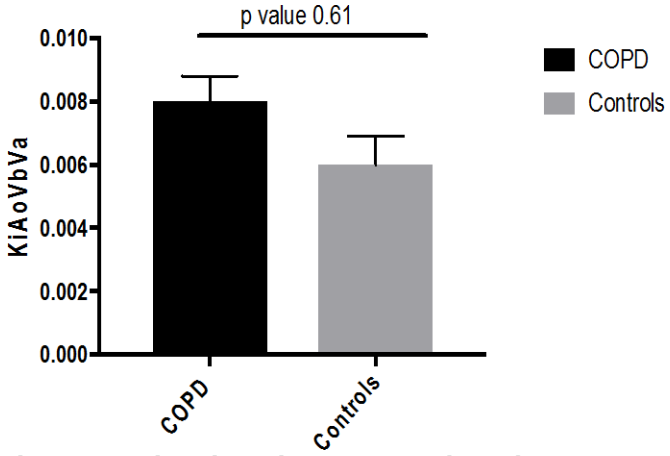


**Figure 3.22b: KiAoVbVa comparison between COPD and controls (Histograms denote Mean and the bars the SEM, p=0.61).**

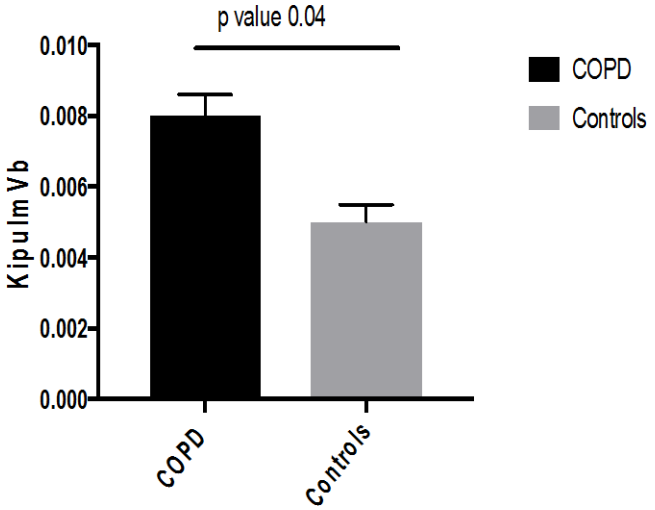


**Figure 3.22c: KiPulmVb: comparison between COPD and Controls. (Histograms denote Mean and the bars the SEM, p=0.04).**

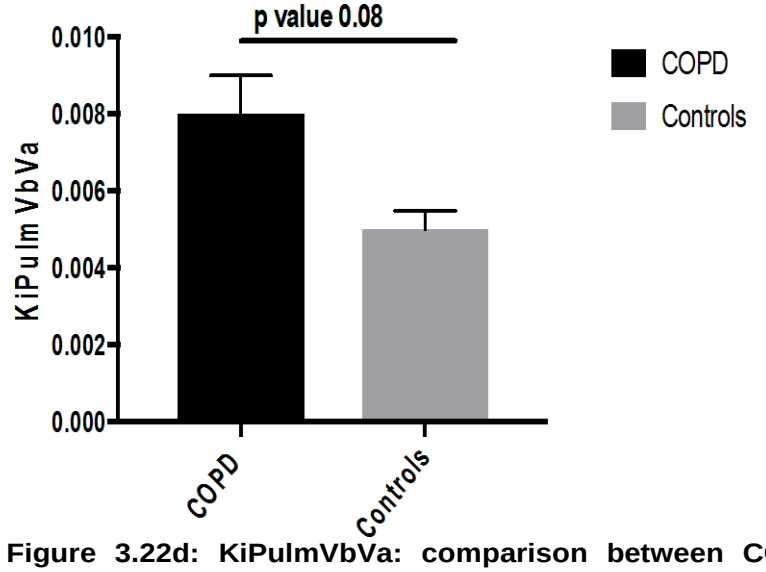


**Figure 3.22d: KiPulmVbVa: comparison between COPD and the controls. (Histograms denote Mean and the bars the SEM, p=0.08).**

### 3.8.4 Comparison between subgroups of COPD and controls

Similar results were also obtained for KiPumVb and KiPulmVbVa when the COPD group was subdivided according to their smoking status, with higher inflammation observed in the smoking COPD patients. KiAoVb and KiAoVbVa showed a trend

to higher values in the smoking COPD patients, which just failed to reach statistical significance. (Table 3.9 and Figures 3.23 a-c summarise these observations). A post hoc analyses using KiPulmVb also showed significant differences between the smoker COPD patients and the controls (p=0.01) [Figure 3.23c].

| Parameters | COPD ex-smoker (mean ± SEM) | COPD current smoker (mean ± SEM) | Controls (mean ± SEM) | p value |
|---|---|---|---|---|
| **kiAovb** | 0.008 ±0.0002 | 0.013±0.0003 | 0.008±0.0001 | 0.06 |
| **KiAoVbVa** | 0.007±0.0009 | 0.013±0.0003 | 0.007±0.0006 | 0.07 |
| **KiPulmVb** | 0.008±0.0001 | 0.010±0.0001 | 0.006±0.0004 | 0.04 |
| **KiPulmVbVa** | 0.007±0.0006 | 0.010±0.0001 | 0.006±0.0004 | 0.06 |

**Table 3.9 shows the summary of the results between COPD smokers, ex-smokers and the controls.**

Figures 3.23 a, b, c and d show the results for the parameters in the compartmental analysis in COPD ex-smokers, COPD smokers and the healthy controls.

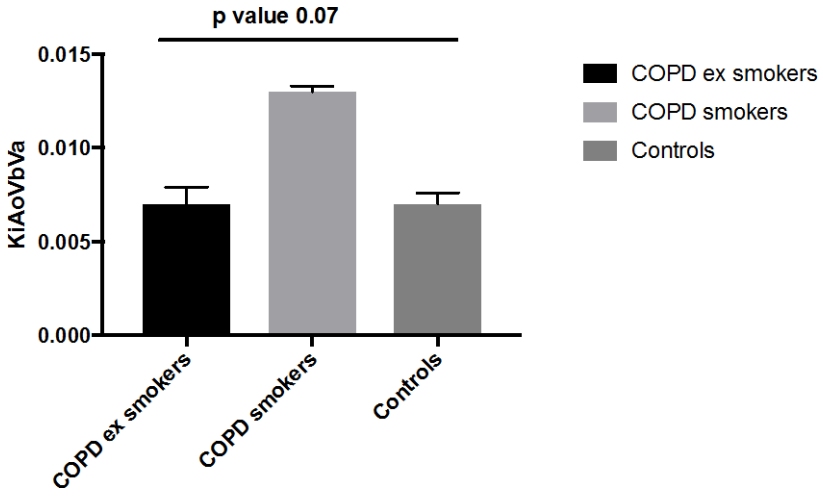


**Figure 3.23a: KiAoVbVa between the three groups (histograms denote the mean and the bars the SEM, p=0.07)**

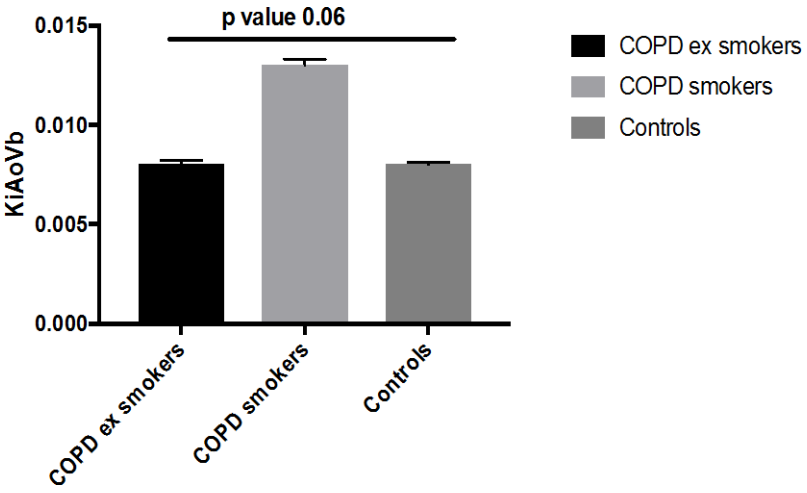


**Figure 3.23b: KiAoVb between the three groups (histograms denote the mean and the bars the SEM, p value 0.06).**

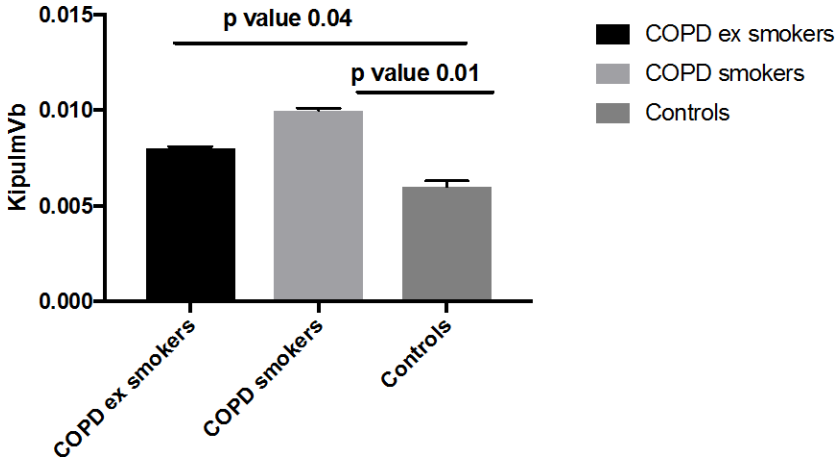


**Figure 3.23c: KiPulmVb between the three groups (histograms denote the mean and the bars the SEM, p=0.04, comparsion between COPD smokers and the controls show a p=0.01).**

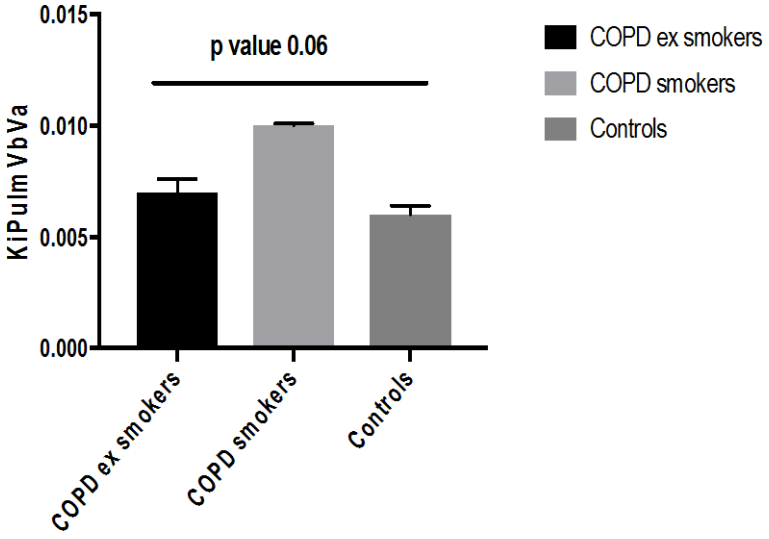


**Figure 3.23d: KiPulmVbVa between the three groups (histograms denote the mean and the bars the SEM, p=0.06).**

### 3.8.5 Correlation of kinetic marker of inflammation with other variables

From the above results, given that KiPulmVb was the parameter that demonstrated most significant difference between COPD (smokers and ex-smokers) compared with controls, I chose this parameter to explore possible correlations with clinical parameters ($FEV_1$, $FEV_1$pp, FVC, FVCpp, $FEV_1$/FVC ratio, St George's questionnaire score, CAT score, MRC score), and markers of inflammation (neutrophil count, MPO, IL8, A2MG, IL6, WBC, CRP and fibrinogen) in COPD patients.

Using Pearsons Correlations Coefficient analysis ***no significant correlations*** were however shown between KiPulmVb and any of these combined groups of COPD and controls (Tables 3.10 and 3.11), or in COPD patients alone (Tables 3.12 a and b).

| | $FEV_1$ | $FEV_1$pp | FVC | FVCpp | $FEV_1$/FVC | SGRQ | CAT | mMRC |
|---|---|---|---|---|---|---|---|---|
| R value | -0.20 | -0.27 | 0.23 | 0.15 | -0.12 | 0.11 | 0.19 | 0.09 |
| p value | 0.29 | 0.15 | 0.22 | 0.43 | 0.53 | 0.56 | 0.32 | 0.64 |
| N = | 26 | 26 | 26 | 26 | 26 | 26 | 26 | 26 |

**Table 3.10: Correlations of KiPulmVb with clinical variables in the combined COPD and control group**

| | IL8 | A2MG | IL6 | WBC | CRP | Fib | MPO |
|---|---|---|---|---|---|---|---|
| R value | -0.11 | 0.16 | -0.13 | 0.29 | -0.15 | -0.12 | -0.13 |
| p value | 0.57 | 0.41 | 0.52 | 0.13 | 0.43 | 0.52 | 0.52 |
| N = | 26 | 26 | 26 | 26 | 26 | 26 | 26 |

**Table 3.11: Correlation of KiPulmVb with markers of inflammation (all serum samples) in combined COPD and control groups.**

Tables 3.12a and b show no significant correlations of KipulmVb with the various clinical parameters and inflammatory markers respectively in the COPD patients.

| | $FEV_1$ | $FEV_1$pp | FVC | FVCpp | $FEV_1$/FVC | SGRQ | CAT | mMRC |
|---|---|---|---|---|---|---|---|---|
| R value | 0.07 | -0.05 | 0.35 | 0.26 | -0.18 | -0.22 | -0.06 | -0.18 |
| p value | 0.72 | 0.79 | 0.09 | 0.21 | 0.39 | 0.30 | 0.75 | 0.39 |
| N = | 20 | 20 | 20 | 20 | 20 | 20 | 20 | 20 |

**Table 3.12a Correlation of KiPulmVb with various clinical parameters in COPD patients.**

| Pearson correlation coefficients of KiPulmVb with the various blood inflammatory markers in COPD patients | | | | | | | |
|---|---|---|---|---|---|---|---|
| | MPO | IL8 | A2MG | IL6 | WBC | CRP | Fibrinogen |
| R value | -0.17 | -0.14 | 0.13 | -0.14 | 0.26 | -0.19 | -0.21 |
| p value | 0.42 | 0.51 | 0.53 | 0.49 | 0.22 | 0.38 | 0.32 |
| N = | 20 | 20 | 20 | 20 | 20 | 20 | 20 |

**Table 3.12b: Correlation of KiPulmVb with markers of inflammation (all serum samples) in the COPD group.**

In seven COPD patients who managed to provide us with an induced sputum sample, I measured markers of inflammation (sputum MPO, IL8, A2MG, IL6 and neutrophil count) and found no significant correlation with KiPulmVb (Table 3.13).

| Pearson correlation coefficients of KiPulmVb with the various cytokines from the induced sputum in COPD | | | | | |
|---|---|---|---|---|---|
| | **MPO** | **IL8** | **A2MG** | **IL6** | **WBC** |
| R value | -0.02 | 0.33 | 0.27 | 0.66 | 0.09 |
| p value | 0.96 | 0.46 | 0.54 | 0.10 | 0.83 |
| N = | 7 | 7 | 7 | 7 | 7 |

**Table 3.13: Correlation of KiPulmVb with markers of inflammation in the sputum of COPD patients.**

## 3.9 Key summary points from the kinetic modelling analysis

☐ The data between both the visits for the COPD patients were reproducible.

☐ Kinetic modelling analysis accounts for both air and blood volume fraction components.

☐ Markers such as KiPulmVb and KiPulmVbVa hold promise to be better indicators of lung inflammation in dynamic FDG PET scanning.

☐ Smokers showed more lung inflammation compared to the non-smokers.

## 3.10 SUV analyses

### 3.10.1 SUV measurement

SUV is a semi-quantitative ratio of tissue radioactivity ([$^{18}$F FDG uptake) within the region of interest to the injected tracer activity, adjusted for body weight and the dose of the FDG injected.

### 3.10.2 Reproducibility

SUVmax measured, as an index of SUV measurement, was reproducible with all data points within two standard deviations in a Bland-Altman plot analysis (Figure 3.24a). Figure 3.24b shows the mean plus SEM data for SUVmax between visits 1 and 2 of the COPD patients and, although not a measure of reproducibility, the similar results are reassuring to observe.

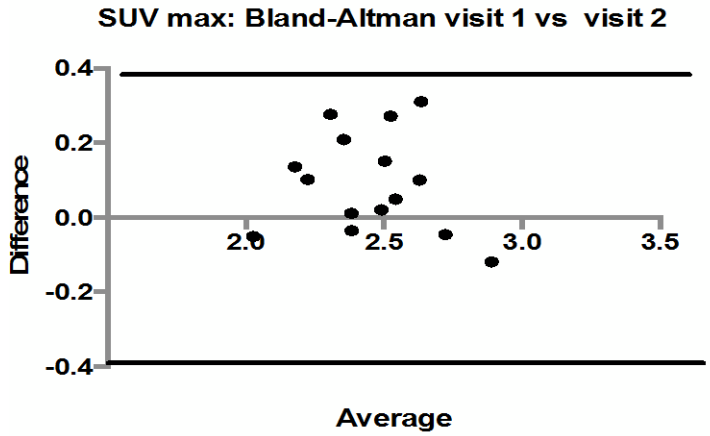


**Fig 3.24a: Bland Altman plot comparing SUV max between the two visits.**

Figure 3.24b shows the histograms of mean +SEM for the SUVmax between the 2 visits with non-significant difference (p=0.25).

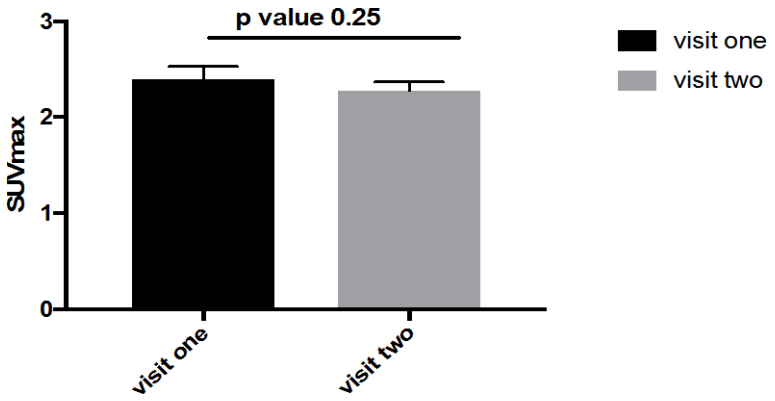


**Figure 3.24b: SUVmax in visit 1 and 2 in COPD patients (Histograms denote Mean and the bars the SEM, p value 0.25).**

### 3.10.3 Correlation with lung density

A good correlation was noted between the SUV max and lung density from full inspiratory CT scan (Figure 3.25) similar to results from the Patlak analyses (R2 0.76, p=0.05).

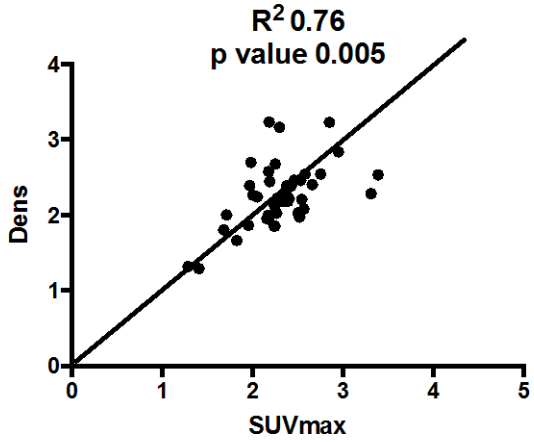


**Fig 3.25: Relationship between SUVmax and the CT lung density ($R^2$ 0.76, p=0.05).**

The SUVmax corrected for density was therefore also calculated. Table 3.14a and 3.14b show the mean and the SEM results for SUV max, as well as SUVmax corrected for density for the COPD patients between visit 1 and 2 respectively.

**COPD Visit=1**

| Variable | Mean | SEM | N |
|---|---|---|---|
| SUV Max | 2.399 | 0.01 | 25 |
| SUVcorrDENS | 2.246 | 0.09 | 25 |

**COPD Visit=2**

| Variable | Mean | SEM | N |
|---|---|---|---|
| SUV Max | 2.280 | 0.08 | 18 |
| SUVcorrDENS | 2.291 | 0.09 | 18 |

**Table 3.14a and 3.14b**

### 3.10.4 Comparison between COPD and the controls

Table 3.15a and 3.15b show the mean and the SEM for the SUVmax and SUVmax corrected for density between the COPD patients and the controls.

**COPD**

| Variable | Mean | SEM | N |
|---|---|---|---|
| SUV Max | 2.280 | 0.08 | 18 |
| SUVcorrDENS | 2.291 | 0.09 | 18 |

**Table 3.15a**

**Group=Control**

| Variable | Mean | SEM | N |
|---|---|---|---|
| Max | 2.084 | 0.05 | 6 |
| SUVcorrDENS | 1.943 | 0.03 | 6 |

**Table 3.15b**

There was however no significant difference between the COPD and the controls using SUVmax as the index of measurement. Figure 3.26 depicts this finding (p value 0.16).

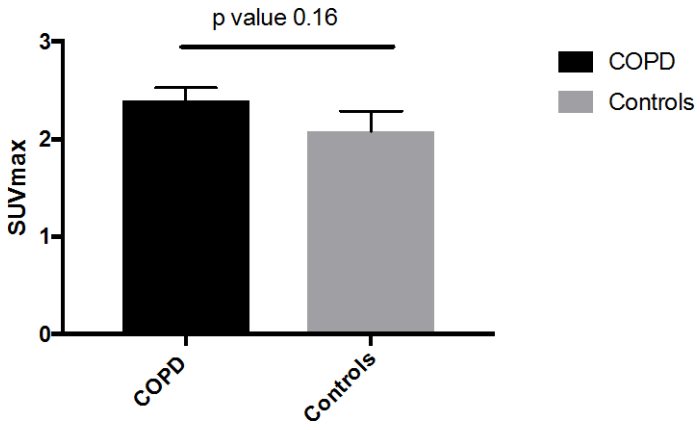


**Figure 3.26: shows no statistically significant difference in SUVmax between the COPD and the healthy controls (Histograms denote the mean and the bars the SEM, p=0.16).**

The SUV max corrected for density showed higher numerical values in COPD than controls, although this difference just failed to reach statistical significances (p value 0.05). Figure 3.27 summarises these findings.

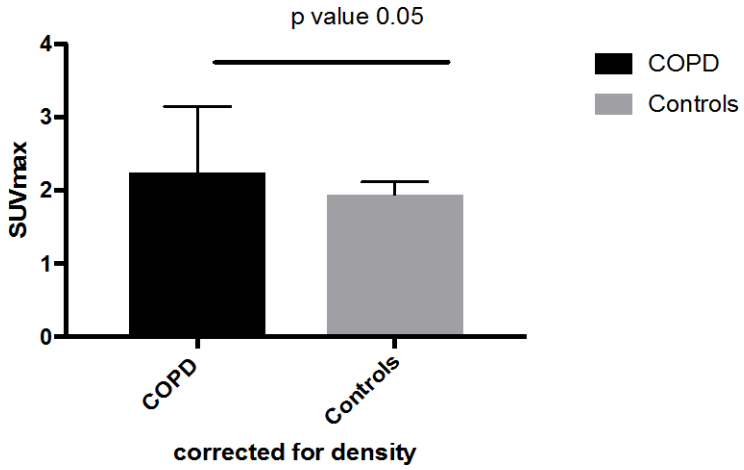


**Figure 3.27: SUVmax corrected for density shows higher value in COPD compared to controls (histograms denote the mean and the bars the SEM, p=0.05).**

### 3.10.5 SUV using kinetic modelling correction

I also assessed the SUV after correcting for air and blood fraction based on the aorta using the kinetic model analyses (applying a 1-Va-Vb correction), and found the

corrected SUV max was significantly higher in the COPD patients compared to the healthy controls (p value 0.04). Figure 3.28 summarises this observation.

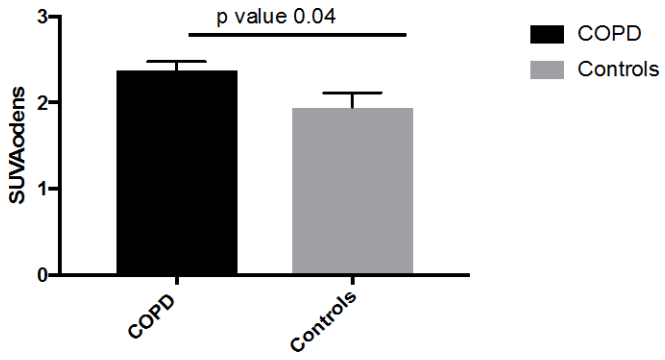


**Figure 3.28: SUV corrected for density using kinetic modelling analyses in COPD and controls (Histograms denote Mean and the bars the SEM, p=0.04).**

## 3.11 Key summary points of SUV analyses

☐ Lung SUVmax was reproducible between visits 1 and 2 in the COPD patients.

☐ When corrected for lung density SUVmax shows differences between COPD and controls and could be a potential marker of lung inflammation in COPD patients.

## 3.12 Assessment of vascular inflammation

### 3.12.1 Assessment of vascular inflammation

Vascular inflammation in the aorta was also assessed in the COPD patients and the healthy controls using combined $^{18}$F-FDG PET/CT scan technique as a sub study. Since these analyses needed only static PET scan data, I also included data from 10 ex-smokers with normal spirometry who had undertaken a previous PET scan.

Aortic $^{18}$F-FDG uptake was measured as maximum standardised uptake value (SUV). Emphysema as before was expressed as % of low attenuation areas with HU of less than −950 within both lungs.

Table 3.16 shows the characteristics for these groups.

| Parameters | COPD patients (n=24) | Healthy volunteers (n=8) | Ex-smokers (n=10) |
|---|---|---|---|
| **Age (years)** | 66.4 ± 7.5 | 59.7 ± 12.8 | 61.6 ± 5.5 |
| **Sex (M: F)** | 18: 6 | 4: 4 | 6: 4 |
| **Smoking history (pack years)** | 39.0 ± 7.1 | 0 | 32.8 ± 19.6 |
| **FEV1 (% predicted)** | 48.4 ± 16.5 | 104.5 ± 17.5 | 97.3 ± 17.6 |
| **Emphysema ((% < -950HU)** | 13.9 ± 13.0 | 0.66 ± 0.6 | 2.4 ± 4.7 |

**Table 3.16 shows the important characteristics in the three groups.**

### 3.12.2 Reproducibility between the two visits for COPD patients

Figure 3.29a shows reproducibility of aortic arch SUVmax between visits 1 and 2 for the COPD patients with most data points within two standard deviations in a Bland-Altman plot analysis.

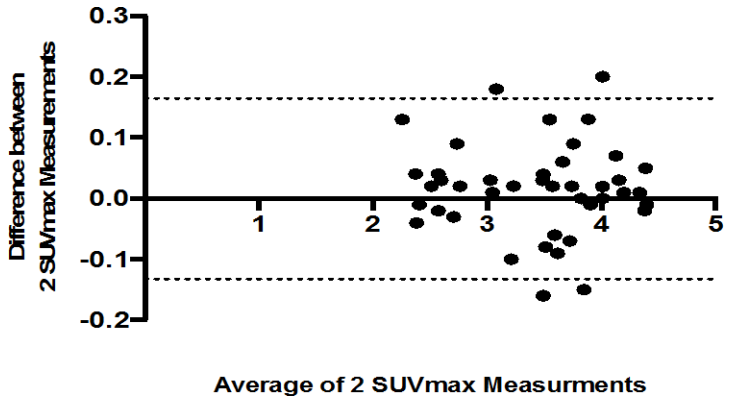


**Figure 3.29a: shows good reproducibility of mean SUVmax (Aortic arch) between the two visits.**

Figure 3.29b shows reproducibility between visits 1 and 2 for the COPD patients in respect of SUV max from ascending aorta with most data points within two standard deviations in a Bland-Altman plot analysis.

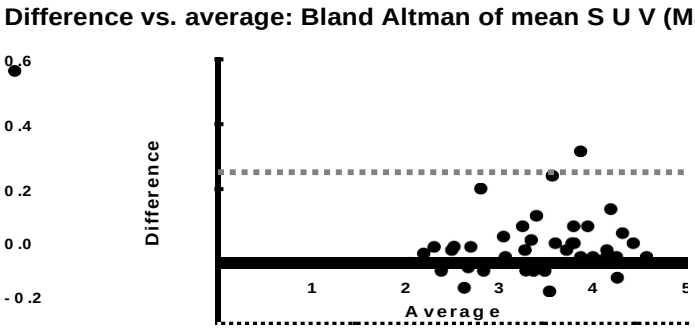


**Figure 3.29b**: **shows good reproducibility of mean SUVmax AA (Ascending aorta) between the two visits.**

Figure 3.29c shows reproducibility between visits 1 and 2 for the COPD patients in respect of SUV max from descending arch with most data points within two standard deviations in a Bland-Altman plot analysis.

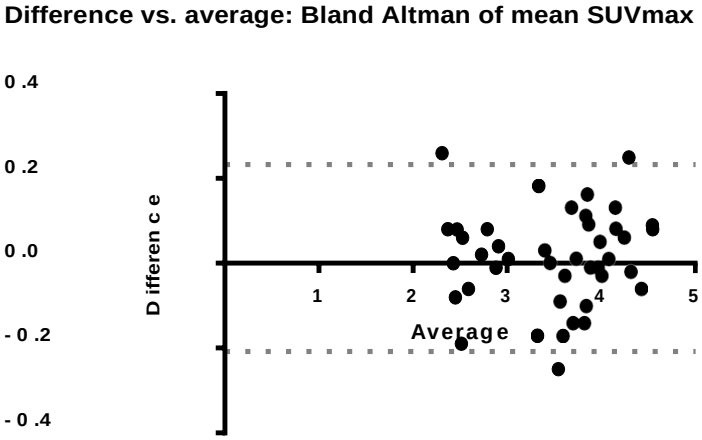


**Figure 3.29c: shows good reproducibility of Mean SUV (max) of DA (SUV of Descending Aorta).**

Figure 3.29d shows acceptable reproducibility of the TBR data as well between the two visits of the COPD patients with most data points within two standard deviations in a Bland-Altman plot analysis.

**Difference vs. average: Bland Altman of mean TBR Aorta**

**Figure 3.29d: reproducibility of mean TBR between two visits of COPD patients.**

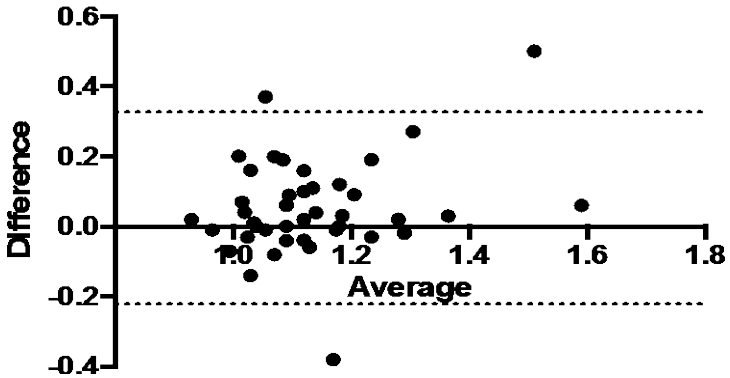


### 3.12.3 Comparison between COPD and the controls

Aortic maximum SUV (SUVmax) [mean±SEM] was significantly higher in COPD patients (3.77 ± 0.30), compared with healthy volunteers (3.25 ± 0.45) and ex-smokers (2.81 ± 0.34) with a p value of <0.05 (Figure 3.30a).

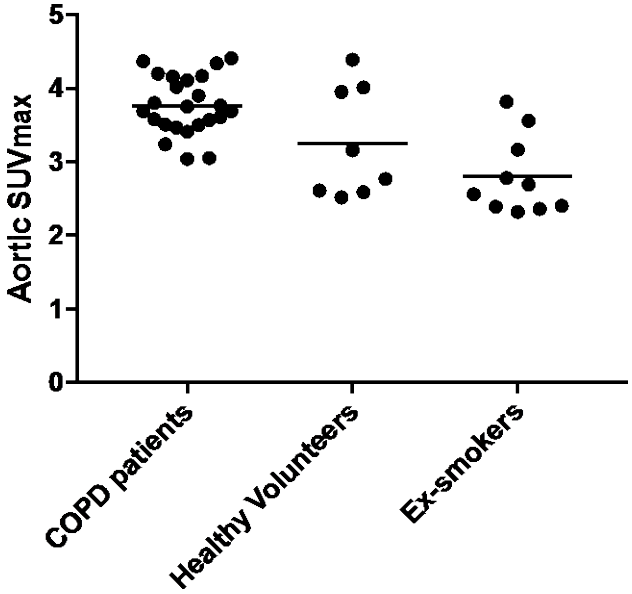


**Figure 3.30a: Aortic maximum SUV (SUVmax) was significantly higher in COPD patients compared to the controls (ex- and non-smokers) (p<0.001).**

However, when assessed with the Mean and Max Target to Background ratio (TBR) as the other index of measuring vascular inflammation, there were no significant differences between the COPD and the healthy controls groups for all. Mean TBR COPD (1.17 ± 0.20), Mean TBR Healthy Volunteers (1.133 ± 0.12) and Mean TBR Ex- smokers (1.152 ± 0.1) (mean ± SEM) with a p value of 0.85 (Figure 3.30b).

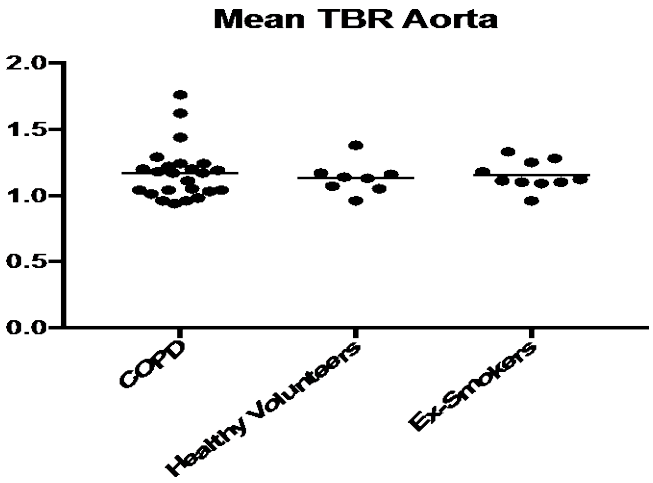


**Figure 3.30b: Mean TBR values between COPD and the controls (p=0.85).**

### 3.12.4 Correlations of SUV max aortic arch (SUVmax and TBR with clinical parameters (in COPD patients)

Positive correlations were observed in the COPD patients with these following markers.

☐ **St George's Questionnaire:** SUVmax (r = 0.53, p=0.006), TBR (TBR from ascending arch) (r = -0.54, p=0.0058)

☐ **CAT score:** SUVmax (r = 0.56, p=0.0043), TBR (r = 0.44, p=0.02)

☐ **$FEV_1$/FVC Ratio:** SUVmax (r = 0.46, p=0.02), TBR (r = -0.41, p=0.04)

No significant correlations were demonstrated between these indices and other parameters in COPD patients. They are as follows:

- **$FEV_1$:** SUVmax (r=0.12, p=0.56) TBR (r= 0.18, p=0.68)
- **CRP:** SUVmax (r=0.10, p=0.6) TBR (r= 0.11, p=0.7)
- **WCC:** SUVmax (r=0.19, p=0.46) TBR (r= 0.20, p=0.57)
- **Fibrinogen:** SUVmax (r=0.25, p=0.13) TBR (r= 0.28, p=0.18)

### 3.12.5 Correlations in all groups

Further analyses in the combined results of all three groups showed positive correlations with the following variables:

☐ **$FEV_1$:** SUVmax (r = -0.50, p=0.0007)

☐ **FVC:** SUVmax (r = -0.37, p=0.0015)

☐ **$FEV_1$/FVC Ratio:** SUVmax (r = -0.428, p=0.004)

☐ **Smoking:** Emphysema score (r = 0.56, p=0.0002)

☐ **Fibrinogen:** TBR ($r = 0.44$, $p=0.017$)

☐ **Emphysema score** (less than -950 HU): $FEV_1$ ($r = -0.52$, $p=0.0005$), Predicted $FEV_1$ ($r = -0.59$, $p<0.0001$), $FEV_1$/FVC ratio ($r = -0.68$, $p<0.0001$)

## 3.13 Key summary points of vascular analyses

In summary, the SUVmax measurements were reproducible. Aortic maximum SUV (mean±SEM) was significantly higher in COPD patients compared with the healthy volunteers. However, similar results were not elicited when TBR was used as the index of inflammation. $^{18}$F-FDG PET/CT could therefore potentially be a reproducible method for assessing vascular inflammation in COPD patients.

# Chapter 4. Discussion

## 4.1 Significance of dynamic PET/CT scanning

There is a growing body of literature supporting the use of FDG PET imaging to assess the neutrophilic burden in the lungs in a number of pulmonary diseases.

We also know that chronic lung inflammation is a characteristic feature of COPD and involves cells such as neutrophils, macrophages, T lymphocytes and augmented concentrations of inflammatory cytokines, and the resultant neutrophil alveolar infiltration would be expected to be associated with an increased cellular metabolism and glucose consumption, and consequently increase in FDG activity in COPD lungs. Existing evidence also suggests that neutrophils contribute primarily to the increased uptake of $^{18}$F FDG in lung inflammation and that the FDG-PET signal potentially correlates with the presence of activated neutrophils [154, 176].

Further understanding of the mechanisms that lead to increased $^{18}$F FDG uptake using dynamic PET scans in inflammatory conditions would be therefore helpful in interpreting what its uptake means in the context of lung inflammation and consequent potential targeted anti-inflammatory treatment in chronic lung conditions like COPD. This, along with further standardisation of all the methodologies including assessing reproducibility, is crucial to enhance our understanding of this imaging technique, both in clinical practice and for translational research.

The advantages of PET imaging include its non-invasiveness, the opportunity of quantification, and the ability to assess the entire lung as it enables quantification of radioactivity throughout the lungs, in airspaces and interstitium, enabling study of the behaviour of key inflammatory cells in their native micro-environment [176]. Investigation of $^{18}$F FDG uptake in the lungs in diffuse lung diseases such as COPD

may therefore be an important tool in assessing lung inflammation, monitoring disease progression, as well as assessing treatment efficacy.

Some clinical studies have previously used PET to acquire static lung images. In such studies the subject is injected with the radioactive ligand and scanned after it has reached equilibrium in the body, usually after 45-50 minutes. In contrast, dynamic scan starts image acquisition immediately and follows the course of the tracer dynamically. This permits the radiotracer concentration within the body to be observed in real time, and therefore is considered potentially more informative and quantitative [176].

It is well known that pattern and distribution of structural parenchymal abnormalities can be assessed by high resolution CT scanning (HRCT). However, HRCT is a purely structural imaging technique on which only indirect inferences regarding inflammation can be made. PET, on the other hand, potentially offers the ability to noninvasively investigate cellular metabolism in vivo. Combining PET/CT imaging thus has the potential to provide both structural and inflammatory information and provides advances in the field. [176].

### 4.1.1 Evidence so far supporting the use of dynamic PET scanning in lung diseases as a biomarker of lung inflammation

The United States Food and Drug Administration define a biomarker as "a defined characteristic that is measured as an indicator of normal biological processes, pathogenic processes, or responses to an exposure or intervention, including therapeutic interventions" [142, 177]. It is also known that the utility of any imaging biomarker will rely on a number of factors, including its reliability and accuracy in quantifying the process it is intended to measure, its reproducibility within subjects, and its dependence on observer interpretation [142].

Studies have previously shown that positron emission imaging following injection of $^{18}$F-fluorodeoxyglucose could be used to monitor neutrophil metabolic activity in vivo [154] and have also shown marked increase in FDG uptake in the lungs in animal models of pneumonia [178]. An in vitro study has previously also shown that the uptake of deoxyglucose by neutrophils reflects both priming and activation of the cell [179]. The sustained neutrophil presence and activation in lung inflammation [154] is likely to be orchestrated by alveolar and interstitial macrophages. Accumulation of macrophages can also be measured noninvasively by PET imaging of 11C-labelled PK11195 (a ligand that binds specifically in macrophages) and increased lung uptake, as has previously been demonstrated in rabbit lungs in response to particulate challenge [180]. There is also evidence that chronic activation of neutrophils is associated with the development of pulmonary fibrosis [181]. Studies have also shown that there was an increase in the radiotracer concentration of FDG in regions of increased lung fibrosis in idiopathic pulmonary fibrosis (IPF) [182].

FDG PET studies have shown interesting results in ARDS and acute lung injury. Bellani and colleagues [183] studied the utilisation of FDG PET in patients with ARDS and found that the relationship of FDG uptake and lung density followed two patterns; most of the patients had highest FDG uptake in regions with the highest density and, in some patients, the uptake was higher in normally or poorly aerated regions than in non-aerated regions. This study again reinforced the potential of FDG as a possible surrogate of lung inflammation, as the normally aerated lungs in ARDS are known to have higher influx of inflammatory cells [183].

These studies have thus been considered to be useful for further development of techniques for non-invasive imaging of the various components of the inflammatory process in the lungs, and for assessing the therapeutic modification of lung inflammation [181].

***Current evidence in COPD:*** Very few studies have previously investigated the effectiveness of dynamic PET imaging in COPD patients [152, 154, 184]. One such study has shown increased pulmonary uptake of $^{18}$FDG in patients with COPD and that this FDG uptake related to the presence of emphysema [152]. This study however only studied the Patlak analysis as a method of assessing FDG uptake in the lungs. Also, the reproducibility of the Patlak analyses was not assessed in this study. In another study, however, good reproducibility was shown in the assessment of FDG PET as a surrogate of inflammation in COPD patients [184].

However this was performed on a small number of COPD patients, again using just the Patlak analyses. Jones and her colleagues also showed similar results in six stable COPD patients [154] and found correlations between the lung PET signal and markers of inflammation in sputum in a small study of six COPD patients. Hence further exploration to optimise all of the methods to assess FDG uptake in the lungs, as a surrogate measure of lung inflammation in COPD patients, in a larger cohort of COPD patients was merited.

### 4.1.2 Significance of my study

A primary goal in this study was therefore to standardize the protocol for FDG PET imaging of lung inflammation, its reproducibility and, in particular, to investigate the various methods of analysis of FDG PET imaging in COPD as the target condition for potential anti-inflammatory therapies.

My study thus aimed to compare the various methods of assessing FDG lung uptake in dynamic (Patlak analyses, 2 compartmental kinetic modelling) and static (SUV measurement) FDG PET lung imaging in COPD patients and in healthy controls. As is known, blood and air comprises a significant proportion of the lung and could result in a significant underestimation of the FDG uptake in the lung parenchyma. Without correcting for these effects, the sensitivity of the PET signal from the lungs would be reduced. This was the justification for the application of the various

methods in this study to investigate and correct for these effects.

***In the following sections each aspect of my study will be discussed in more details.***

## 4.2 Feasibility study

The main aim of the feasibility phase was to develop a local protocol and method of analysis FDG PET/CT as a surrogate marker of lung inflammation in COPD patients. This was successfully achieved in this phase by applying various arterial input functions (AIF). This phase of the study demonstrated comparability of the use of blood-derived (venous and arterial) and image-derived techniques in COPD patients and is the first study to demonstrate this in COPD patients. As a result, it is now possible to assess dynamic FDG pet imaging less invasively without the need for arterial blood sampling.

### 4.2.1 Challenges of image-derived analysis of dynamic FDG PET technique

A prerequisite for the analysis of the lungs is the acquisition of an input function in the form of a blood time–activity curve. The input function typically involves sequential blood sampling, a process that is invasive, prone to measurement artefacts, exposes the clinical staff to radiation and blood, and adds costly laboratory procedures. To avoid or minimize manual blood sampling, substantial effort has been devoted to developing alternative techniques such as *image derived input functions.*

AIFs could thus also be derived from dynamic images without the need for blood sampling. This is achieved from a volume of interest (VOI) drawn over a large thoracic vessel such as pulmonary artery or the aorta. The application of accurate

VOI is dependent on image segmentation, and could be affected by motion artefacts [185], which were corrected for in my study. One disadvantage of this method is that the time-activity curve is for whole blood and not plasma, and that the activity determined may be affected by partial volume effect (PVE) [164]. This is due to the limited spatial resolution of PET, which results in a confounding factor in the reconstructed image from any object smaller than the spatial resolution of the system. The PVE is of two types; spillover effects (or cross-contamination) and the tissue fraction effect (TFE) [155, 186, 187]. The simplest method to lessen spillover effects is to enhance the spatial resolution [156], which was applied in my study. The way to deal with TFE is discussed in a later section.

A correction for image-derived arterial input functions (AIF) based on comparing two late blood calibration samples with the AIF from a blood pool region of interest (ROI) using a 2-parameter model describing the activity of blood and that from the spillover into the time-activity curve for the blood pool ROI, has also been described [156]. My results are based on image-derived AIFs without correction by whole blood samples, as also reported by Holman [155], and without the plasma to whole blood ratio correction (~1.07) reported by Coello and colleagues [188]. Correction of image-derived AIFs by whole blood samples based on an average of the last 30 minutes were also investigated in my study, but results have not been reported because of some technical errors with some of the blood samples, particularly in the healthy controls.

### 4.2.2 Other challenges of combined PET/CT imaging methodology

The annihilation photons in PET are subject to attenuation as they travel through the imaged object. This effect reduces the number of photons detected in each line of response [189]. CT-based *attenuation correction* is an important step in correcting for this in quantitative FDG PET imaging. This results in shorter acquisition times, improves image quality and quantitative accuracy. However, due to the temporal

difference between PET and a single attenuation map from CT, typically available in routine clinical scanning, motion artefacts and errors observed in matching the attenuation-corrected scan to the PET images could add to the errors. Reducing the spatial mismatch of the PET and CT reconstructed images remains a challenge and has been extensively explored in the literature [187]. This, together with PVE, can lead to further errors in analysis [189, 190]. A model of a joint correction approach, incorporating a model of motion blurring, PVE, and object size/shape could be a way forward [190].

CT scanning also introduces challenges with respect to the effect of respiratory motion on the co-registration of the PET-CT images, which has important implications for the reliability of region of interest placement for small lung regions. Artefacts can result from patient and organ motion and differences between the breathing protocols used in PET and CT. These artefacts affect the accuracy of the registration and attenuation correction, seriously compromising the accuracy of activity quantification [191, 192]. Asking the patient to hold the breath during the CT scan, as is usually performed in diagnostic CT studies, can lead to artefacts because of the certain mismatch between a specific stage of the breath cycle during the CT and the average of many breathing cycles in the PET images. Nonetheless, even if the patient is allowed to breathe normally during the whole PET/CT study, because of the fast CT scan time, the diaphragm is visualised in a single position that is different from the mean position of PET images or in the course of respiratory motion. Therefore, mismatch of attenuation correction CT and PET can cause artefacts particularly near the diaphragm [193, 194]. A respiratory-gated analysis to take into account this issue would be desirable, but this was not applied in this study.

## 4.3 Reproducibility

Using the Bland Altman analyses my study demonstrated a good reproducibility between visits 1 and 2 of the COPD patients with regard to all of the parameters of PET imaging that I investigated. This is again the first study to investigate the reproducibility of dynamic PET scanning in stable COPD patients, using Patlak analysis and kinetic modelling methods as well as SUV measurements. All of the results showed good repeatability between the two visits for all of the parameters. Thus, dynamic PET/CT using the protocol and analysis techniques used in this study can be utilised to assess the effects of interventions in future studies.

Models used to assess FDG activity usually use an iterative fitting method to find the least squares between the measured and calculated values over time, which may lead to methodological challenges such as the over fitting of model parameters and result in poor reproducibility, especially when handling noisy data [195]. It was therefore reassuring to see a good repeatability of the data in my study. Chen and her colleagues also showed good reproducibility in a cohort of COPD patients; however this study only assessed the indices of the Patlak analysis [184].

However, all indices of repeatability in my study were performed by one observer. A study in 13 IPF patients investigated the reproducibility of pulmonary $^{18}$F-FDG PET/CT [182]. The study demonstrated excellent short-term reproducibility between the two scans (2 weeks apart) with very good intra-observer agreement.
Some bias was observed between observers, and the authors concluded that serial studies would benefit from analysis by the same observer. This is the approach that I adopted in my study.

It would nevertheless be important to perform a study, with *inter observer's repeatability* comparing all the different indices of PET analyses (SUV vs Patlak analyses vs kinetic model analyses) in a COPD cohort.

## 4.4 Static vs. dynamic PET scanning

### 4.4.1 Static imaging

Static PET imaging of the lung measures the standardized uptake value (SUV). SUV is a simple and straightforward index of tracer uptake, but it introduces quantification bias since it is neither directly linked to any physiological process nor independent on blood flow and blood-to-tissue tracer transportation [185].

In contrast, dynamic PET studies offer the possibility of full kinetic modelling. Kinetic modelling offers a quantitative description of tracer behaviour by taking into account the blood flow and the transportation rate constants between the blood and the tissue, which is particularly important in lung studies.

My study showed that the SUVmax when corrected for the lung density showed a trend to higher values in the COPD group compared to the controls. This difference was greater and reached a statistical significance ($p=0.04$) when the SUVmax was calculated using correction for Va and Vb. Similar results were shown by Torigian and colleagues who calculated lung parenchymal volume (L) (in $cm^3$), excluding large and small pulmonary vessels, emphysema volume (E) (in $cm^3$) based on a -910HU threshold, fraction of lung emphysema (F=E/L), and mean attenuation (HU) of non-emphysematous lung parenchyma from the CT images [196]. They also calculated a partial volume correction (PVC) of lung SUVmax to account for air, emphysema and lung tissue density, and this corrected SUVmax (corrected for the mixture of air and lung parenchyma at the microscopic level) showed a strong and positive correlation with extent of lung emphysema. The uncorrected SUVmax in this study however did not show significant correlations. This reinforces the fact that pulmonary inflammation may only be detectable when $^{18}$F-FDG uptake is corrected for the partial volume effect using data provided by chest CT images.

### 4.4.2 Dynamic PET imaging

The hypothesis in my study was that dynamic PET scanning would be a more robust way of assessing lung inflammation in COPD patients. It nonetheless failed to show a significantly enhanced inflammatory signal in the COPD patients compared with control subjects using the conventional Patlak analyses.

This is in contrast to other previous studies in COPD using Patlak analyses that demonstrated more positive outcomes in this condition [152, 154, 184].

FDG PET studies in other chronic lung diseases, such as cystic fibrosis, and in acute inflammatory lung diseases, such as pneumonia, have also shown significantly raised FDG uptake as measured by Ki compared to healthy controls [178, 197]. However, these conditions are characterised by increased bacterial colonisation, with marked increased numbers of neutrophils present in the lungs in these conditions. In stable COPD by contrast, neutrophilic inflammation in the lungs is less prominent and FDG PET may not be sensitive enough to pick up the subtle increase in neutrophilic inflammation in the lungs in COPD patients.

In addition, it is important to remember that lack of FDG activity does not necessarily signify lack of lung inflammation in the COPD patients. For example, in patients with bronchiectasis an enhanced indium-111 labelled granulocyte activity indicated significant migration of neutrophils, which correlated the sputum volume and the extent of bronchiectasis on CT [143], but there was little FDG uptake on PET imaging [178]. In a further study, Jones and colleagues provided an explanation for this by demonstrating that $^{18}$FDG uptake is associated with some but not all neutrophil activities requiring energy, and is also related to the migrational and the polaroid state of the cell [179].

The other explanation of a poor inflammatory signal using Patlak analyses, as observed in my study, may be the need to consider for correction for the potential contributing factors such as the TFE in the lung, which is a high vascular organ.

### 4.4.3 Correction for the tissue fraction effect

The TFE, as mentioned previously, is a component of the partial volume effect and is the result of the finite size of an image voxel. A single voxel within the lung will contain air and multiple tissue components including blood and lung parenchyma. The resulting voxel value, when being assessed for lung inflammation, will then be an average of the tracer concentrations within that voxel (including blood and air) and not just the signal from the lung parenchyma.

The significance of correcting the air component of the TFE has been investigated in previous studies [198, 199]. In one such study Groves *et al* had shown increased FDG uptake in denser regions of lung fibrosis, where there is a greater tissue component compared to the more normal areas of lung parenchyma [200]. Thus, in regions of the lungs with enlarge air spaces, as is often the case in severe COPD patients with emphysematous lung, the TFE will have more of an influence on the signal. As shown in a previous study, if the TFE is taken into account the uptake distribution could be more uniform across the lung with reduced inter- and intra-subject variability [198].

In my study a clear relationship was shown between lung density (as measured by CT scanning) and the FDG uptake. One way of correcting for the air component and thus enhancing the inflammatory signal when using the Patlak method could be to correct the effect of density. In my study I was able to show that the difference in the FDG PET signal from the lungs between control and COPD was greater when corrected for density, although this difference still failed to reach statistical significance.

An optimal assessment of lung inflammation using the dynamic FDG PET scanning may therefore need better correction for the TFE. The compartmental model analysis allows for this and includes a correction for the blood volume effect. Using this approach I showed increased FDG uptake in the lungs, suggesting increased inflammation in the lungs of COPD patients compared to the healthy controls as measured by an increase in the kinetic modelling indices (KipulmVb and KipulmVbVa).

A similar approach has also been recently advocated by Coello *et al* who suggested a quantitative analysis, which corrects for the presence of air and blood in the lung, enabling direct estimation of the metabolic rate of FDG in lung tissue [188]. This is a more robust way of correcting for the blood and the air effect and is equivalent to method 2 of the compartmental analysis in my study.

In diffuse diseases like COPD, estimation of $^{18}$F-FDG analysed previously using the Patlak graphical approach have used Patlak intercept as a surrogate to correct for air [178]. These previous studies [152, 154, 184] employing the Patlak method did not specifically include any correction for blood activity to the lung ROI. The concept of the use of Patlak intercept to correct for the amount of air in the lungs was introduced by Jones and colleagues in previous studies [154, 179], but is still not a fully validated technique. The intercept component of the linear regression, as we know, is used to calculate the influx constant from a Patlak plot and represents this initial volume of distribution in both the tissue and the blood. Such a correction could be particularly significant in the lungs because lung "tissue" on PET images, as discussed, includes air and blood as well as the parenchymal tissue itself. Changes in density due to atelectasis, pulmonary oedema, or inflammatory recruitment of cells might also alter the volume of distribution of $^{18}$F-FDG and its subsequent rate of uptake. In one such study of a sheep model using bronchoalevolar lavage, Prost *et al* showed that enhanced lung water as in ARDS could generate additional volume to distribution to FDG [201]. This volume is not a precursor for phosphorylation and can artifactually increase lung FDG uptake independent of lung

inflammation.

Thus, optimal ways to correct for such regional variation including the TFE would indeed be the compartmental modelling technique, as also shown in my study. This technique improved the difference in FDG uptake between controls and COPD.

Using CT data to estimate the air fraction and the compartmental modelling applied to lung $^{18}$F-FDG data to account for the blood fraction, it is therefore potentially possible to quantify the glucose metabolic rate for all lung components (ie, lung cells and water) with $^{18}$F-FDG PET; hence improving the inflammatory signal from the lung. Holman *et al* has shown in Idiopathic Pulmonary Fibrosis patients that without correcting for the TFE, regions of high density (fibrosis) appeared to have a higher uptake than lower density (lung with normal appearance on CT scan) reinforcing the need to do so [155]. However, this was reversed after air and blood correction. Similarly, patients with severe emphysema (with lower density areas) if not corrected for the TFE, would arguably give lower uptake signals. This also potentially offers an explanation for the higher slope and intercept using conventional Patlak analyses, in the healthy control group in my study, which would be expected to have higher lung tissue density compared to COPD lungs.

### 4.4.4 Accounting for areas of emphysema

Another important facet to consider whilst optimising the signal thus would be to account for areas of emphysema in COPD patients. In a study performed by Karimi *et al* smoking volunteers with normal pulmonary function were compared with patients with mild to moderate COPD [202]. Higher density spectrum (%HDS), which is percentage of pixels in the lung with attenuation between -750 and -900 HU, were calculated from the inspiratory CT-scans in these subjects. This was then

correlated with markers of systemic inflammation and lung inflammation assessed by bronchoalveolar lavage. The study showed increased lung density in the healthy smokers compared to the COPD patients, and they also recorded that the increased lung density on CT was associated with increased inflammatory cell numbers in BAL in the healthy smokers. This again emphasises the fact that, in COPD patients with emphysema, loss of lung tissue may counterbalance the expected increase in inflammation related uptake and supports the importance of correcting for the TFE as well as the effect of emphysema when assessing the inflammatory signal in COPD patients using dynamic FDG PET scanning. Potentially this also offers an explanation as to why the corrected Ki (slope divided by intercept) when corrected for areas of emphysema, enhanced the inflammatory signal (corrected Ki) to an extent in the COPD patients, compared to the healthy controls using conventional Patlak analyses. However, this difference failed to reach statistical significance in my study.

In a study by Win *et al*, the authors compared the FDG PET signal in the normal regions of the lungs in IPF patients with controls and found, although only after an air fraction correction, that the normal regions of the lung in patients with IPF have an increased uptake compared with the lungs of control subjects [203]. This result is similar to the results from my study, which showed that removing areas of emphysema in the COPD patients and focussing on the non-emphysematous lung parenchyma could result in further improvement of FDG lung uptake in COPD patients compared with healthy controls.

### 4.4.5 Other potential ways to optimise the signal in in the lungs from dynamic FDG PET scanning methodology

The standard methods of calculating Vb from dynamic PET data result in global (whole lung) or regional estimates. However, in lung diseases such as COPD where the quantity of blood reaching regions of diseased lung is heterogeneous,

determination of Vb on a local (voxel-wise) level would be even more advantageous. Holman *et al* applied such a voxel based Vb analyses in IPF patients [204]. The study showed the time delay of the image derived input function (IDIF) varied considerably between different voxels within the IPF lung (maximum difference 17s). This suggests that calculation of a reproducible Vb in the lung requires use of a compartment model that accounts for this time delay and ideally should be performed on a voxel basis. The computation time for voxel based modelling with delay estimation is significant but a similar analysis on the COPD cohort would be desirable**.**

As discussed in the methods chapter, a scale factor of (1-Vb)/(1-Vb-Va) is implicit in all methods of kinetic modelling to estimate Ki corrected for air and blood volume fractions (since Vb+Va+parenchyma =1). Holman *et al* [155, 204] and the group at University College London (personal communication) recommend removal of areas in voxel based parameter images where the tissue fraction (1-Va-Vb) is less than 5% to avoid an unrealistic corrected Ki. This may however lead to an inaccurate measurement in some COPD patients with severe emphysema, where Va could be high resulting in few areas in the lungs with tissue fraction greater than 5%. Coello *et al* claim that their method (qABL method: quantitative analyses which correct for the presence of air and blood in the lung) avoids artefactual increase of Ki in regions with emphysema [188], but my experience with a similar algorithm is that all methods have similar potential problems. Further analysis using a voxel-based analysis thus could be a way forward.

### 4.4.6 Further factors to consider from the study

The results from the dynamic analyses seem to be sensitive to CT density, and relaxed expiration attenuation correction CT has been used to assess density in my study. However, results using density from an average of full inspiration and relaxed expiration (approximating average inspiration) show how density changes the

relative corrected Ki in normal and COPD lungs because of different breathing patterns. In most COPD patients, relaxed expiration has a similar lung volume to full inspiration, but larger differences between full inspiration and relaxed expiration are observed in normal subjects. A failure to match the attenuation correction CT with average PET in the COPD group properly may have influenced the results. Some groups recommend the use of an average of respiratory-gated 4D CT to generate an attenuation correction CT, with density equivalent to average PET; but this will increase the radiation dose [205].

Previous studies have also raised concern that a bolus injection of FDG may not lead to reliable quantification of the PET data using kinetic modelling analyses [206]. For the quantitative evaluation of FDG uptake into the target tissue, kinetic modelling utilises the plasma FDG activity-time profile. Results are, therefore, exclusively dependent on the uptake kinetics in the studied tissue and are not affected by inter- and intra-individual differences in systemic FDG disposition. However, a non-homogenous FDG distribution in the blood pool during the first 30 seconds after a rapid bolus injection, as was the case in this study, can still lead to errors in the measurements. This is because blood radioactivity in general is not assessed directly in the tissue of interest [207]. FDG infusion over a longer duration instead of rapid bolus injection might allow for more reliable assessment of the peak in the time-activity curve required for Vb estimation in the compartmental model analysis.

### 4.4.7 Comparison between smoker and ex-smoker COPD patients with controls

In this study I anticipated that the lung inflammation would be higher in the current smoker COPD compared to the ex-smokers, and this has been shown where an increased FDG PET uptake, presumably reflecting increased pulmonary inflammation, was present in current smoker group compared to the ex-smokers. Although the Patlak analysis showed a trend towards increased uptake in the

current COPD smokers, the compartmental analyses showed statistically significant results in favour of COPD smokers using some of the indices. This is important as it reinforces the importance of smoking cessation even in established COPD patients, and corroborates the conclusions generated from previous studies that show inflammation from persistent smoking in COPD patients is, as expected, associated with an increased all-cause mortality rate and exacerbation frequency [51].

## 4.5 Lobar data analyses

In my study, measurement of the FDG signal in the lung lobes showed that the upper lobe in COPD patients had a trend towards higher inflammatory signal compared to the controls, although this difference failed to reach statistical significance. This result is similar to the study performed by Parr *et al* where they showed higher values of corrected Patlak Ki in upper lobes of lungs of COPD patients that correlated inversely with per cent predicted $FEV_1$ and positively with CT-determined emphysema severity [152]. Since emphysema predominates in the upper lobes this might suggest that increased inflammation occurs in association with areas of emphysema. However, another explanation might be related to the fact that the upper lobes have lower density due to emphysema causing high Patlak slope/intercept as intercept correlates with density, as also shown in this study.

In contrast to the findings, Wright *et al* assessed the pathological abnormalities of the small airways in the upper and lower lobes of 13 surgically resected lung specimens from COPD patients [208]. The study showed slightly increased degrees of respiratory bronchiolar inflammation in the lower lobes compared to the upper lobes but no significant differences between the two sites, or any other relationship between the presence of pathological abnormalities in the small airways and the presence of centrilobular emphysema in these patients. Thus, more detailed lobar analyses studies are necessary to understand the regional variation in inflammatory uptake in COPD.

These conflicting findings also continue to emphasize the need to continue defining the relationship of the different $^{18}$F-FDG PET quantitative parameters to outcome measures; to help determine which metrics are the best surrogate measures of inflammation using this methodology. This also reinforces the possibility that although corrected Ki using Patlak analyses has been used as the endpoint in many previous publications on lung $^{18}$F-FDG uptake, it does not adequately account for the impact of air and blood in the lungs. The analyses in my study for the lobar data were also part of the Patlak methodology and I did not take into account the TFE using the compartmental modelling analyses because of time constraints.

## 4.6 Assessment of vascular inflammation

My study showed increased vascular (aortic) inflammation in COPD patients compared to the controls, *when* SUVmax was used as index of measurement of vascular inflammation. SUVmax was also linked with the severity of the airflow limitation as it correlated inversely with the $FEV_1$ per cent predicted. This supports the theory that increased vascular inflammation may partly account for the increased risk of cardiovascular disease in COPD patients [115, 209]. The underlying mechanism is unclear - although elastin degradation may play a role in this enhanced inflammation noticed in COPD patients [210]. However, as mentioned before, no significant difference was found between the COPD patients and the controls when analysing using target to background (TBR: standardized uptake value (SUV) normalized to $^{18}$F-FDG blood pool activity) as the other index of measurement of vascular inflammation.

### 4.6.1 Significance of TBR

This is considered an important index of measuring vascular inflammation using PET methodology. In a study performed by Vanflettern *et al*, increased

inflammation was shown in the abdominal aorta in COPD patients with lung cancer, compared to healthy controls [211]. In this study the parameter chosen to measure the aortic inflammation was TBRmax and the TBR was calculated by normalizing the arterial SUV for blood pool activity by dividing the SUV values in the arteries by the average blood mean SUV estimated from the superior vena cava. However, these were patients who had underlying lung cancer that may have influenced the results.

Similarly, in another study by Figueroa *et al* TBR strongly predicted subsequent cardiovascular disease in a group of participants who underwent PET-CT for oncological evaluation and did not have a prior history of cardiovascular disease, independent of traditional risk factors [212], reinforcing TBR as an important marker to be considered whilst measuring vascular inflammation.

### 4.6.2 Potential explanation for low TBR

In my study the degree of uptake in the aorta was measured at 50 minutes after $^{18}$F-FDG administration. Most cardiovascular studies recommend assessing vascular uptake at a later time-point (60 minutes or later) [213, 214] and might in part explain why my TBR readings were lower in the COPD patients. Also, careful selection of the index vessel to measure the blood pool activity to calculate TBR is of paramount importance [215]. This ensures that the delay between injection of tracer and data acquisition, and consequently tracer uptake in the arterial target structure (eg aorta) and the washout of tracer from the venous blood pool will be the same for the arterial and the venous vessel. The superior venae cava was used as the "index vessel" in my study as this was not a vascular tailored study and is very likely to be affected by intense uptake of FDG by the myocardium; hence potentially giving lower values for the TBR in my study.

Although TBR is an important aspect of assessing vascular inflammation, SUVmax remains an equally important index of measuring vascular inflammation [216, 217]. Therefore, irrespective of the discrepancy of results between the two different measures in my study, vascular inflammation is to be expected in COPD patients and indeed is independently associated with cardiovascular complications as frequently observed in these patients. Intervention studies report a 6-15% reduction in markers of aortic inflammation with anti-inflammatory treatments such as anti-tumour necrosis-α therapy, or high-dose statins [218, 219] and could form the basis of similar such studies in properly vascular tailored studies in COPD. A similar prospective analysis thus involving COPD patients and healthy controls, with a vascular tailored FDG-PET protocol, analysing SUV and TBR as inflammatory indices, using both static and kinetic modelling approach, would be needed to determine the association between aortic inflammation and outcomes in COPD.

## 4.7 Summary of the study

In summary my study showed that:

☐ Dynamic $^{18}$FDG PET scanning is potentially a novel reproducible method of assessing for lung inflammation in COPD patients.

☐ Image derived methodology is a robust method of deriving arterial input functions.

☐ The conventional Patlak assessment is not fully adequate to explore the role of dynamic PET scanning as a biomarker of lung inflammation, as it does not fully account for the effects of lung density and other TFE. My study showed no difference in results between COPD and controls using this method.

☐ Tissue kinetic modelling is indeed the way of enhancing the signal for lung inflammation as it takes account of the air and the blood effect. Using this method

my study showed more lung inflammation in COPD patients using some indices, compared with control subjects, particularly in COPD patients who were current smokers.

## 4.8 Limitations of the study

☐ One of the major limitations of the study was the sample size that may account for the lack of statistical significance for most of the assessments between COPD and the healthy controls. This was done primarily to keep the subject number low due to associated risk of radiation. A larger study investigating all the methods of assessment in a prospective cohort would be desirable.

☐ My study showed good reproducibility of all measured indices. However to make the methodology even more robust, as mentioned before, inter observer measurements would have been ideal.

☐ The issues regarding respiratory motion correction have been mentioned before. Respiratory-gated analyses using a respiratory motion detector as specified earlier would be desirable.

☐ The kinetic model analyses technique is sensitive to the location of the volume of interest (VOI). In this study I observed that the pulmonary artery image- derived arterial input function could have higher peaks than aorta AIFs: higher peak for image-derived arterial input functions from the pulmonary artery than from the aorta has been shown by other groups too [188]. This higher peak for image-derived arterial input functions from the pulmonary artery, than from the aorta, may have an implication on Vb estimation and needs further exploration.

☐ My study found no correlation of KiPulmVb with any of the markers of serum and sputum inflammation. Although a correlation would have been interesting, this

is not entirely unexpected. The patients in this study were all scanned during their stable state and the inflammation in lung parenchyma that I wanted to demonstrate would be expectedly chronic and subtle. Also, all the markers of inflammation that I looked into (CRP, Fibrinogen, WCC and the cytokines) are more reflective of systemic and airway inflammation (particularly the sputum markers), and therefore may not correlate with a PET index of measuring subtle lung parenchymal inflammation. A more detailed dynamic PET study in the future encompassing ways to look at the airway inflammation would be very informative.

☐ Further ways to correct for the TFE when analysing the lobar data using the compartmental method of analyses needs exploration.

☐ A vascular tailored imaging protocol was not followed in my study as this was predominantly a lung study, and could have influenced the results of the vascular inflammation.

☐ Other disadvantages of $^{18}$FDG PET as a biomarker: the PET scan itself entails the subjects needing to lie on the scanner for an hour. This adds to the burden of motion artefacts and although methods to correct for this have been discussed and implemented, it still raises the practicality of using PET scan as a modality of measuring lung inflammation in a chronic lung disease cohort.

Also as discussed before, FDG competes with glucose for uptake in the cells and any hyperglycaemic state can give potentially false negative FDG uptake [148]. A vast majority of the COPD patients can have associated diabetes as comorbidity [39,44] and again questions the usefulness of FDG as the most appropriate biomarker of lung inflammation in this cohort.

The suitability of FDG (that measures neutrophilic inflammation) in a chronic stable lung cohort of COPD, where the inflammation is to an extent also mediated thorough macrophages, has already been discussed before.

## 4.9 Future directions

- ***New PET tracers:*** Together with a further investigation of the role of $^{18}$F FDG, newer radio ligands also hold promise in chronic lung diseases. One such radiotracer for inducible nitric oxide synthase (iNOS), $^{18}$F (+/−) NOS, could be potentially used for imaging inflammation [176]. iNOS is expressed in response to inflammatory cytokines [220] and can add to the burden of oxidative stress. $^{18}$F(+/−)NOS is an iNOS-targeted PET tracer that has been tested in an animal model of lung inflammation [220] and has shown promise in endotoxin treated lungs of healthy volunteers [221]. Given the oxidative stress burden in COPD, this tracer potentially holds promise for this cohort.

Similarly, $^{18}$F-Fluciclatide has shown promising results for imaging in pulmonary fibrosis. Fluciclatide is an arginine-glycine-aspartic acid peptide with high affinity for integrins [176]. This has been radiolabeled with F-18 for PET imaging of angiogenesis and active fibrosis and assessed in a Phase 1 trial [222]. A recent study shows increased $^{18}$F-fluciclatide uptake, as quantified using the maximum standard uptake value (SUV), in patients with lung fibrosis, compared to healthy volunteers, particularly in areas of the lung with the most severe fibrosis [223].

A translocator protein–targeted tracer $^{11}$C-PK11195 has also been used to image the presence of macrophages in COPD and asthma patients and age-matched healthy controls and compared with $^{18}$F-FDG [154]. The study showed increased

$^{11}$CPK11195 activity in both asthmatics and COPD patients in contrast to the $^{18}$F-FDG signal which was increased only in the COPD cohort. The data from this pilot study suggest that 11C-PK11195 may be useful in imaging the macrophage burden in the lungs. Chen and colleagues showed similar results where they demonstrated PET imaging with [$^{11}$C] PBR28 and [$^{18}$F] FDG could help to differentiate macrophage dominant from neutrophilic inflammation in COPD [224]. This was however in an animal model and needs further exploration in human studies.

☐ ***Role of combined MR/PET imaging:*** Without the use of contrast agents, MRI provides higher soft-tissue contrast, and therefore holds potential benefits of providing superior co-registration of resulting images in comparison to CT scans [225]. Radiation exposure is also lower than with hybrid PET/computed tomography scanning, and is therefore of added value. The fact that this modality can combine the full potential of anatomic and multiparametric imaging of MRI with the molecular information of PET could be of immense value to investigate its role as an inflammatory biomarker. However, unlike CT attenuation correction where the Hounsfield units are directly related to density, attenuation correction for different tissues in the human body based on MRI is a major problem [226]. MRI relies on the presence of hydrogen nuclei and tissue relaxation properties, rather than on tissue densities and a consensus approach to magnetic resonance attenuation correction (MRAC) is yet to be agreed on [226, 227]. Nevertheless, this imaging technique holds potential and need future further research exploration.

☐ ***Optical imaging using confocal laser endomicroscopy:*** This diagnostic technique aims to look at development of methodologies to attain real-time identification of inflammation and infection process in human subjects [228]. Several attempts to chemical probe designing and validation have been undertaken

so far, however none have yet been successfully translated into clinical practice. A combined protocol of dynamic PET imaging with such confocal imaging could potentially be an interesting way of assessing lung inflammation in the future.

## 4.10 Conclusions

In conclusion, $^{18}$FDG PET scanning holds promise to be used as a novel non-invasive biomarker of lung inflammation in COPD patients. The methodology is reproducible; careful attention however needs to be given to the tissue fraction effect including density effects when interpreting the results of this heterogeneous lung disease with chronic subtle lung inflammation. Future prospective analyses of a larger number of COPD patients, addressing these issues and investigating all the newer techniques, would greatly add to our understanding of this imaging technique.

## References


1. Murray CJ, Lopez AD. Alternative projections of mortality and disability by cause 1990-2020: Global Burden of Disease Study. Lancet 1997; 349:1498-1504.

2. Chapman KR, Mannino DM, Soriano JB, Vermeire PA, Buist AS, Thune MJ, Connelle C, Jemale A Lee TA, Miravitlles M, Aldington S, Beasley R. Epidemiology and costs of chronic obstructive pulmonary disease, Eur Respir J 2006; 27:188-207.

3. Celli BR, MacNee W, Agusti A, AnzuetoA, Berg B, Buist AS et al. Standards for the diagnosis and treatment of patients with COPD: a summary of the ATS/ERS position paper. Eur Respir J 2004; 23(6):9329-9346.

4. Global Initiative for Chronic Obstructive Lung Disease (GOLD). GOLD 2017 Global strategy for the diagnosis, management and prevention of COPD. From the Global Strategy for the Diagnosis, Management and Prevention of COPD, Global Initiative for Chronic Obstructive Lung Disease (GOLD) 2017. Available from: http://goldcopd.org.

5. Han MK, Agusti A, Calverley PM, et al. Chronic obstructive pulmonary disease phenotypes: the future of COPD. Am J Respir Crit Care Med 2010; 182:598-604.

6. Scottish Public Health Observatory. Chronic obstructive pulmonary disease (COPD): mortality data [online], 2015. Available at: http://www.scotpho.org.uk/health-wellbeing-and-disease/chronic-obstructive-pulmonary-disease-copd/data/mortality- data

7. World Health Statistics. Geneva: World Health Organisation, 2008.

8. Burney and Jarvis. 2006;NHS Evidence - The Burden of COPD in the UK [online]: Available at : http://www.library.nhs.uk/RESPIRATORY/ViewResource.aspx?resID=187247 [Accessed January 23, 2011].

9. Scottish Public Health Observatory. Chronic obstructive pulmonary disease (COPD): mortality data [online] 2015. Available at: http://www.scotpho.org.uk/health-wellbeing-and-disease/chronic-obstructive-pulmonary-disease-copd/data/secondary- care-data

10. Lundbäck B, Lindberg A, Lindström M, et al. Not 15 but 50% of smokers develop COPD? - Report from the Obstructive Lung Disease in Northern Sweden Studies. Respir Med 2003; 97:115-122.

11. US Department of Health and Human Services. The health benefits of smoking cessation. A report of the Surgeon General, 1990. DHHS Publication No CDC 90-8416. Rockville, Maryland: Centers for Disease Control, Office on Smoking and Health, 1990.

12. Fletcher C, Peto R. The natural history of chronic airflow obstruction. BMJ 1977; 1:1645-1648.

13. Kohansal R, Martinez-Camblor P, Agusti A, et al. The natural history of chronic airflow obstruction revisited: an analysis of the Framingham offspring cohort. Am J Respir Crit Care Med 2009; 180:3-10.

14. Hagstad S, Bjerg A, Ekerljung L. Passive smoking exposure is associated with increased risk of COPD in never smokers. Chest 2014; 145(6):1298-1304.

15. Curran HV, Brignell C, Fletcher S, et al. Cognitive and subjective dose-response effects of acute oral delta 9-tetrahydrocannabinol (THC) in infrequent cannabis users. Psychopharmacology (Berl) 2002; 164:61-70.

16. Gates P1, Jaffe A, Copeland J. Cannabis smoking and respiratory health: consideration of the literature. Respirology 2014; 19(5):655-62.

17. Hii SW, Tam JDC, Thompson BR, et al. Bullous lung disease due to marijuana. Respirology 2008; 13:122-127.

18. Tan C, Hatam N, Treasure T. Bullous disease of the lung and cannabis smoking: insufficient evidence for a causative link. J R Soc Med 2006; 99: 77-80.

19. Taylor DR, Fergusson DM, Milne BJ, et al. A longitudinal study of the effects of tobacco and cannabis exposure on lung function in young adults. Addiction 2002; 97:1055-1061.

20. Omland O, Wurtz ET, Aasen TB, et al. Occupational chronic obstructive pulmonary disease: a systematic literature review. Article Scand J Work Environ Health, 2014.

21. Dement J, Welch L, Ringen K, et al. A case-control study of airways obstruction among construction workers. Am J Ind Med 2015; 58(10):1083-1097.

22. Ramírez-Venegas A, Sansores RH, Pérez-Padilla R, et al. Survival of patients with chronic obstructive pulmonary disease due to biomass smoke and tobacco. Am J Respir Crit Care Med 2006; 173:393-397.

23. Zhai G, Valdes AM, Cherkas L, et al. The interaction of genes and smoking on forced expiratory volume: a classic twin study. Chest 2007; 132:1772-1777.

24. Lomas D, Parfrey H. α1-Antitrypsin deficiency • 4: Molecular pathophysiology. Thorax 2004; 59:529-535.

25. Silverman EK, Chapman HA, Drazen JM, et al. Genetic epidemiology of severe, early- onset chronic obstructive pulmonary disease. Risk to relatives for airflow obstruction and chronic bronchitis. Am J Respir Crit Care Med 1998; 157:1770-1778.

26. Baraldo S, Turato G, Lunardi F, et al. Immune activation in α1-antitrypsin-deficiency emphysema. Beyond the protease-antiprotease paradigm. Am J Respir Crit Care Med 2015; 191(4):402-409.

27. Lee JH, Cho MH, Hersh CP, et al. Genetic susceptibility for chronic bronchitis in chronic obstructive pulmonary disease. Respir Res 2014; 15:113.

28. Cunningham TJ, Ford ES, Croft JB, et al. Sex-specific relationships between adverse childhood experiences and chronic obstructive pulmonary disease in five states. Int J Chron Obstruct Pulmon Dis 2014; 9:1033-1042.

29. Hogg JC. Childhood viral infection and the pathogenesis of asthma and chronic obstructive lung disease. Am J Respir Crit Care Med 1999; 160(5 Pt 2):S26- 28.

30. Ishii M, Teramoto S. Childhood respiratory infection in the pathogenesis of COPD. ihon Rinsho 2007; 65(4):617-622.

31. Barker DJ, Godfrey KM, Fall C, et al. Relation of birth weight and childhood respiratory infection to adult lung function and death from chronic obstructive airways disease. BMJ 1991; 303:671-675.

32. Stern D, Morgan W, Wright A, et al. Poor airway function in early infancy and lung function by age 22 years: a non-selective longitudinal cohort study. Lancet. 2007; 370:758-764.

33. Baumann S, Godtfredsen NS, Lange P, et al. The impact of birth weight on the level of lung function and lung function decline in the general adult population. The Inter99 study. Respir Med. 2015; 109(10):1293-1299.

34. MacNee W. Systemic inflammatory biomarkers and co-morbidities of chronic obstructive pulmonary disease. Ann Med 2013; 45(3):291-300.

35. MacNee W. Pulmonary and systemic oxidant/antioxidant imbalance in chronic obstructive pulmonary disease. Proc Am Thorac Soc 2005; 2:50-60.

36. Rode L, Bojesen SE, Weischer M, et al. Short telomere length, lung function and chronic obstructive pulmonary disease in 46,396 individuals. Thorax 2013; 68(5):429- 435.

37. Tsuji T, Aoshiba K, Nagai A. Cigarette smoke induces senescence in alveolar epithelial cells. Am J Respir Cell Mol Biol 2004; 31:643-649.

38. Yao H, Chung S, Hwang JW, et al. SIRT1 protects against emphysema via FOXO3mediated reduction of premature senescence in mice. J Clin Invest 2012; 122(6):2032-2045.

39. Szulakowski P, Crowther AJ, Jimenez LA, et al. The effect of smoking on the transcriptional regulation of lung inflammation in patients with chronic obstructive pulmonary disease. Am J Respir Crit Care Med 2006; 174:41-50.

40. Barnes PJ, Celli BR. Systemic manifestations and comorbidities of COPD. Eur Respir J 2009; 33:1165-1185.

41. Lambers C, Hacker S, Posch M, et al. T cell senescence and contraction of T cell repertoire diversity in patients with chronic obstructive pulmonary disease. Clin Exp Immunol 2009; 155:466-475.

42. Fairclough L, Urbanowicz RA, Corne J, Lamb JR. Killer cells in chronic obstructive pulmonary disease. Clin Sci(Lond) 2008; 114:533-541.

43. Miniati M, Monti S, Basta G, Cocci F, et al. Soluble receptor for advanced glycation end products in COPD: relationship with emphysema and chronic cor pulmonale: a case–control study. Respir Res 2011; 12:37.

44. Churg A, Wright JL. Proteases and emphysema. Curr Opin Pulm Med 2005; 11:153- 159.

45. Agusti AG. Systemic effects of chronic obstructive pulmonary disease. Proc Am Thorac Soc 2005; 2(4):367-70; discussion 371-372.

46. Vernooy JH, Kucukaycan M, Jacobs JA, et al. Local and systemic inflammation in patients with chronic obstructive pulmonary disease: soluble tumor necrosis factor receptors are increased in sputum. Am J Respir Crit Care Med 2002; 166:12181224.

47. Hsiao HM, Sapinoro RE, Thatcher TH, et al. A novel anti-inflammatory and pro- resolving role for resolvin d1 in acute cigarette smoke-induced lung inflammation. PLoS One 2013; 8(3):e58258.

48. Kanner RE, Anthonisen NR, Connett JE. Lower respiratory illnesses promote FEV1 decline in current smokers but not ex-smokers with mild chronic obstructive pulmonary disease: results from the lung health study. Am J Respir Crit Care Med 2001; 164:358-364.

49. Saetta M, Turato G, Facchini FM, et al. Inflammatory cells in the bronchial glands of smokers with chronic bronchitis. Am J Respir Crit Care Med 1997; 156:1633-1639.

50. Vestbo J. Systemic inflammation and progression of COPD. Thorax 2007; 62(6):469- 470.

51. Agusti A, Edwards LD, Rennard SI, MacNee W, et al. Persistent systemic inflammation is associated with poor clinical outcomes in COPD: a novel phenotype. PLoS One 2012; 7: e37483.

52. Hurst JR, Donaldson GC, Perera WR, et al. Use of plasma biomarkers at exacerbation of chronic obstructive pulmonary disease. Am J Respir Crit Care Med 2006; 174:867- 874.

53. Sevenoaks MJ, Stockley RA. Chronic obstructive pulmonary disease, inflammation and co-morbidity – a common inflammatory phenotype? Respir Res 2006; 7:70.

54. Gea J, Barreiro E, Orozco-Levi M. Systemic Inflammation in COPD. Clin Pulm Med 2009; 16:233-242.

55. Luppi F, Franco F, Beghe, B, Fabbri M. Treatment of chronic obstructive pulmonary disease and its comorbidities. Proc Am Thorac Soc 2008; 5:848-856.

56. Maclay JD, McAllister DA, MacNee W. Cardiovascular risk in chronic obstructive pulmonary disease. Respirology 2007; 12:634-641.

57. Rahman I, Morrison D, Donaldson K, MacNee W. Systemic oxidative stress in asthma, COPD, and smokers. Am J Respir Crit Care Med 1996; 154(4 Pt 1):1055-1060.

58. Yao H, Rahman I. Current concepts on oxidative/carbonyl stress, inflammation and epigenetics in pathogenesis of chronic obstructive pulmonary disease. Toxicol Appl Pharmacol 2011; 254(2):72-85.

59. Igishi T, Hitsuda Y, Kato K, et al. Elevated urinary 8-hydroxydeoxyguanosine, a biomarker of oxidative stress, and lack of association with antioxidant vitamins in chronic obstructive pulmonary disease. Respirology 2003; 8:455-460.

60. Rahman I, van Schadewijk AA, Crowther AJ, et al. 4-Hydroxy-2-nonenal, a specific lipid peroxidation product, is elevated in lungs of patients with chronic obstructive pulmonary disease. Am J Respir Crit Care Med 2002; 166:490–495.

61. Rahman I, MacNee W. Oxidant/antioxidant imbalance in smokers and chronic obstructive pulmonary disease. Thorax 1996; 51(4):348-350.

62. Repine JE, Bast A, Lankhorst I. Oxidative stress in chronic obstructive pulmonary disease. Oxidative Stress Study Group. Am J Respir Crit Care Med 1997; 156:341e57.

63. Fischer BM, Pavlisko E, Voynow JA. Pathogenic triad in COPD: oxidative stress, protease–antiprotease imbalance, and inflammation. Int J Chron Obstruct Pulmon Dis 2011; 6:413-421.

64. Rahman I, Li XY, Donaldson K, et al. Glutathione homeostasis in alveolar epithelial cells in vitro and lung in vivo under oxidative stress. Am J Physiol Lung Cell Mol Physiol 1995; 269:L285–L292.

65. Snider GL, Ciccolella DE, Morris SM, et al. Putative role of neutrophil elastase in the pathogenesis of emphysema. Ann NY Acad Sci 1991; 624:45-59.

66. Cavarra E, Lucattelli M, Gambelli F, et al. Human SLPI inactivation after cigarette smoke exposure in a new in vivo model of pulmonary oxidative stress. Am J Physiol Lung Cell Mol Physiol 2001; 281:L412-L417.

67. Shapiro SD. Proteinases in chronic obstructive pulmonary disease. Biochem Soc Trans 2002; 30:98-102.

68. Parameswaran GI, WronaCT, Murphy TF, Sethi S. *Moraxella catarrhalis* acquisition, airway inflammation and protease-antiprotease balance in chronic obstructive pulmonary disease. BMC Infect Dis 2009; 9:178.

69. Moyzis RK, Buckingham JM, Cram LS, et al. A highly conserved repetitive DNA sequence, (TTAGGG)n, present at the telomeres of human chromosomes. Proc Natl Acad Sci USA 1988; 85:6622-6626.

70. von Zglinicki T. Oxidative stress shortens telomeres. Trends Biochem Sci 2002; 27:339- 344.

71. Anthonisen NR, Connett JE, Kiley JP, et al. Effects of smoking intervention and the use of an inhaled anticholinergic bronchodilator on the rate of decline of FEV1. The Lung Health Study. JAMA 1994; 272:1497-1505.

72. Lee J, Sandford AJ, Connett JE, et al. The relationship between telomere length and mortality in chronic obstructive pulmonary disease (COPD). PLoS One 2012; 7(4):e35567.

73. Mui TS, Man JM, McElhaney JE, et al. Telomere length and chronic obstructive pulmonary disease: evidence of accelerated aging. J Am Geriatr Soc 2009; 57(12):2372- 4.

74. ThériaultM-E, Paré M-E, Maltais F, Debigaré. R Satellite cells senescence in limb muscle of severe patients with COPD. PLoS One 2012; 7(6):e39124.

75. Alder JK, Guo N, Kembou F, et al. Telomere length is a determinant of emphysema susceptibility. Am J Respir Crit Care Med 2011; 184:904-912.

76. Faner R, Rojas M, MacNee W, Agustí A. Abnormal lung aging in chronic obstructive pulmonary disease and idiopathic pulmonary fibrosis. Am J Respir Crit Care Med 2012; 186(4):306-313.

77. Miller KM, Tjeertes JV, Coates J, et al. Human HDAC1 and HDAC2 function in the DNA-damage response to promote DNA nonhomologous end-joining. Nat Struct Mol Biol 2010; 17:1144-1151.

78. Wagner M, Brosch G, Zwerschke W, et al. Histone deacetylases in replicative senescence: evidence for a senescence-specific form of HDAC-2. FEBS Lett 2001; 499:101-106.

79. Bitterman KJ, Anderson RM, Cohen HY, et al. Inhibition of silencing and accelerated aging by nicotinamide, a putative negative regulator of yeast sir2 and human SIRT1. J Biol Chem 2002; 277:45099e107.

80. Lee IH, Cao L, Mostoslavsky R, et al. A role for the NAD-dependent deacetylase Sirt1 in the regulation of autophagy. Proc Natl Acad Sci USA 2008; 105:3374-3379.

81. Wallace DC. A mitochondrial paradigm of metabolic and degenerative diseases, aging, and cancer: A dawn for evolutionary medicine. Annu Rev Genet 2005; 39:359- 407.

82. Balaban RS, Nemoto S, Finkel T. Mitochondria, oxidants, and aging. Cell 2005; 120:483-495.

83. MacNee W. Accelerated lung aging: a novel pathogenic mechanism of chronic obstructive pulmonary disease (COPD). Biochem Soc Trans 2009; 37: 819-823.

84. Neeper M, Schmidt AM, Brett J, et al. Cloning and expression of a cell surface receptor for advanced glycosylation end products of proteins. J Biol Chem 1992; 267:14998- 15004.

85. Kirstein M, Brett J, Radoff S, et al. Advanced protein glycosylation induces transendothelial human monocyte chemotaxis and secretion of platelet-derived growth factor: role in vascular disease of diabetes and aging. Proc Natl Acad Sci USA 1990; 87(22):9010-9014.

86. Smith DJ, Yerkovich ST, Towers MA, et al. Reduced soluble receptor for advanced glycation end-products in COPD. Eur Respir J 2011; 37(3):516-22.

87. Ferhani N, Letuve S, Kozhich A, et al. Expression of high-mobility group box 1 and of receptor for advanced glycation end products in COPD. Am J Respir Crit Care Med 2010; 181:917-927.

88. Lee SH, Goswami S, Grudo A, et al. Antielastin autoimmunity in tobacco smoking- induced emphysema. Nat Med 2007; 13:567-569.

89. Willemse BW, ten Hacken NH, Rutgers B, et al. Effect of 1-year smoking cessation on airway inflammation in COPD and asymptomatic smokers. Eur Respir J 2005; 26:835- 845.

90. Sin DD, Anthonisen NR, Soriano JB, Agusti AG. Mortality in COPD: role of comorbidities. Eur Respir J 2006; 28(6):1245-1257.

91. Gan WQ, Man SF, Senthilselvan A, et al. Association between chronic obstructive pulmonary disease and systemic inflammation: a systematic review and a meta- analysis. Thorax 2004; 59:574-580.

92. Celli BR, Locantore N, Yates J, et al; ECLIPSE Investigators. Inflammatory biomarkers improve clinical prediction of mortality in chronic obstructive pulmonary disease. Am J Respir Crit Care Med 2012; 185(10):1065-1072.

93. Takabatake N, Nakamura H, Abe S, et al. The relationship between chronic hypoxemia and activation of the tumor necrosis factor-α system in patients with chronic obstructive pulmonary disease. Am J Respir Crit Care Med 2000; 161:1179-1184.

94. Preedy, VR, Smith DM, Sugden PH. The effects of 6 hours of hypoxia on protein synthesis in rat tissues in vivo and in vitro. Biochem J 1985; 228:179-185.

95. Pinto-Plata VM, Mullerova H, Toso JF, et al. C-Reactive protein in patients with COPD, control smokers and non-smokers. Thorax 2006; 61:23-28.

96. Alessandri C, Basili S, Violi F, et al; Chronic Obstructive Bronchitis and Haemosta- sis Group. Hypercoagulability state in patients with chronic obstructive pulmonary disease. Thromb Haemost 1994; 72(3): 343-346.

97. Ashitani J-I, Mukae H, Arimura Y, Matsukura S. Elevated plasma procoagulant and fibrinolytic markers in patients with chronic obstructive pulmonary disease. Intern Med 2002; 41(3):181-185.

98. Sin DD, Leung R, Gan WQ, Man SP. Circulating surfactant protein D as a potential lung-specific biomarker of health outcomes in COPD: a pilot study. BMC Pulm Med 2007; 7:13.

99. Bozinovski S, Hutchinson A, Thompson M, et al. Serum amyloid A is a biomarker of acute exacerbations of chronic obstructive pulmonary disease. Am J Respir Crit Care Med 2008; 177:269-278.

100. Sparrow D, Glynn RJ, Cohen M, Weiss ST. The relationship of the peripheral leukocyte count and cigarette smoking to pulmonary function among adult men. Chest 1984; 86:383-386.

101. Burnett D, Chamba A, Hill SL, Stockley RA. Neutrophils from subjects with chronic obstructive lung disease show enhanced chemotaxis and extracellular proteolysis. Lancet 1987; 2:1043-1046.

102. Aldonyte R, Jansson L, Piitulainen E, Janciauskiene S. Circulating monocytes from healthy individuals and COPD patients. Respir Res 2003; 4:11.

103. Hodge SJ, Hodge GL, Reynolds PN, et al. Increased production of TGF-beta and apoptosis of T lymphocytes isolated from peripheral blood in COPD. Am J Physiol Lung Cell Mol Physiol 2003; 285:L492-L499.

104. Domagala-Kulawik J, Hoser G, Dabrowska M, Chazan R. Increased proportion of Fas positive CD8+ cells in peripheral blood of patients with COPD. Respir Med 2007; 101:1338-1343.

105. Mapel DW, Dedrick D, Davis K. Trends and cardiovascular co-morbidities of COPD patients in the Veterans Administration Medical System, 1991-1999. COPD 2005; 2(1):35-41.

106. Anthonisen NR, Connett JE, Enright PL, Manfreda J; Lung Health Study Research Group. Hospitalizations and mortality in the Lung Health Study. Am J Respir Crit Care Med 2002; 166(3):333-339.

107. Divo M, Cote C, de Torres JP, et al. Comorbidities and risk of mortality in patients with chronic obstructive pulmonary disease. Am J Respir Crit Care Med 2012; 186(2):155-161.

108. Holguin F, Folch E, Redd SC, Mannino DM. Comorbidity and mortality in COPD- related hospitalizations in the United States, 1979 to 2001. Chest 2005; 128:2005-2011.

109. Bang KM, Gergen PJ, Kramer R, Cohen B. The effect of pulmonary impairment on all- cause mortality in a national cohort. Chest 1993; 103(2):536-540.

110. Campo G, Guastaroba P, Marzocchi A, et al. Impact of chronic obstructive pulmonary disease on long-term outcome after ST-segment elevation myocardial infarction receiving primary percutaneous coronary intervention. Chest 2013; 144(3):750-757.

111. Hole DJ, Watt GC, Davey-Smith G, et al. Impaired lung function and mortality risk in men and women: finding from the Renfrew and Paisley prospective population study. BMJ 1996; 313:711-715 [discussion: 5-6].

112. Sin DD, Man SF. Why are patients with chronic obstructive pulmonary disease at increased risk of cardiovascular diseases? The potential role of systemic inflammation in chronic obstructive pulmonary disease. Circulation 2003; 107(11):1514-1519.

113. Van Gestel YRBM, Flu W-J, van Kuijk J-P, et al. Association of COPD with carotid wall intima-media thickness in vascular surgery patients. Respir Med 2010; 104(5):712-716.

114. Williams M, Murchison J, Edwards L, et al. Coronary artery calcification is increased in patients with COPD and associated with increased morbidity and mortality. Thorax 2014; 69:718-723.

115. Rabinovich RA, Miller BE, Wrobel K, et al, Evaluation of COPD Longitudinally to Identify Predictive Surrogate Endpoints (ECLIPSE) Investigators. Circulating desmosine levels do not predict emphysema progression but are associated with cardiovascular risk and mortality in COPD. Eur Resp J 2016; 47:42-49.

116. Agusti AG, Noguera A, Sauleda J, et al. Systemic effects of chronic obstructive pulmonary disease. Eur Respir J 2003; 21:347-360.

117. Gosselink R, Troosters T, Decramer M. Peripheral muscle weakness contributes to exercise limitation in COPD. Am J Respir Crit Care Med 1996; 153:976-980.

118. Shrikrishna D, Hopkinson NS. Chronic obstructive pulmonary disease: consequences beyond the lung. Clin Med2012; 12:71-74.

119. Decramer M, Gosselink R, Troosters T, et al. Muscle weakness is related to utilization of health care resources in COPD patients. Eur Respir J 1997; 10:417-423.

120. Swallow EB, Reyes D, Hopkinson NS, et al. Quadriceps strength predicts mortality in patients with moderate to severe chronic obstructive pulmonary disease. Thorax 2007; 62:115-120.

121. Seymour JM, Spruit MA, Hopkinson NS, et al. The prevalence of quadriceps weakness in COPD and the relationship with disease severity. Eur Respir J 2010; 36:81-88.

122. Shrikrishna D, Hopkinson NS. Skeletal muscle dysfunction in chronic obstructive pulmonary disease. Respir Med: COPD Update 2009; 5:7-13.

123. Hopkinson NS, Polkey MI. Does physical inactivity cause chronic obstructive pulmonary disease? Clin Sci 2010; 118:565-572.

124. Shrikrishna D, Patel M, Tanner RJ, et al. Quadriceps wasting and physical inactivity in patients with COPD. Eur Respir J 2012; 40(5):1115-1122.

125. Wust RC, Degens H. Factors contributing to muscle wasting and dysfunction in COPD patients. Int J Chron Obstruct Pulmon Dis 2007; 2:289-300.

126. Schols AMWJ, Soeters PB, Dingemans AMC, et al. Prevalence and characteristics of nutritional depletion in patients with stable COPD eligible for pulmonary rehabilitation. Am Rev Respir Dis 1993; 147:1151-1156.

127. Marquis K, Debigare R, Lacasse Y, et al. Midthigh muscle cross-sectional area is a better predictor of mortality than body mass index in patients with chronic obstructive pulmonary disease. Am J Respir Crit Care Med 2002; 166:809-813.

128. Byun MK, Cho EN, Change J, et al. Sarcopenia correlates with systemic inflammation in COPD. Int J Chron Obstruct Pulmon Dis 2017; 12:669-675.

129. Londhe P, Guttridge DC. Inflammation induced loss of skeletal muscle. Bone 2015; 80:131-142.

130. Graat-Verboom L, Wouters EF, Smeenk FW, et al. Current status of research on osteoporosis in COPD: a systematic review. Eur Respir J 2009; 341:209-218.

131. Calverley PM, Anderson JA, Celli B, et al. Salmeterol and fluticasone propionate and survival in chronic obstructive pulmonary disease. N Engl J Med 2007; 356: 775–789.

132. Vrieze A, de Greef MH, Wijkstra PJ, Wempe JB. Low bone mineral density in COPD patients related to worse lung function, low weight and decreased fat-free mass. Osteoporos Int 2007; 18:1197-1202.

133. Liang B, Feng Y. The association of low bone mineral density with systemic inflammation in clinically stable COPD. Endocrine 2012; 42(1):190-195.

134. Tantucci C. COPD and osteoporosis: something more than a comorbidity. Endocrine 2012; 42(1):5-6.

135. Mineo TC, Ambrogi V, Mineo D, et al. Bone mineral density improvement after lungvolume reduction surgery for severe emphysema. Chest 2005; 127(6):1960-1966.

136. Briot K, Geusens P, Em Bultink I, et al. Inflammatory diseases and bone fragility. Osteoporos Int 2017; 28(12):3301-3314.

137. O'Donnell R, Breen D, et al. Inflammatory cells in the airways in COPD. Thorax 2006; 61(5):448-454.

138. Rouhani F, Paone G, Smith NK, et al. Lung neutrophil burden correlates with increased pro-inflammatory cytokines and decreased lung function in individuals with alpha(1)-antitrypsin deficiency. Chest 2000; 117(5 Suppl 1):250S-251S.

139. Tetley TD. Inflammatory cells and chronic obstructive pulmonary disease. Curr Drug Targets Inflamm Allergy 2005; 4(6):607-618.

140. Cosio MG, Majo J, Cosio MG. Inflammation of the airways and lung parenchyma in COPD: role of T cells. Chest 2002; 121:160-165S.

141. Freeman CM, Han MK, Martinez FJ, et al. Cytotoxic potential of lung CD8+ T Cells increases with chronic obstructive pulmonary disease severity and with in vitro stimulation by IL-18 or IL-15. J Immunol 2010; 184:6504-6513.

142. Chen DL, Cheriyan J, Chilvers E, et al. Quantification of Lung PET Images: Challenges and Opportunities. J Nucl Med 2017; 58(2):201-207.

143. Efthimiadis A, Jayaram L, Weston S, et al. Induced sputum: time from expectoration to processing. Eur Respir J 2002; 19(4):706-708.

144. Barnes PJ, Chowdhury B, Kharitonov SA, et al. Pulmonary biomarkers in chronic obstructive pulmonary disease. Am J Respir Crit Care Med 2006; 174:6-14.

145. Clements PJ, Golding JG, Kleerup EC, et al. Regional differences in bronchoalveolar lavage and thoracic high resolution computed tomography results in dyspneic patients with systemic sclerosis. Arthritis Rheum 2004; 50(6):1909-1901.

146. Lee W, Thomas PS. Oxidative stress in COPD and its measurement through exhaled breath condensate. Clin Transl Sci 2009; 2(2):150-155.

147. Chen DL, Ferkol TW, Mintun MA, et al. Quantifying pulmonary inflammation in cystic fibrosis with positron emission tomography. Am J Respir Crit Care Med 2006; 173:1363-1369.

148. Chen DL, Bedient TJ, Kozlowski J, et al. [18F]Fluorodeoxyglucose positron emission tomography for lung antiinflammatory response evaluation. Am J Respir Crit Care Med 2009; 180(6):533-539.

149. Chen DL, Rosenbluth DB, Mintun MA, Schuster DP. FDG-PET imaging of pulmonary inflammation in healthy volunteers after airway instillation of endotoxin. J Appl Physiol 2006; 100:1602-1609.

150. Rodrigues R, Miller P, Bozza F, et al. FDG-PET in patients at risk for acute respiratory distress syndrome: a preliminary report. Intensive Care Med 2008; 34:2273–2278.

151. Doot RK, Dunnwald LK, Schubert EK, et al. Dynamic and static approaches to quantifying $^{18}$F-FDG uptake for measuring cancer response to therapy, including the effect of granulocyte CSF. J Nucl Med 2007; 48(6):920-925.

152. Subramanian DR, Jenkins L, Edgar R, et al. Assessment of pulmonary neutrophilic inflammation in emphysema by quantitative positron emission tomography. Am J Respir Crit Care Med 2012; 186(11):1125-1132.

153. Harris RS, Venegas JG, Wongviriyawong C, et al. 18F-FDG uptake rate is a biomarker of eosinophilic inflammation and airway response in asthma. J Nucl Med 2011; 52(11):1713-1720.

154. Jones HA, Clark RJ, Rhodes CG, et al. In vivo measurement of neutrophil activity in experimental lung inflammation. Am J Respir Crit Care Med1994; 149(6):1635-1639.

155. Holman BF, Cuplov V, Millner L, et al. Improved correction for the tissue fraction effect in lung PET/CT imaging. Phys Med Biol 2015; 60(18):7387–7402.

156. Schroeder T, Vidal Melo MF, Musch G, et al. Image-derived input function for assessment of 18F-FDG uptake by the inflamed lung. J Nucl Med 2007; 48:1889-1896.

157. Patlak CS, Blasberg RG, Fenstermacher JD. Graphical evaluation of blood-to-brain transfer constants from multiple-time uptake data. J Cereb Blood Flow Metab 1983; 3:1-7.

158. Mair G, Maclay J, Miller JJ, et al. Airway dimensions in COPD: Relationships with clinical variables. Respir Med 2010; 104:1683-1690.

159. Khurana S, Ravi A, Sutula J, et al. Clinical characteristics and airway inflammation profile of COPD persistent sputum producers. Respir Med 2014; 108(12):1761-1770.

160. Hounsfield GN. Nobel Award address. Computed medical imaging. Med Phys 1980; 7(4):283-290.

161. Regan EA, Hokanson JE, Murphy JR, et al. Genetic epidemiology of COPD (COPDGene) study design. COPD 2010; 7(1):32-43.

162. Gevenois PA, De Vuyst P, de Maertelaer V, et al. Comparison of computed density and microscopic morphometry in pulmonary emphysema. Am J Respir Crit Care Med 1996; 154(1):187-192.

163. Schreiter V, Steffen I, Huebner H, et al. Ventilation/perfusion SPECT/CT in patients with pulmonary emphysema. Evaluation of software-based analysing. Nuklearmedizin 2015; 54(1):31-35.

164. de Geus-Oei LF, Visser EP, Krabbe PF, et al. Comparison of image-derived and arterial input functions for estimating the rate of glucose metabolism in therapymonitoring 18F-FDG PET studies. J Nucl Med 2006; 47(6):945-949.

165. Ochs M, Nyengaard JR, Jung A, et al. The number of alveoli in the human lung Am J Respir Crit Care Med 2004; 169:120-124.

166. Wollmer P, Rhodes CG, Hughes JM. Regional extravascular density and fractional blood volume of the lung in interstitial disease Thorax 1984; 39(4):286-293.

167. Sokoloff L, Reivich M, Kennedy C, et al. The [14C]deoxyglucose method for the measurement of local cerebral glucose utilization: theory, procedure, and normal values in the conscious and anesthetized albino rat. J Neurochem 1977; 28:897-916.

168. Gunn RN, Gunn SR, Cunningham VJ. Positron emission tomography compartmental models. J Cereb Blood Flow Metab 2001; 21:635-652.

169. Hawkins RA, Phelps ME, Huang SC. Effects of temporal sampling, glucose metabolic rates, and disruptions of the blood-brain barrier on the FDG model with and without a vascular compartment: studies in human brain tumors with PET. J Cereb Blood Flow Metab 1986; 6:170-183.

170. Huang SC, Phelps ME. Principles of tracer kinetic modeling in positron emission tomography and autoradiography. In: Phelps ME, Mazziotta JC, Schelbert HR, eds. Positron Emission Tomography and Autoradiography: Principles and Applications for the Brain and Heart. New York, NY: Raven Press; 1986:287–346.

171. Coello C, Fisk M, Wilson F, et al. Quantitative analysis of dynamic 18F-FDG in lungs of HV and COPD subjects. J Nucl Med 2016; 57:482.

172. Thie JA. Understanding the standardized uptake value, its methods, and implications for usage. J Nucl Med 2004; 45:1431-1434.

173. Kinahan PE, Fletcher JW. Positron emission tomography-computed tomography standardized uptake values in clinical practice and assessing response to therapy. Semin Ultrasound CT MR 2010; 31(6):496-505.

174. Borst GR, Belderbos JSA, Boellaard R, et al. Standardised FDG uptake: a prognostic factor for inoperable non-small cell lung cancer. Eur J Cancer 2005; 41:1533-1541.

175. Tarkin JM, Joshi FR, Rudd JHF. PET imaging of inflammation in atherosclerosis. Nat Rev Cardiol 2014; 11(8):443-457.

176. Chen DL, Schiebler ML, Goo JM, van Beek EJR. PET imaging approaches for inflammatory lung diseases: Current concepts and future directions. Eur J Radiol 2017; 86:371-376.

177. Biomarker Qualification Program. http://www.fda.gov/Drugs/DevelopmentApprovalProcess/DrugDevelopmentToolsQualificationProgram/ucm284076.htm. Accessed Nov 20, 2016.

178. Jones HA, Sriskandan S, Peters AM, et al. Dissociation of neutrophil emigration and metabolic activity in lobar pneumonia and bronchiectasis. Eur Respir J 1997; 10:795- 803.

179. Jones HA, Cadwallader KA, White JF, et al. Dissociation between respiratory burst activity and deoxyglucose uptake in human neutrophil granulocytes: Implications for interpretation of 18F-FDG PET images. J Nucl Med 2002; 43:652-657.

180. Jones HA, Valind SO, Clark IC, et al. Kinetics of lung macrophages monitored *in vivo* following particulate challenge in rabbits. Toxicol Appl Pharmacol 2002; 183:46- 54.

181. Jones HA, Schofield JB, Krausz T, et al Pulmonary fibrosis correlates with duration of tissue neutrophil activation. Am J Respir Crit Care Med 1998; 158:620-628.

182. Win T, Lambrou T, Hutton BF, et al. 18F-Fluorodeoxyglucose positron emission tomography pulmonary imaging in idiopathic pulmonary fibrosis is reproducible: implications for future clinical trials. Eur J Nucl Med Mol Imaging 2012; 39(3):521-528.

183. Bellani G, Messa C, Guerra L, et al. Lungs of patients with acute respiratory distress syndrome show diffuse inflammation in normally aerated regions: a [18F]-fluoro-2- deoxy-D-glucose PET/ CT study. Crit Care Med 2009; 37:2216-2222.

184. Chen DL, Azulay DO, Atkinson JJ, et al. Reproducibility of positron emission tomography (PET)-measured [18F]Fluorodeoxyglucose ([18F]FDG) uptake as a marker of lung inflammation in chronic obstructive pulmonary disease (COPD). Am J Respir Crit CareMed 2011; 813:A6449.

185. Coulson JM, Rudd JHF, Duckers JM, et al. Excessive aortic inflammation in chronic obstructive pulmonary disease: An 18F-FDG PET pilot study. J Nucl Med 2010; 51:1357-1360.

186. Soret M, Bacharach SL, Buvat I. Partial-volume effect in PET tumor imaging. J Nucl Med 2007; 48(6):932-945.

187. Sun T, Mok GS. Techniques for respiration-induced artifacts reductions in thoracic pet/ct. Quant Imaging Med Surg 2012; 2:46-52.

188. Coello C, Fisk M, Mohan D, et al. Quantitative analysis of dynamic 18F-FDG PET/CT for measurement of lung inflammation. EJNMMI Res 2017; 7(1):47.

189. Kalantari F, Wang J. Attenuation correction in 4D-PET using a single-phase attenuation map and rigidity-adaptive deformable registration. Med Phys 2017; 44(2):522-532.

190. Chang G, Chang T, Pan T, et al. Joint correction of respiratory motion artifact and partial volume effect in lung/thoracic PET/CT imaging. Med Phys 2010; 37(12):6221- 632.

191. Brechtel K, Klein M, Vogel M, et al. Optimized contrast-enhanced CT protocols for diagnostic whole-body 18F-FDG PET/CT: technical aspects of single-phase versus multiphase CT imaging. J Nucl Med 2006; 47:470-476.

192. Goerres GW, Burger C, Schwitter MR, et al. PET/CT of the abdomen: optimizing the patient breathing pattern. Eur Radiol 2003; 13:734-739.

193. Papathanassiou D, Becker S, Amir R, et al. Respiratory motion artefact in the liver dome on FDG PET/CT: comparison of attenuation correction with CT and a caesium external source. Eur J Nucl Med Mol Imaging 2005; 32(12):1422-1428.

194. Richard MA, Fouquet JP, Lebel R, Lepage M. MRI-guided derivation of the input function for PET kinetic modeling. PET Clin 2016; 11(2):193-202.

195. Bruyant PP. Analytic and iterative reconstruction algorithms in SPECT. J Nucl Med 2002; 43(10):1343-1358.

196. Torigian DA, Dam V, Chen X, et al. In vivo quantification of pulmonary inflammation in relation to emphysema severity via partial volume corrected (18)F-FDG-PET using computer-assisted analysis of diagnostic chest CT. Hell J Nucl Med 2013; 16(1):12-18.

197. Currie DC, Pavia D, Agnew JE, et al. Impaired tracheobronchial clearance in bronchiectasis. Thorax 1987; 42:126-130.

198. Lambrou T, Groves AM, Erlandsson K, et al. The importance of correction for tissue fraction effects in lung pet: preliminary findings Eur J Nucl Med Mol Imaging 2011; 38:2238.

199. Win T, Screaton NJ, Porter J, et al. Novel positron emission tomography/computed tomography of diffuse parenchymal lung disease combining a labeled somatostatin receptor analogue and 2-deoxy-2[18f]fluoro-dglucose. Mol Imaging 2012; 11:91-98.

200. Groves AM, Win T, Screaton NJ, et al. Idiopathic pulmonary fibrosis and diffuse parenchymal lung disease: implications from initial experience with 18f-fdg pet/ct. J Nucl Med 2009; 50:538.

201. de Prost N, Tucci MR, Vidal Melo MF. Assessment of lung inflammation with $^{18}$F-FDG PET during acute lung injury. AJR Am J Roentgenol 2010; 195(2):292-300.

202. Karimi R, Tornling G, Forsslund H, et al. Lung density on high resolution computer tomography (HRCT) reflects degree of inflammation in smokers. Respir Res 2014; 15:23.

203. Win T, Thomas BA, Lambrou T, et al. 2014 Areas of normal pulmonary parenchyma on HRCT exhibit increased FDG pet signal in IPF patients Eur J Nucl Med Mol Imaging 2014; 41:337-342.

204. Holman B, Hutton B, Thielemans K. Method to determine the voxel-wise blood volume in the lung from dynamic PET data. J Nucl Med 2017; 58(supplement 1):Abstract 1310.

205. Park SJ, Ionascu D, Killoran J, et al. Evaluation of the combined effects of target size, respiratory motion and background activity on 3D and 4D PET/CT images. Phys Med Biol 2008; 53:3661-3679.

206. Alf MF, Martić-Kehl MI , Schibli R, Krämer SD. FDG kinetic modeling in small rodent brain PET: optimization of data acquisition and analysis. EJNMMI Research 2013, 3:61.

207. Graham MM. Physiologic smoothing of blood time-activity curves for PET data analysis. J Nucl Med 1997; 38:1161-1168.

208. Wright JL, Wiggs BJ, Hogg JC. Airway disease in upper and lower lobes in lungs of patients with and without emphysema. Thorax 1984; 39(4):282-285.

209. Sin DD, Wu L, Man SF. The relationship between reduced lung function and cardiovascular mortality: a population-based study and a systematic review of the literature. Chest 2005; 127:1953-1959.

210. Maclay JD, McAllister DA, Rabinovich R, et al. Systemic elastin degradation in chronic obstructive pulmonary disease. Thorax 2012; 67(7):606-612.

211. Vanfleteren LE, van Meerendonk AM, Franssen FM, et al. A possible link between increased metabolic activity of fat tissue and aortic wall inflammation in subjects with COPD. A retrospective 18F-FDG-PET/CT pilot study. Respir Med 2014; 108(6):883-890.

212. Figueroa AL, Abdelbaky A, Truong QA, et al. Measurement of arterial activity on routine FDG PET/CT images improves prediction of risk of future CV events. JACC Cardiovasc Imaging 2013; 6:1250-1259.

213. Bucerius J, Mani V, Moncrieff C, et al. Optimizing 18F-FDG PET/CT imaging of vessel wall inflammation: the impact of 18F-FDG circulation time, injected dose, uptake parameters, and fasting blood glucose levels. Eur J Nucl Med Mol Imaging 2014; 41:369-383.

214. Blomberg BA, Thomassen A, Takx RA, et al. Delayed 18F-fluorodeoxyglucose PET/CT imaging improves quantitation of atherosclerotic plaque inflammation: results from the CAMONA study. J Nucl Cardiol 2014; 21:588-597.

215. Gholami S, Salavati A, Houshmand S, et al. Assessment of atherosclerosis in large vessel walls: A comprehensive review of FDG-PET/CT image acquisition protocols and methods for uptake quantification. J Nucl Cardiol 2015; 22:468-479.

216. Bucerius J, Duivenvoorden R, Mani V, et al. Prevalence and risk factors of carotid vessel wall inflammation in coronary artery disease patients: FDG-PET and CT imaging study. JACC Cardiovasc Imaging 2011; 4(11):1195-1205.

217. Mehta NN, Yu Y, Saboury B, et al. Systemic and vascular inflammation in patients with moderate to severe psoriasis as measured by [18F]-Fluorodeoxyglucose positron emission tomography/computed tomography (FDG-PET/CT): a pilot study. Arch Dermatol 2011; 147(9):1031-1039.

218. Maki-Petaja KM, Elkhawad M, Cheriyan J, et al. Anti-tumor necrosis factor-α therapy reduces aortic inflammation and stiffness in patients with rheumatoid arthritis. Circulation 2012; 126:2473-2480.

219. Tawakol A, Fayad ZA, Mogg R, et al. Intensification of statin therapy results in a rapid reduction in atherosclerotic inflammation: results of a multicenter fluorodeoxyglucosepositron emission tomography/computed tomography feasibility study. J Am Coll Cardiol 2013; 62:909-917.

220. Korhonen JR, Lahti A, Kankaanranta H, Moilanen E. Nitric oxide production and signaling in inflammation. Curr Drug Targets Inflamm Allergy 2005; 4(4):471-479.

221. Huang HJ, Isakow W, Byers DE, et al. Imaging pulmonary inducible nitric oxide synthase expression with PET. J Nucl Med 2015; 56(1):76-81.

222. Kenny LM, Coombes RC, Oulie I, et al. Phase I trial of the positron-emitting Arg-Gly- Asp(RGD) peptide radioligand 18F-AH111585 in breast cancer patients, J Nucl Med 2008; 49(6):879-886.

223. Mirsadraee S, Marin A, Jenkins W, et al. The identification of systemic integrin activation in idiopathic and systemic sclerosis pulmonary fibrosis using 18F- fluciclatide positron emission tomography, Insights Imaging2016; 7(Suppl 1):S424.

224. Chen D, Agapov E, Solingapuram K, et al. PET imaging with [$^{11}$C]PBR28 and [$^{18}$F]FDG distinguishes macrophage from neutrophil lung inflammation. Eur Respir J 2012; 40:1693.

225. Werner MK, Schmidt H, Schwenzer NF. MR/PET: A new challenge in hybrid imaging. Am J Roentgenol 2012; 199:272-277.

226. Hofmann M, Steinke F, Scheel V, et al. MRI-based attenuation correction for PET/MRI: a novel approach combining pattern recognition and atlas registration. J Nucl Med 2008; 49(11):1875-1883.

227. Salomon A, Goedicke A, Schweizer B, et al. Simultaneous reconstruction of activity and attenuation for PET/MR. IEEE Trans Med Imaging 2011; 30(3):804-813.

228. Mills B, Akram AR, Scholefield E, et al. Optical screening of novel bacteria-specific probes on ex vivo human lung tissue by confocal laser endomicroscopy J Vis Exp 2017; 129, e56284.

**Abstracts and publications generated so far related to this study:**

1. Quantification of Lung PET Images: Challenges and Opportunities. Delphine L Chen, Joseph Cheriyan, Edwin Chilvers, Gourab Choudhury, et al. Jan 2017 Journal of Nuclear Medicine. DOI 10.2967/jnumed.116.184796
2. Role of Inflammation and Oxidative Stress in the Pathology of Ageing in COPD: Potential Therapeutic Interventions. G Choudhury and W MacNee. Sep 2016. COPD Journal of Chronic Obstructive Pulmonary Disease. COPD Journal of Chronic Obstructive Pulmonary Disease 14(1):1-14
3. $^{18}$F-fluorodeoxyglucose (18FDG) PET pulmonary imaging in COPD. G Choudhury, M Connell, A Fletcher, E Van Beek, W MacNee. September 2015. European Respiratory Journal 46(suppl 59):OA4988. DOI 10.1183/13993003.congress- 2015.OA4988
4. $^{18}$F-Fluorodeoxyglucose (18FDG) PET pulmonary imaging: Role in detecting vascular inflammation. Janice Wong, A Vasey, S Ferguson, G Choudhury. September 2015. European Respiratory Journal 46(suppl 59):OA4989. DOI 10.1183/13993003.congress-2015.OA4989
5. $^{18}$F-fluorodeoxyglucose (18FDG) Pet Pulmonary Imaging: Comparative Methodology in COPD Patients. Gourab Choudhury, A Fletcher, M Connell, W MacNee. December 2014. Thorax 69(Suppl 2):A13-A13
6. Dynamic PET pulmonary imaging in COPD patients, comparing various modalities. G Choudhury, M Connell, A Fletcher, E Van Beek, W. MacNee. ERS 2014
7. $^{18}$F-fluorodeoxyglucose (18F-FDG) PET/CT assessment of aortic inflammation and calcification in COPD. Susan Fernandes, G Choudhury et al. DOI. 10.1183/1393003.congress- 2017.PA785.
8. $^{18}$F-Fluorodeoxyglucose ($^{18}$FDG) PET pulmonary imaging: Methodology: Is there a relationship with lung density? G Choudhury, M Connell, A Fletcher, S Ferguson, W MacNee; Scottish Thoracic Society Meeting April 2016.

# APPENDIX

## Section One: supplemental statistical analyses result

**Table 1: Wilcoxon scores for variable *slope* for different modalities of input functioning with no statistical difference.**

| Wilcoxon Scores (Rank Sums) for Variable Slope Classified by Variable Site | | | | | |
|---|---|---|---|---|---|
| **Site** | **N** | **Sum of scores** | **Expected under HO** | **SEM Under HO** | **Mean score** |
| **Image derived** | 6 | 63.0 | 81.00 | 16.431 | 10.50 |
| **Venous blood** | 5 | 60.0 | 67.50 | 15.370 | 12.00 |
| **Venous plasma** | 5 | 43.0 | 67.50 | 15.370 | 8.60 |
| **Arterial blood** | 5 | 98.0 | 67.50 | 15.370 | 19.60 |
| **Arterial plasma** | 5 | 87.0 | 67.50 | 15.370 | 17.40 |

| Kruskal-Wallis Test | |
|---|---|
| **Chi-Square** | 7.6479 |
| **DF** | 4 |
| **Pr > Chi-Square** | 0.1054 |

**Table 2: Wilcoxon scores for variable *intercept* for different modalities of input functioning with no statistical difference between all the methods (p value 0.35).**

| Wilcoxon Scores (Rank Sums) for Variable Intercept Classified by Variable Site | | | | | |
|---|---|---|---|---|---|
| **Site** | **N** | **Sum of scores** | **Expected under HO** | **SEM Under HO** | **Mean score** |
| **Image derived** | 6 | 89.0 | 81.00 | 16.431 | 14.833 |
| **Venous blood** | 5 | 91.0 | 67.50 | 15.370 | 18.200 |
| **Venous plasma** | 5 | 63.0 | 67.50 | 15.370 | 12.600 |
| **Arterial blood** | 5 | 66.0 | 67.50 | 15.370 | 13.200 |
| **Arterial plasma** | 5 | 42.0 | 67.50 | 15.370 | 8.400 |

| Kruskal-Wallis Test | |
|---|---|
| **Chi-Square** | 4.3704 |
| **DF** | 4 |
| **Pr > Chi-Square** | 0.3582 |

**Table 3: Non-parametric analyses of the slope data using Wilcoxon scores between visit 1 and 2 also showing no statistical difference (p value 0.36).**

| Wilcoxon Scores (Rank Sums) for Variable Slope Classified by Variable Visit | | | | | |
|---|---|---|---|---|---|
| **Visit** | **N** | **Sum of scores** | **Expected under HO** | **SEM Under HO** | **Mean score** |
| **2** | 17 | 330.0 | 365.50 | 39.024 | 19.411 |
| **1** | 20 | 373.0 | 387.50 | 39.024 | 22.920 |

| Kruskal-Wallis Test | |
|---|---|
| **Chi-Square** | 0.8275 |
| **DF** | 1 |
| **Pr > Chi-Square** | 0.3630 |

**Table 4: Non-parametric analyses of the intercept data using Wilcoxon scores between visit one and two also showing no statistical significance (p value 0.09).**

| Wilcoxon Scores (Rank Sums) for Variable Intercept Classified by Variable Visit | | | | | |
|---|---|---|---|---|---|
| **Visit** | **N** | **Sum of scores** | **Expected under HO** | **SEM Under HO** | **Mean score** |
| **2** | 17 | 300.0 | 365.50 | 39.024 | 17.647 |
| **1** | 20 | 313.0 | 377.50 | 39.024 | 24.120 |

| Kruskal-Wallis Test | |
|---|---|
| **Chi-Square** | 2.8171 |
| **DF** | 1 |
| **Pr > Chi-Square** | 0.0933 |

**Table 5: Patlak slope in COPD patients and controls.**

| Wilcoxon Scores (Rank Sums) for Variable Intercept Classified by Variable Group | | | | | |
|---|---|---|---|---|---|
| **Group** | **N** | **Sum of scores** | **Expected under HO** | **SEM Under HO** | **Mean score** |
| **COPD** | 19 | 222.0 | 247.0 | 15.716234 | 11.684 |
| **Control** | 6 | 103.0 | 78.0 | 15.716234 | 17.166 |

| Kruskal-Wallis Test | |
|---|---|
| **Chi-Square** | 2.5304 |
| **DF** | 1 |
| **Pr > Chi-Square** | 0.1117 |

**Table 6: Patlak intercept in COPD patients and controls.**

| Wilcoxon Scores (Rank Sums) for Variable Intercept Classified by Variable Group | | | | | |
|---|---|---|---|---|---|
| **Group** | **N** | **Sum of scores** | **Expected under HO** | **SEM Under HO** | **Mean score** |
| **COPD** | 19 | 192.0 | 247.0 | 15.716 | 10.105 |
| **Control** | 6 | 133.0 | 78.0 | 15.716 | 22.166 |

| Kruskal-Wallis Test | |
|---|---|
| **Chi-Square** | 12.2470 |
| **DF** | 1 |
| **Pr > Chi-Square** | 0.0005 |

**Table 7: Comparative data (slope/intercept) between the two visits of the COPD patients.**

| Wilcoxon Scores (Rank Sums) for Variable Slope/ Intercept Classified by Variable Visit | | | | | |
|---|---|---|---|---|---|
| **Visit** | **N** | **Sum of scores** | **Expected under HO** | **SEM Under HO** | **Mean score** |
| **2** | 17 | 362.0 | 365.50 | 39.024 | 21.294 |
| **1** | 20 | 541.0 | 537.50 | 39.024 | 24.640 |

| Kruskal-Wallis Test | |
|---|---|
| **Chi-Square** | 0.0080 |
| **DF** | 1 |
| **Pr > Chi-Square** | 0.98 |

**Table 8: shows no significant difference of slope/intercept between COPD and controls (p value 0.70).**

| Wilcoxon Scores (Rank Sums) for Variable Slope/ Intercept Classified by Variable Group | | | | | |
|---|---|---|---|---|---|
| **Group** | **N** | **Sum of scores** | **Expected under HO** | **SEM Under HO** | **Mean score** |
| **COPD** | 19 | 241.0 | 247.0 | 15.716 | 12.684 |
| **Control** | 6 | 84.0 | 78.0 | 15.716 | 14.000 |

| Kruskal-Wallis Test | |
|---|---|
| **Chi-Square** | 0.145 |
| **DF** | 1 |
| **Pr > Chi-Square** | 0.70 |

**Table 9: Comparison of KiAoVb between visits 1 and 2.**

| Wilcoxon Scores (Rank Sums) for Variable KiAoVb Classified by Variable Visit | | | | | |
|---|---|---|---|---|---|
| **Visit** | **N** | **Sum of scores** | **Expected under HO** | **SEM Under HO** | **Mean score** |
| **1** | 14 | 503.0 | 500.00 | 34.156 | 20.120 |
| **2** | 20 | 277.0 | 280.00 | 34.156 | 19.785 |

| Kruskal-Wallis Test | |
|---|---|
| **Chi-Square** | 0.0077 |
| **DF** | 1 |
| **Pr > Chi-Square** | 0.9300 |

**Table 10: Comparison of KiPulmVb between visits 1 and 2.**

| Wilcoxon Scores (Rank Sums) for Variable KiPulmVb Classified by Variable Visit | | | | | |
|---|---|---|---|---|---|
| **Visit** | **N** | **Sum of scores** | **Expected under HO** | **SEM Under HO** | **Mean score** |
| **1** | 25 | 511.0 | 500.00 | 34.156 | 20.440 |
| **2** | 14 | 269.0 | 280.00 | 34.156 | 19.214 |

| Kruskal-Wallis Test | |
|---|---|
| **Chi-Square** | 0.1037 |
| **DF** | 1 |
| **Pr > Chi-Square** | 0.747 |

**Table 11: Comparison of KiAoVbVa between visits 1 and 2.**

| Wilcoxon Scores (Rank Sums) for Variable KiAoVbVa Classified by Variable Visit | | | | | |
|---|---|---|---|---|---|
| **Visit** | **N** | **Sum of scores** | **Expected under HO** | **SEM Under HO** | **Mean score** |
| **1** | 25 | 490.0 | 500.00 | 34.156 | 19.600 |
| **2** | 14 | 290.0 | 280.00 | 34.156 | 20.714 |

| Kruskal-Wallis Test | |
|---|---|
| **Chi-Square** | 0.085 |
| **DF** | 1 |
| **Pr > Chi-Square** | 0.769 |

**Table 12: Comparison of KiPulmVbVa between visits 1 and 2.**

| Visit | N | Sum of scores | Expected under HO | SEM Under HO | Mean score |
|---|---|---|---|---|---|
| 1 | 25 | 506.0 | 500.00 | 34.156 | 20.240 |
| 2 | 14 | 274.0 | 280.00 | 34.156 | 19.571 |

| Kruskal-Wallis Test | |
|---|---|
| Chi-Square | 0.0309 |
| DF | 1 |
| Pr > Chi-Square | 0.8606 |

**Table 13: KiAoVb between COPD and controls.**

| Wilcoxon Scores (Rank Sums) for Variable KiAoVb Classified by Variable Group | | | | | |
|---|---|---|---|---|---|
| Group | N | Sum of scores | Expected under HO | SEM Under HO | Mean score |
| COPD | 25 | 397.0 | 400.0 | 20.0 | 15.880 |
| Control | 6 | 99.0 | 96.0 | 20.0 | 16.500 |

| Kruskal-Wallis Test | |
|---|---|
| Chi-Square | 0.0225 |
| DF | 1 |
| Pr > Chi-Square | 0.86 |

**Table 14: KiaAoVbVa between COPD and controls.**

| Wilcoxon Scores (Rank Sums) for Variable KiAoVbVa Classified by Variable Group | | | | | |
|---|---|---|---|---|---|
| **Group** | **N** | **Sum of scores** | **Expected under HO** | **SEM Under HO** | **Mean score** |
| **COPD** | 25 | 410.0 | 400.0 | 20.0 | 16.400000 |
| **Control** | 6 | 86.0 | 96.0 | 20.0 | 14.333333 |

| Kruskal-Wallis Test | |
|---|---|
| **Chi-Square** | 0.2500 |
| **DF** | 1 |
| **Pr > Chi-Square** | 0.6171 |

**Table 15: KiPulmVb between COPD and controls.**

| Wilcoxon Scores (Rank Sums) for Variable KiPulmVb Classified by Variable Group | | | | | |
|---|---|---|---|---|---|
| **Group** | **N** | **Sum of scores** | **Expected under HO** | **SEM Under HO** | **Mean score** |
| **COPD** | 25 | 440.0 | 400.0 | 20.0 | 17.600000 |
| **Control** | 6 | 56.0 | 96.0 | 20.0 | 9.333333 |

| Kruskal-Wallis Test | |
|---|---|
| **Chi-Square** | 4.0000 |
| **DF** | 1 |
| **Pr > Chi-Square** | 0.04 |

**Table 16: KiPulmVbVa between COPD and controls.**

| Wilcoxon Scores (Rank Sums) for Variable KiPulmVbVa Classified by Variable Group | | | | | |
|---|---|---|---|---|---|
| **Group** | **N** | **Sum of scores** | **Expected under HO** | **SEM Under HO** | **Mean score** |
| **COPD** | 25 | 435.0 | 400.0 | 20.0 | 17.400000 |
| **Control** | 6 | 61.0 | 96.0 | 20.0 | 10.166667 |

| Kruskal-Wallis Test | |
|---|---|
| **Chi-Square** | 3.0625 |
| **DF** | 1 |
| **Pr > Chi-Square** | 0.0801 |

**Table 17: Comparison of SUVmax between visits 1 and 2.**

| Wilcoxon Scores (Rank Sums) for SUV Max Classified by Variable Visit | | | | | |
|---|---|---|---|---|---|
| **Visit** | **N** | **Sum of scores** | **Expected under HO** | **SEM Under HO** | **Mean score** |
| **2** | 18 | 350.0 | 396.00 | 40.620192 | 19.444444 |
| **1** | 25 | 596.0 | 550.00 | 40.620192 | 23.840000 |

| Kruskal-Wallis Test | |
|---|---|
| **Chi-Square** | 1.2824 |
| **DF** | 1 |
| **Pr > Chi-Square** | 0.2574 |

**Table 18: Comparison of SUVmax between COPD and controls.**

| Wilcoxon Scores (Rank Sums) for SUVmax Classified by Variable Group | | | | | |
|---|---|---|---|---|---|
| **Group** | **N** | **Sum of scores** | **Expected under HO** | **SEM Under HO** | **Mean score** |
| **COPD** | 19 | 269.0 | 247.00 | 15.716234 | 14.157895 |
| **Control** | 6 | 56.0 | 78.00 | 15.716234 | 9.333333 |

| Kruskal-Wallis Test | |
|---|---|
| **Chi-Square** | 1.9595 |
| **DF** | 1 |
| **Pr > Chi-Square** | 0.1616 |

**Table 19: Comparison of SUVcorrDENS corrected for density between COPD and controls.**

| Wilcoxon Scores (Rank Sums) for SUVcorrDENS Classified by Variable Group | | | | | |
|---|---|---|---|---|---|
| **Group** | **N** | **Sum of scores** | **Expected under HO** | **SEM Under HO** | **Mean score** |
| **COPD** | 19 | 277.0 | 247.00 | 15.716234 | 14.578947 |
| **Control** | 6 | 48.0 | 78.00 | 15.716234 | 8.000000 |

| Kruskal-Wallis Test | |
|---|---|
| **Chi-Square** | 3.6437 |
| **DF** | 1 |
| **Pr > Chi-Square** | 0.0563 |

**Table 20: Comparison of SUV corrected density using kinetic modelling analyses between COPD and controls.**

| Wilcoxon Scores (Rank Sums) for SUVaoDENS Classified by Variable Group | | | | | |
|---|---|---|---|---|---|
| **Group** | **N** | **Sum of scores** | **Expected under HO** | **SEM Under HO** | **Mean score** |
| **COPD** | 25 | 440.0 | 400.00 | 20.0 | 17.600 |
| **Control** | 6 | 56.0 | 96.00 | 20.0 | 9.333 |

| Kruskal-Wallis Test | |
|---|---|
| **Chi-Square** | 4.0000 |
| **DF** | 1 |
| **Pr > Chi-Square** | 0.0455 |

## Section Two: principles of running an ELISA experiment

ELISA protocol commences with a capture antibody, specific for a protein of interest, coated onto the wells of microplates. Samples, including a standard containing protein of interest, control specimens, and unknowns, are pipetted into these wells. During the first incubation, the protein antigen binds to the capture antibody. After washing, a detection antibody is added to the wells, and this antibody binds to the immobilized protein captured during the first incubation. After removal of excess detection antibody, an HRP conjugate (secondary antibody) is added and binds to the detection antibody. After a third incubation and washing to remove the excess HRP conjugate, a substrate solution is added and is converted by the enzyme to a detectable form (colour signal). The intensity of this coloured product is directly proportional to the concentration of antigen present in the original specimen.

## Section Three: Sputum processing

### Procedure

1. **Sputum selection:** Before processing the sample, discard the specimen cup containing the salivary portion of the expectorate to avoid potential confusion with the sample specimen waste cup. The sputum sample is poured into a Petri dish for visual examination or inspection. The colour (clear, yellow, green), purulence and signs of blood contamination are noted in the CRF (Sputum Sample Quality page). The Petri dish should then be placed on a dark background. All solid or dense looking material as compared to clear surrounding fluid is defined and referred to as "sputum plug". Plugs are typically gelatinous (more dense) and mucoid in appearance. Using fine or pointed sterile forceps, select the sputum plugs from the saliva and transfer them onto the Petri dish lid. If blood is in the sample, avoid selecting it. Then, using larger blunt ended forceps, gather the sputum plugs into one mass and then condense by moving the entire mass around the lid in circular motions. The aim is to spread the saliva around the lid but to keep sputum in one mass. Transfer the concentrated sputum with the blunt ended forceps to a pre-weighed 15 ml polypropylene centrifuge tube with screw top (use of polystyrene tubes is not recommended as they cause cell adhesion). The selection procedure and condensation/removal of saliva are important in reducing squamous cell contamination. In order to further reduce contamination with squamous epithelial cells, it can be helpful (but not necessary) to use an inverted microscope to help in identifying the plugs in the sputum sample. It is also helpful to hold the Petri dish up to the light and look through the bottom of it in order to see whether plugs are "hiding" underneath layers of bubbles. Always select as much plug material as possible.

**Sputum weight:** Once all the plug material has been selected and placed into a 15ml polypropylene test tube, record the weight of the test tube using a microbalance or scale that is accurate to at least 2 decimal places. The weight of the selected plug is determined by subtracting the weight of the test tube from the weight of the test tube + sputum plug and this weight is recorded on the CRF. A minimum of 0.5 g of selected sputum **is recommended** to enable the sample to be fully processed (but 0.15 g may suffice). Keep the sample tube on ice and make sure it is processed as soon as possible (within 2 hours).

2. **Addition of DTT:** A ratio of 4:1, of ml of 0.1% DTT: grams of sputum plug is necessary (ie, 0.1% DTT is added to the sputum in the ratio of 4ml DTT to 1g sputum plugs). Please see the example in Appendix 2.

3. **Liquefaction:** Following the addition of DTT, the sample is vortexed for 15 seconds and aspirated with a pipette if necessary to ensure thorough homogenization (mixing) of the sample (ie, no visible clumps still suspended in solution). The sample is then agitated on a rotating tumbler for 15 minutes at room temperature. If a rotating tumbler is not available, one can use a rolling mixer or rocker.

****NOTE: It is important to be exact with the 15-minute incubation in DTT - do not extend this incubation period as prolonged incubation with DTT can be detrimental to the sample**. At the end of the 15-minute incubation period, DPBS (or PBS) in the same volume as the 0.1% DTT volume is added to the sample. The sample is then vortexed for 15 seconds and put on the tumbler for an additional 5 minutes.

4. **Filtration: **NOTE: This filtration step may need to be repeated if the sample is large. Mucus can block the mesh and a new filter is needed for the remaining sample.**

Once the tumbling is complete, the sample is filtered through a 48-55 μm pore nylon mesh filter (that sits in a conical plastic funnel) into a 50ml polypropylene test tube. It is advisable to pre-wet the mesh filter with DPBS/PBS so that it adheres to the sides of the funnel. Do not let the filter fold over onto itself or form creases. The bottom of the filter should be as flat and smooth as possible. If 48-55 μm pore nylon mesh filter is not available, a BD Falcon Cell Strainer may be used.

****NOTE: A BD Falcon Strainer should only be used with 50ml tubes if the sample is of large enough volume.**

Use a pipette (1ml) to deliver the sample through the filter and do not aggressively discharge the sample onto the filter. The sample should ideally drip through the filter and not "run" through it.

5. **Centrifugation of filtrate:** Once the filtrate is collected it is centrifuged at 4$^{O}$C for 5 minutes at 1000 rpm (400-500 x g, depending on centrifuge, it may be necessary to spin for up to 10 min at 2000 rpm) to precipitate the cells into a soft pellet. Use a pipette to remove the supernatant layer. The pellet may or may not be visibly obvious so take care not to disturb it when pipetting out the supernatant layer.

****NOTE: Do not decant (tip) the sample tube to remove the supernatant.** If a layer of mucus is observed at the top of the tube following centrifugation, it should be removed with a pipette tip prior to removing the supernatant.

6. **Supernatant aliquots:** The supernatant should be aliquoted into pre-chilled labelled screw-cap 2ml polypropylene cryotubes with blue snap cap inserts; ideally 3 aliquots of not less than 200 ul each should be obtained (if less than 600 ul is produced then less aliquots should be provided to maintain the volume of each aliquot). All sputum supernatant aliquots should be labelled and stored at -70ºC until required for analysis.

**Aliquot 1:** 200 ul (biomarkers). Label from Sample Data Sheet 3, Line 46. Indicate the relevant sample code. Record the box and position of the aliquot. **Aliquot 2:** diluted (25x) sputum supernatant aliquot for MPO analysis. In a cryotube add 50 ul of fresh sample into 1200 ul of stabilizing buffer (provided by GSK).
Label from Sample Data Sheet 3, Line 48. Indicate the relevant sample code. Record the box and position of the aliquot.

**Aliquots 3 and 4:** 2ml of the remainder is added to each tube (add protease inhibitor at 10µl/mL).

Label from Sample Data Sheet 3, Line 47. Indicate the relevant sample code. Record the box and position of the aliquots.

7. **Re-suspension:** Immediately following removal of the supernatant, the cell pellet must be fully re-suspended in an appropriate volume of cold PBS to ensure that it does not dry out. It is recommended that the sample pellet be re- suspended to give a concentration of approximately 500,000 cells/ml. The volume required is usually between 0.3 and 1.0 ml, depending on the size and viscosity of the pellet. A

more thick or viscous pellet would require a higher re- suspension volume closer to 1ml (and on some occasions, larger pellets require 1.5ml). Once the buffer is added to the pellet, it is mixed by gentle vortexing using cell saver tips or gentle pipette aspiration. Keep the cell suspension on ice while performing the next step: quick cell counting (within 15 min).

8. **Quick Cell count:** Assess total cell count for viability and qualitative level of squamous cell contamination using a Neubauer haemocytometer.

****NOTE: The New Improved Bright Line Neubaur Haemocytometer is recommended**) and the Trypan Blue exclusion method, as follows:

- First locate the Neubauer haemocytometer and make sure it is clean, has a cover slip and is ready for use. It is strongly recommended that the haemocytometer and coverslip are cleaned with 70% ethanol or methanol to ensure better quality when counting.
- Remove a 10 µl aliquot of the cell suspension and mix it with 10 µl of 0.4% Trypan blue in an eppendorf tube. Trypan blue is commercially purchased as a 0.4% solution (so there is no need to dilute it).
- Gently aspirate the sample using a pipette 2-3 times to ensure good mixing.
- Place the cover slip on top of the haemocytometer (a number 1 cover slip is used). Formation of Newton's rings between the external support and the cover slip shows that the cover slip is correctly positioned. Inject 10µl of the stained mixture into one end (injection port) of the haemocytometer and repeat for the other injection port. Be careful not to flood the chamber of the hemcytometer (a 10µl volume should adequately fill the chamber and not overflow it).

****NOTE: Introduction of bubbles may occur when aspirating the sample to mix with the Trypan Blue dye and when loading the haemocytometer.** This

should be avoided as much as possible as bubbles may have a large impact on cell count.

Place the haemocytometer under the microscope for cell counting. Perform a cell count within 5 minutes, following the instructions outlined below. Find the counting grids (four 4x4 square grids in each corner quadrant with a more detailed centre grid) by adjusting the focus of the microscope (usually 20x magnification power is enough to see the grid lines). Initially focus the grid based on the clarity of the grid lines and not the cells. Use the upper left 4x4 quadrant grid as the starting grid for your cell counts.

9. **Cytospin slide preparation:** Assemble the cytospin slide apparatus (microscope slide, filter paper, sample bucket, and metal/plastic clip). Make sure that the filter card circle lines up with the filter cup circle by observing the reverse side of the metal/plastic clip when assembled (See the cytospin instructions if you are unsure). Disposable cytofunnels (filter paper and sample bucket) are available and are recommended in order to reduce potential contamination and avoid disinfection steps. Please see the manufacturer's instructions regarding the type of cytospin apparatus you have. It is recommended to use single cytofunnels (i.e. filter papers with one hole) and not the double cytofunnels (2 holes).

Adjust the sample suspension to any concentration between 0.5- 1.0 x $10^6$ cells/ml using DPBS or PBS. See Appendix 2 for examples of how to do this. Prepare 2 slides for differential cell staining. Please ensure these slides are affixed with the correct label (use of a lead pencil is recommended as this will not come off when the slides are being stained).

Add 65µl of cell suspension to the cytospin bucket. Deposit the 65µl of sample

directly at the bottom of the bucket (ie, do not let it drip down the sides to settle on the bottom).

****NOTE: The volume of cell suspension to be added to the cytospin should be 65 μl if the cell concentration is close to the 1 x $10^6$ cells/ml. The volume should be increased to 100 μl if the sample concentration is closer to the 0.5 x $10^6$ cells/ml level.** Load the cytospin slide apparatus with the two slides into the centrifuge making sure that the centrifuge is appropriately balanced before spinning. Set the cytospin at 450 rpm with medium acceleration for 6 minutes. The remaining sample should be kept on ice during this time.

When the cytospin is finished, carefully and quickly remove each slide apparatus and remove the slide from the assembly. Be sure not to disturb the sample pellet (which will appear as a round dot of sample) on the slide. Let the slides air dry for at least 15 minutes.

At this stage the slide quality and density should be checked under a microscope to ensure the quality of your samples.

10. **Differential cell staining:** Following air-drying, the 2 slides are stained according to the manufacturer's instructions for the stain kit used.

****NOTE: Please follow manufacturer's instructions of the kit you are using.** Once the slides have been stained and air dried, mount with DPX (or similar mounting media) and size 0 cover slips, store at room temperature.

- **Label:** Affix each slide on the side with the appropriate bar code label taken

from Sample Data Sheet (SDS) 3, lines 50 and 51. Indicate the relevant sample code on the SDS.

## Storage of sputum supernatant and cell samples for analysis

The sputum supernatants and cell TRIzol lysate and slides will be stored at -70° C (supernatant, TRIzol lysate) and room temperature (slides) for shipment as described above. The number of aliquots of supernatant and TRIzol lysate is recorded in the CRF.

**Modified MRC score:**

| Table 2.5. Modified MRC dyspnea scale[a] | |
|---|---|
| PLEASE TICK IN THE BOX THAT APPLIES TO YOU (ONE BOX ONLY) (Grades 0–4) | |
| **mMRC Grade 0.** I only get breathless with strenuous exercise. | ❑ |
| **mMRC Grade 1.** I get short of breath when hurrying on the level or walking up a slight hill. | ❑ |
| **mMRC Grade 2.** I walk slower than people of the same age on the level because of breathlessness, or I have to stop for breath when walking on my own pace on the level. | ❑ |
| **mMRC Grade 3.** I stop for breath after walking about 100 meters or after a few minutes on the level. | ❑ |
| **mMRC Grade 4.** I am too breathless to leave the house or I am breathless when dressing or undressing. | ❑ |

[a] Fletcher CM. BMJ 1960; 2: 1662.